HOKKAIDO UNIVERSITY

Title	Design of Quantum Dot-Based High Performance Nanoparticle Platform for Nanoparticle-Based Drug Delivery (NDD) system
Author(s)	TAN, ROGER SALVACION
Citation	北海道大学. 博士(生命科学) 甲第12011号
Issue Date	2015-09-25
DOI	10.14943/doctoral.k12011
Doc URL	http://hdl.handle.net/2115/60374
Type	theses (doctoral)
File Information	ROGER_SALVACION_TAN.pdf

Instructions for use

Hokkaido University Collection of Scholarly and Academic Papers : HUSCAP

Doctoral Dissertation

Design of Quantum Dot-Based High Performance Nanoparticle Platform for Nanoparticle-Based Drug Delivery (NDD) System

（ナノ微粒子による薬物送達システム

－量子ドット型高性能ナノ微粒子プラットフォームの設計）

Roger Salvacion Tan

Submitted for the Degree of
Doctor of Life Science in
the Graduate School of Life Science

HOKKAIDO UNIVERSITY

2015

Design of Quantum Dot-Based High Performance Nanoparticle Platform for Nanoparticle-Based Drug Delivery (NDD) System

（ナノ微粒子による薬物送達システム

－量子ドット型高性能ナノ微粒子プラットフォームの設計）

ABSTRACT

Nanoparticle drug delivery (NDD) platforms have emerged as a promising approach to enhance the efficacy of the existing drugs and potent therapeutic agents though encapsulation of poorly soluble agents. However, the early design of NDD vehicles was governed by the intrinsically poor pharmacokinetic properties of conventional chemotherapeutics. Low drug solubility, rapid metabolism and clearance, and most importantly a lack of selectivity regularly lead to therapeutic failure by causing severe systemic toxicity in healthy neighboring tissues, thus prohibiting the dose escalation necessary to eliminate tumor cells. Prime pre-requisite to a successful NDD is the ability to mediate the facile and efficient delivery of the nanoparticles to the cell to ultimately deliver various drugs towards the target intracellular space and various specific subcellular compartments of mammalian cells. The traceability of the delivered drug is also a crucial aspect in monitoring the biodistribution, intracellular trafficking, and long-term fate of drugs and NP-drug delivery vehicles in order to assess and characterize the pharmacokinetic properties as well as the targeting specificity of the delivered drug, which are lacking in the current NDD platforms. In this study, a novel strategy for the development of high performance nanoparticle platform was established by means of cell surface mimetic quantum dots (QDs)-anchored peptides/glycopeptides as a model system for NDD vehicles with defined functions facilitating intracellular trafficking after initial endocytosis.

This study describes the standardized protocol for the preparation of multifunctional QDs that allow for efficient cellular uptake and rapid escape from endolysosomal entrapment followed by subsequent molecular delivery to the target cellular compartment. The established protocol took advantage of the facile chemoselective ligation of ketone-functionalized peptides and glycopeptides onto the surface of the aminooxy/phospholylcholine self-assembled monolayer coated QDs (AO/PCSAM-QDs) in mild reaction condition. Displaying ketone-functionalized hexahistidine derivative onto the AO/PCSAM-QD surface during intracellular delivery facilitated both endocytic entry and rapid endolysosomal escape of the conjugates in various human cell lines. Combined use of hexahistidylated AO/PCSAM-QDs with serglycin-like glycopeptides, a proteoglycan initiators (PGIs), elicited an entry, controlled intracellular

trafficking, golgi localization and subsequent excretion of the QD conjugates, as also observed in the real-time live cell imaging. The results suggested that this approach can potentially provide an ideal platform for the design of high performance NDD system that could track every stages of NDD.

Therefore, it is noteworthy that PCSAM coating strategy could become a universal tool for spatially oriented immobilization of engineered proteins including antibody and antibody-drug conjugates on various metal-based nanoparticles.

Acknowledgement

I would like to thank...

- My supervisor, Professor Shin-Ichiro Nishimura for always taking time, for excellent guidance and for sharing his vast knowledge.
- Dr. Kentaru Naruchi for valuable discussions, sharing ideas and guidance regarding research path, as well as uplifting encouragements.
- Dr. Hiroshi Hinou for the discussions, guidance and kind assistance especially in terms of technical instrumental problems matters.
- Dr. Maho Amano for your kind advice and discussion for research improvement.
- Professor Masataka Kinjo and Dr. Akira Kitamura for kind assistance in fluorescence imaging.
- Dr. Fayna Maria Garcia-Martin and Dr. Sylvia Pujals for assistance in spectral analysis.
- My colleagues both from Nishimura laboratory and Medicinal Chemistry Pharmaceuticals Co. Ltd., (MCP).
- Former members of Advanced Chemical Biology group, Ms. Misaki Arai, Mr. Yuya Abe, Mr. Seiji Handa, Mr. Seiya Kikuchi, Mr. Hiroyoshi Fujii, Ms. Yuka Iida, Ms. Yukina Umemoto, Mr. Yukihiko Wakimoto, Dr. Junya Ishida, Dr. Takayuki Furukawa.
- Ms. Kana Masui, Ms. Mayo Hirota, Ms. Maki Morita, and Ms. Tomoko Takahashi.
- International Graduate Program (IGP) of Hokkaido University.
- Ministry of Education, Culture, Sports, Science and Technology (MEXT), Japan
- My friends around the world.

- My Families and relatives.

- The almighty God for everything.

ABBRIVIATIONS

Ac	Acetyl
*t*Bu	*tert*-butyl
QDs	Quantum Dots
CPPs	Cell Penetrating Peptides
k-His_6	Ketone functionalized hexa-histidine
k-Arg_6	Ketone functionalized hexa-arginine
SAMs	Self-assembled monolayers
AOSH	11,11'-dithio bis[undec-11-*yl* 12-(aminooxyacetyl)amino hexa(ethyleneglycol)]
PCSH	11-mercaptoundecylphosphorylcholine
AO/PCSAM-QDs	aminooxy/phosphorylcholine self-assembled monolayer-coated QDs
SPPS	Solid-Phase Peptide Synthesis
MALDI-TOF/MS	Matrix-Assisted Laser Desorption/Ionization-Time of Flight/ Mass Spectrometry
RP-HPLC	Reversed-Phase High Performance Liquid Chromatography
TOPO	Trioctylphosphine oxide
TOPO-QD	Trioctylphosphine oxide-coated Quantum Dots
FCS	Fluorescence Correlation Spectroscopy
HSPGs	Heparan Sulphate Proteoglycans
GAGs	Glycosaminoglycans
PyBOP	Benzotriazol-1-yloxytris(pyrrolidino)phosphonium hexafluorophosphate
HBTU	*N*-[(*1*H-benzotriazol-1-yl)(dimethylamino)methylene]-*N*-methylmethanaminium hexafluorophosphate *N*-oxide
HOAt	1-hydroxy-7-azabenzotriazole
DCM	Dichloromethane
DMF	*N,N*-dimethylformamide
DIEA	*N,N*-diisopropylethylamine
TFA	Trifluoroacetic acid
Ac_2O	Acetic anhydride
Fmoc	9-fluorenylmethoxycarbonyl
EDT	1,2-etanedithiol
Arg	Arginine
His	Histidine
DHB	2,5-dihydroxybenzoic acid
HCl	Hydrochloric acid
AcOH	Acetic acid
Boc	*tert*-butoxycarbonyl
BSA	Bovine Serum Albumin
Pbf	2,2,4,6,7-pentamethyldihydrobenzofuran-5-sulphonyl
Trt	Trityl
TIS	Triisopropylsilane
RT/r.t	Room Temperature
PBS	Phosphate-buffered saline
EDTA	Ethylenediamine tetraacetic acid
DMSO	Dimethyl sulphoxide
Ser	Serine
Gly	Glycine
ER	Endoplasmic reticulum
PGI	Proteoglycan initiator

TABLE OF CONTENTS

			Page
Title Page			**i**
Abstract			**ii**
Acknowledgement			**iv**
Abbreviation			**vi**
Table of Contents			**vii**
List of Tables			**viii**
List of Schemes			**ix**
List of Figures			**x**
CHAPTER			
1	**General Introduction**		1
	1.1	General Introduction	2
	1.2	References	6
2	**Hexahistidine-Mediated Endolysosomal Escape of Cell Surface Mimetic Quantum Dots-Anchored Glycopeptides**		9
	2.1	General Introduction	10
	2.2	Results and Discussion	14
	2.3	Experimental	56
	2.4	References	64
3	**Effect of Glycosylation on Intracellular Trafficking of Synthetic Peptides**		69
	3.1	General Introduction	70
	3.2	Results and Discussion	72
	3.3	Experimental	102
	3.4	References	111
4	**Conclusion**		116
	4.1	Conclusion	117

LIST OF TABLES

TABLE		Page
2.1	High resolution masses of peptides and glycopeptide taken using MALDI-TOFMS……...	15
3.1	List of high resolution masses of compounds **1-4** taken using MALDI-TOFMS……...	75
3.2	Semi-quantitative assessment of the amount of QDs inside the cell....……..……...……...	96

LIST OF SCHEMES

SCHEME		Page
2.1a	Diagram for SPPS of ketone-functionalized glycopeptide……....	15
2.1b	Diagram for SPPS of *k*-His_6 and *k*-Arg_6……...	16

LIST OF FIGURES

FIGURE		Page
2.1	Peptides and glycopeptide structures……..	14
2.2a	Structure and high resolution mass spectrum of *k*-Arg_6.....	16
2.2b	Structure and RP-HPLC chromatogram of *k*-Arg_6……	17
2.3a	Structure and high resolution mass spectrum of *k*-His_6……	17
2.3b	Structure and RP-HPLC chromatogram of *k*-His_6……	18
2.4a	Structure and high resolution mass spectrum of ketone-functionalized glycopeptide……..	18
2.4b	Structure and RP-HPLC chromatogram of ketone-functionalized glycopeptide……..	19
2.5	General protocol for preparation of AO/PCSAM-QDs…….	19
2.6	Direct MALDI-TOFMS of AO/PCSAM-QDs……..	20
2.7	Fluorescence fluctuation profile of AO/PCSAM-QDs measured by Fluorescence Correlation Spectroscopy……	21
2.8	General protocol for preparation of QD conjugates……..	22
2.9	MALDI-TOF/MS Spectrum of AO/PCSAM-QD carrying His_6…..	22
2.10	MALDI-TOF/MS Spectrum of AO/PCSAM-QD carrying Arg_6…..	23
2.11	MALDI-TOF/MS Spectrum of AO/PCSAM-QD carrying glycopeptide……..	23
2.12	MALDI-TOF/MS Spectrum of AO/PCSAM-QD carrying His_6 and glycopeptide……..	24
2.13	Cartoon structure representation and Fluorescence fluctuation profile of AO/PCSAM-QD carrying His_6 and glycopeptide measured by Fluorescence Correlation Spectroscopy……...	25
2.14	Cartoon structure representation and Fluorescence fluctuation profile of AO/PCSAM-QD carrying His_6 measured by Fluorescence Correlation Spectroscopy……	26
2.15	Cartoon structure representation and Fluorescence fluctuation profile of AO/PCSAM-QD carrying Arg_6 measured by Fluorescence Correlation Spectroscopy……	27
2.16	Fluorescence intensity per molecule of QD conjugates measured by FCS. Error bar represents standard error of the mean…….....	27
2.17	Representative images of different cell lines showing lysosomal entrapment of AO/PCSAM-QDs carrying glycopeptides after co-incubation for 2 h……..	28
2.18	Representative fluorescent images after 2 h co-incubation of A549 cells in the presence of 5 nM AO/PCSAM-QDs carrying His_6 (Left) and Arg_6 (Right)……..	30
2.19	Representative cell images showing **c**ellular Uptake of AO/PCSAM-QDs carrying His_6 (green) at different endocytic inhibition conditions……..	32
2.20	Effect of the different temperature incubation on the cellular uptake efficiency of QD conjugates carrying His_6……	32
2.21	Interaction of His_6 and glycopeptide with heparin (n = 3) using microarray…….	35

2.22	Plot showing cellular uptake of AO/PCSAMQDs displaying different ratios of His_6 in OUS-11. At least 15 cells were scored per data point…….	35
2.23	Representative images showing cellular uptake of AO/PCSAMQDs displaying different ratios of His6 in OUS-11…..	36
2.24	Plot showing cellular uptake of AO/PCSAMQDs displaying different ratios of His6 in NHAC-Kn. At least 15 cells were scored per data point…….	37
2.25	Representative images showing cellular uptake of AO/PCSAMQDs displaying different ratios of His6 in NHAC-Kn.	38
2.26	Plot showing cellular uptake of AO/PCSAMQDs displaying different ratios of His6 in HepG2. At least 15 cells were scored per data point……...	39
2.27	Representative images showing cellular uptake of AO/PCSAMQDs displaying different ratios of His6 in HepG2…..	40
2.28	Plot showing cellular uptake of AO/PCSAMQDs displaying different ratios of His6 in HT-29. At least 15 cells were scored per data point……...	41
2.29	Representative images showing cellular uptake of AO/PCSAMQDs displaying different ratios of His6 in HT-29……	42
2.30	Plot showing cellular uptake of AO/PCSAMQDs displaying different ratios of His6 in PC-3. At least 15 cells were scored per data point……	43
2.31	Representative images showing cellular uptake of AO/PCSAMQDs displaying different ratios of His6 in PC-3……...	44
2.32	Plot showing cellular uptake of AO/PCSAMQDs displaying different ratios of His6 in A549. At least 15 cells were scored per data point……...	45
2.33	Representative images showing cellular uptake of AO/PCSAMQDs displaying different ratios of His6 in A549……..	46
2.34a	Representative cell images showing intracellular distribution of QD conjugates (green) when co-incubated with different human cell lines for 2 h…….	47
2.34b	Semi-quantitative scoring of lysosomal escape in different human cell lines…….	48
2.35	Representative cell images showing dynamic intracellular escape of QD-conjugates from lysosomal sequestration and subsequent trafficking of QD conjugates when co-incubated with A549 cells for 2 h……	48
2.36	Selected frams from the real-time imaging of AO/PCSAM-QDs displaying glycopeptides and His6.	50
2.37	Cytotoxicity of ketone-functionalized glycopeptide on different human cell lines after 24 h treatment……	51
2.38	Cytotoxicity of k-His6 on different human cell lines after 24 h treatment. Each data point represents average percent viability…..	52
2.39	Cytotoxicity of AOPCSAM-QDs carrying His6 on different human cell lines after 24 h treatment…….	53
2.40	Cytotoxicity of AOPCSAM-QDs carrying glycopeptides and His6 on different human cell lines after 24 h treatment…….	53
2.41	Cartoon model of observed cellular fate of AO/PCSAM-QD with co-displayed glycopeptide and His6……..	55
3.1	Peptides and glycopeptides sequences and structures……...	72

3.2	Structure and high resolution MALDI-TOFMS of compound **1**…..	73
3.3	Structure and high resolution MALDI-TOFMS of compound **2**…..	74
3.4	Structure and high resolution MALDI-TOFMS of compound **3**…..	74
3.5	Structure and high resolution MALDI-TOFMS of compound **4**…..	75
3.6	Structure and HPLC Chromatogram of compound **1**……	76
3.7	Structure and HPLC Chromatogram of compound **2**……	76
3.8	Structure and HPLC Chromatogram of compound **3**……	77
3.9	Structure and HPLC Chromatogram of compound **4**……	77
3.10	General Protocol for the preparation of QD conjugates AO/PCSAM-QD with *k*-His_6 and compounds **1-4**……	78
3.11	Direct MALDI-TOFMS spectra of AO/PCSAM-QD carrying *k*-His_6 and compound **1**……	78
3.12	Direct MALDI-TOFMS spectra of AO/PCSAM-QD carrying *k*-His_6 and compound **2**……	79
3.13	Direct MALDI-TOFMS spectra of AO/PCSAM-QD carrying *k*-His_6 and compound **3**……	79
3.14	Direct MALDI-TOFMS spectra of AO/PCSAM-QD carrying *k*-His_6 and compound **4**……	80
3.15	Fluorescence correlation profile using FCS of AO/PCSAM-QD carrying *k*-His_6 and compound **1**……...	80
3.16	Fluorescence correlation profile using FCS of AO/PCSAM-QD carrying *k*-His_6 and compound **2**….....	81
3.17	Fluorescence correlation profile using FCS of AO/PCSAM-QD carrying *k*-His_6 and compound **3**……...	81
3.18	Fluorescence correlation profile using FCS of AO/PCSAM-QD carrying *k*-His_6 and compound **4**……...	82
3.19	Fluorescence intensity per molecule of AO/PCSAM-QDs carrying His6 and compounds **1~4**……..	83
3.20a	Representative images showing different intracellular localization pattern of QD-conjugates (green) on different human cancer cell lines……...	86
3.20b	Representative images showing different intracellular localization pattern of QD-conjugates (green) on different narmal healthy human cell lines……	87
3.21	Representative images showing controlled intracellular delivery after 2 h of co-incubation with 5 nM AO/PCSAM-QDs carrying serglycine-like peptides/glycopeptides (green) in normal human lung tissue (OUS-11) and human lung adenocarcinoma (A549)…..	88
3.22	Example images of OUS-11 cells showing the colocalization of QD conjugates with the golgi apparatus (yellow color)……	89
3.23	Example images of HT-29 cells showing the colocalization of QD conjugates with the golgi apparatus (yellow color)……...	90
3.24	Example images of NHAC-Kn cells showing the colocalization of QD conjugates with the golgi apparatus (yellow color)……	91
3.25	Example images of PC-3 cells showing the colocalization of QD conjugates with the golgi apparatus (yellow color)……...	92
3.26	Example images of A549 cells showing the colocalization of QD conjugates with the golgi apparatus (yellow color)……...	93
3.27	Example images of HepG2 cells showing the colocalization of QD conjugates with the golgi apparatus (yellow color)……...	94
3.28	Differences in golgi coloclalization of AO/PCSAMQDs displaying compound **5** and with co-displayed compounds **1**, **2**, **3** and **4** on different human cell lines……..	95

3.29	Cytotoxicity of AO/PCSAM-QDs carrying His_6 and compound **1** on different human cell lines…….	97
3.30	Cytotoxicity of AO/PCSAM-QDs carrying His_6 and compound **2** on different human cell lines…….	97
3.31	Cytotoxicity of AO/PCSAM-QDs carrying His_6 and compound **3** on different human cell lines…….	98
3.32	Cytotoxicity of AO/PCSAM-QDs carrying His_6 and compound **4** on different human cell lines…….	98
3.33	Cytotoxicity of tetrapeptide **1** on different human cell lines……	99
3.34	Cytotoxicity of glycopeptide **2** on different human cell lines……...	99
3.35	Cytotoxicity of tetracosapeptide **3** on different human cell lines…..	100
3.36	Cytotoxicity of glycopeptide **4** on different human cell lines……...	100

Chapter 1

General Introduction

1.1 General Introduction

Nanotechnology involves the engineering of functional systems at the molecular scale. These systems are attractive for disciplines ranging from material science to biomedicine as they are characterized by unique physical, optical and electronic features. One of the most active research areas of nanotechnology is nanomedicine, which applies nanotechnology to highly specific medical interventions for the prevention, diagnosis and treatment of disease[1,2] The overwhelming researches in nanomedicine were translated into commercialization during the past few decades, with many products on the market and a growing number in the pipeline. Nanomedicine is currently dominated by drug delivery systems[3] utilizing nanoparticles (NPs) as a drug carrier. These NPs include dendrimers, liposomes, carbon tubes, buckyballs, quantum dots (QDs),[4,5] gold, silver,[6] and supermagnetic NPs.[7]

Many Nanoparticle drug delivery (NDD) platforms have been developed over the past decades. These platforms have emerged as a promising approach to enhance the efficacy of the existing drugs as well as those new classes of potent therapeutic agents based on the characteristic properties and functions of nanocarriers. These NDD vehicles have great advantages due to their ability to encapsulate poorly soluble cancer therapeutics, as well as their large surface areas for unique potential multi-functionality through attachment of multiple diagnostic and therapeutic agents such as bioactive molecules (drugs), affinity ligands, and imaging probes within a single nanoparticle-platform to achieve molecular targeted and traceable drug delivery to diseased sites.[8] The use of NDD vehicle as nanocarriers for chemotherapeutic agents has been shown to improve drug pharmacological properties by altering its pharmacokinetics and biodistribution. Through enhanced permeability and retention (EPR) effect, nanoparticles preferentially accumulate in faulty tumor vasculatures allowing nanoparticle-based chemotherapeutics to achieve higher intratumoral drug concentration and lower normal tissue concentration,[9] unlike the conventional chemotherapeutics that distribute throughout the body affecting both normal and cancer cells.[10]

The NDD vehicles have been vastly developed through introduction and utilization of lipids, polymers, carbon materials, inorganic nanocrystals, and even hybrid combinations of those materials that aimed towards improving pharmacologic properties of existing therapeutics, as well as enabling delivery of new classes of potent anti-cancer drugs for gene therapy and immunotherapy.[8,11]

However, challenges to achieve the optimal benefit of NDD have to be addressed and resolved for a successful drug delivery.[12,13] The early design of NDD vehicles was governed by the intrinsically poor pharmacokinetic properties of conventional chemotherapeutics. Low drug solubility, rapid metabolism and clearance, and most importantly a lack of selectivity regularly lead to therapeutic failure by causing severe systemic toxicity in healthy tissues, thus prohibiting the dose escalation necessary to eliminate tumor cells.[14] Prime pre-requisite to a successful NDD is the ability to mediate the facile and efficient delivery of the nanoparticles to the cell to ultimately deliver various drugs towards the target intracellular space and various specific subcellular compartments of mammalian cells.[15,16] The traceability of the delivered drug is also an important aspect in monitoring the biodistribution, intracellular trafficking, and long-term fate of drugs and NP drug delivery vehicles in order to assess and characterize the pharmacokinetic properties as well as the targeting specificity of the delivered drug.

Successful development of specific and potent NDD vehicles for a variety of therapeutics also heavily relies upon elucidating design guidelines for nanocarrier engineering, which, in turn, requires an in-depth understanding of NP behavior in complex biological systems, especially in vivo.[17,18] In light of this, tracking the biodistribution, intracellular trafficking, and long-term fate of drugs and NP-drug delivery vehicles represents a particularly valuable tool for pharmacokinetics characterization.

A number of contrast agents have been developed to facilitate detection of nanocarriers with magnetic resonance imaging (MRI), positron emission tomography (PET), ultrasound imaging, and optical imaging at varying levels of sensitivity and resolution.[7] Earlier studies have already demonstrated the critical impact of NP physical properties (e.g. size and shape) and surface chemistry (e.g. hydrophobicity, charge, density and orientation of surface ligands, distribution of ligands with formation of patches, etc.) on nanocarrier biodistribution, drug delivery and release pathway, and interactions with different components of biological systems (e.g. defining the degree of toxicity and immunogenicity), and fine-tuning many parameters simultaneously remains a big challenge. Improvement in this work direction ultimately requires a systematic, comprehensive characterization of nanocarrier behavior at levels ranging from intracellular uptake and trafficking to whole-body biodistribution and clearance. Thus, a cost-effective NP platform for reliable and comparable evaluation of various nanocarrier designs at all stages of NP-based drug delivery is essential.

Quantum dots (QDs) are one of the most attractive candidates likely to be a good platform for NDD. Most NDD vehicles intrinsically have no capacity for monitoring drug delivery and only relied on either co-attachment or co-encapsulation of a fluorophore as an imaging probe. The weak fluorescent signal of conventional organic fluorophore against strong cellular autofluorescence background, fast photobleaching rates, and metabolic degradation have rendered their utility limited for long term imaging and tracking applications. QDs are engineered NPs that structurally possess a metalloid crystalline core, which emit a type of fluorescence depending on its composition and size that, unlike the conventional organic fluorophore, have broad absorption, long term photostability, and resistance to photobleaching.

QDs have shown great promise with potential for many biological and biomedical applications, especially in drug delivery and cellular imaging.[19] It offers great potential as an ideal model system for facilitating systematic monitoring and evaluation of all stages of NDD

with high sensitivity and resolution due to its unique intrinsic photophysical characteristics. The use of QDs as NDD platform gives more advantage for it doesn't need attachment of an imaging probe onto the NP's surface to monitor every stage of NDD, thus, NP's surface area could be utilized more efficiently for attaching more bioactive molecules and affinity ligands for effective delivery.

In order to increase the functionality and water solubility of QDs for its ability to enter cell membranes and unhampered its intracellular and molecular imaging uses,[20] surface modifications and functionalization could be introduced.[21] These modifications in effect increase its cellular uptake, specificity, and efficiency.[22]

In achieving targeted delivery, NDD platforms utilize complementary molecules to the target cells or organelles for a very specific delivery. These complementary molecules range from small molecules, such as small bioactive molecules, DNA fragments,[23] peptides[24] and glycopeptides, and carbohydrates[25] to larger molecules including proteins, glycoproteins, and antibodies.[26] Peptides and glycopeptides are now becoming attractive bioactive molecules and mediator for NDD.[27] They are incorporated in NDD system as an antigens,[28] localization signals,[27,29] and cell penetrating peptides.[30,31] In this study, peptides and glycopeptides were utilized in establishing a high performance cell surface mimetic nanoparticle platform model system for nanoparticle-based drug delivery (NDD).

1.2 References

1. Lobatto, M.; Fuster, V.; Fayad, Z.; Mulder, W. *Nat. Rev. Drug Discov.* **2011**, 10(11), 835-852.
2. Riehemann, K.; Schneider, S.W.; Luger, T.A.; Godin, B.; Ferrari, M.; Fuchs, H. *Angew. Chem. Int. Ed. Engl.***2009**, 48(5), 872-897.
3. Wagner, V.; Dullaart, A.; Bock, A.; Zweck, A. *Nat. Biotechnol.* **2006**, 24(10), 1211-1217.
4. Iga, A.M.; Robertson, J.H.; Winslet, M.C.; Seifalian, A.M. *J Biomed Biotechnol,* **2007**, 76087.
5. Jamieson, T.; Bakhshi, R.; Petrova, D.; Pocock, R.; Imani, M.; Seifalian, A.M. *Biomaterials*, **2007**, 28, 4717–4732.
6. Chaloupka, K.; Malam, Y.; Seifalian, A.M. *Trends in Biotechnology,* **2010**, 28(11), 580-588.
7. Riyahi-Alam, N.; Behrouzkia, Z.; Seifalian, A.; Haghgoo Jahromi, S. *Biol Trace Elem Res.* **2010**, 137:324–334.
8. Wang, A. Z.; Langer, R.; Farokhzad, O. C. *Annu. Rev. Med.* **2012**, 63:185-198.
9. Jain, R. K.; Stylianopoulos, T. *Nat. Rev.* **2010**, 7:653-664.
10. Matsumura, Y.; Maeda, H. *Cancer Res.* **1986**, 46:6387-6392.
11. Jin, Y.; Xiaohu Gao, X. *Nat. Nanotechnol.***2009**, 4 (9) 571-576.
12. Derfus, A. M.; Chan, W. C.; Bhatia, S. N. *Adv. Mater.* **2004**, 16, 961-966.
13. Chen, F.; Gerion, D. *Nano lett.* **2004**, 4, 1827-1832.
14. Probst, C. E.; Zrazhevskiy, P.; Bagalkot, V.; Gao, X. *Advanced Drug Delivery Reviews* **2013**, 65, 703–718.
15. Rajendran, L.; Knölker, H.J.; Simons, K. *Nat. Rev. Drug Discov.* **2010**, 9, 29-42.

16. Delehanty, J. B.; Bradburne, C. E.; Boeneman, K.; Susumu, K.; Farrell, D.; Mei, B. C.; Blanco-Canosa, J. B.; Dawson, G.; Dawson, P. E.; Mattoussi, H.; Medintz, I. L. *Integr. Biol.* **2010**, 2, 265-277.
17. Delehanty, J.B., et al., *Expert Opin. Drug Deliv.* **2009**, 6 (10) 1091–1112.
18. Qi, L.; Gao, X.H. *Expert Opin. Drug Deliv.* **2008**, 5 (3) 263–267.
19. Ghaderi, S.; Ramesh, B.; Seifalian, A. M. *Journal of Drug Targeting*, **2011**, 19(7):475-486.
20. (a) Chen, X.; Kis, A.; Zettl, A.; Bertozzi, C. R. *Proc. Natl. Acad. Sci. U.S.A.* **2007**, *104*, 8218–8222. (b) Michalet, X.; Pinaud, F. F.; Bentolila, L. A.; Tsay, J. M.; Doose, S.; Li, J. J.; Sundaresan, G.; Wu, A. M.; Gambhir, S. S.; Weiss, S. *Science* **2005**, 307 (5709): 538-544. (c) Delehanty, J. B.; Mattoussi, H,; Medintz, I. L. *Anal. Bioanal. Chem.* **2009**, 393 (4): 1091-1105.
21. (a) Xue, F. L.; Chen, J. Y.; Guo, J.; Wang, C. C.; Yang, W. L.; Wang, P. N.; Lu, D. R. *J. Fluoresc.* **2007**, 17(2):149-154. (b) Koshman, Y. E.; Waters, S. B.; Walker, L. A.; Los, T.; de Tombe, P.; Goldspink, P. H.; Russell, B. *J. Mol. Cell Cardiol.* **2008**, 45, 853-856.
22. Smith, A.; Duan, H.; Mohs A.; Nie, S. *Adv. Drug Delivery Rev*. **2008**, 60, 1226–1240.
23. Gill, R.; Willner, I.; Shweky, I.; Banin, U. *J. Phys. Chem. B* **2005**, 109, 23715–23719.
24. Han, H.-S.; Devaraj, N. K.; Lee, J.; Hilderbrand, S. A.; Weissleder, R.; Bawendi, M. G. *J. Am. Chem. Soc*. **2010**, 132, 7838–7839.
25. (a) De la Fuente, J. M.; Penades, S. *Tetrahedron Asymm*. **2005**, 16, 387–391. (b) Robinson, A.; Fang, J. M.; Chou, P. T.; Liao, K. W.; Chu., R. M.; Lee., S. *J. ChemBioChem.* **2005**, 6, 1899–1905. (c) Ohyanagi, T.; Nagahori, N.; Shimawaki, K.; Hinou, H.; Yamashita, T.; Sasaki, A.; Jin, T.; Iwanaga, T.; Kinjo, M.; Nishimura, S-I. *J. Am. Chem. Soc*. **2011**, 133, 12507–12517.
26. Zhu, L., Kate, P. & Torchilin, V. P. *ACS Nano* **2012,** 6, 3491–3498.

27. Delehanty, J.B.; Bradburne, C.E.; Boeneman, K.; Susumu, K.; Farrell, D.; Mei, B. C.; Blanco-Canosa, J.B.; Dawson, G.; Dawson, P. E.; Mattoussi, H.; Medintz, I. L. *Integr. Biol*. **2010**, 2, 265-277.

28. Raymond P. Briñas, R. P.; Sundgren, A.; Sahoo, P.; Morey, S.; Rittenhouse-Olson, K.; Greg E. Wilding, G. E.; Deng, W.; Barchi Jr, J. J. *Bioconjugate Chem.* **2012**, 23, 1513−1523.

29. Chen, F.; Gerion, D. *Nano. Lett.* **2004**, 4 (10), 1827-1832.

30. Michalet, X.; Pinaud, F. F.; Bentolila, L. A.; Tsay, J. M.; Doose, S.; Li, J. J.; Sundaresan, G.; Wu, A. M.; Gambhir, S. S.; Weiss, S. *Science* **2005**, 307 (5709): 538-544.

31. Chen, B.; Liu, Q.; Zhang, Y.; Xu, L.; Fang, X. *Langmuir* **2008**, 24, 11866-11871

Chapter 2

Hexahistidine-Mediated Endolysosomal Escape of Cell Surface Mimetic Quantum Dots-Anchored Glycopeptide

2.1 Introduction

Cellular bio-molecular tracking enables observing real-time bio-molecular dynamism in living cells. This technique can provide great insights on molecular trafficking, translocation and interaction with complementary molecules in response to environmental cues.[1] Fluorescent organic molecules and fluorophores are frequently used in bio-molecular tracking due to their significant smaller size, which can make them easily tag biomolecules and traverse cell membrane more likely unhindered. However, their weak fluorescent signal against strong cellular autofluorescence background, fast photobleaching rates, and metabolic degradation, which are of great concern in this field, have rendered their utility limited for long term imaging of biological processes.[2] To solve these problems, researchers have turned their attention to quantum dots (QDs) as substitute for organic fluorophores. QDs are nanometer-sized inorganic semiconductor crystalline cluster of a few hundred to a few thousand of atoms. Fluorescence emission wavelength of QD can be fine-tuned by controlling QD size and its chemical composition.[3]

Multicoloured QDs have the ability to be simultaneously excited using single light source due to their tuneable, narrow, and symmetric emission peaks with broad excitation profiles and minimal spectral overlap. This intrinsic and prolonged fluorescence of QDs advantageously surpasses the sensitivity and resolution of organic dyes and fluorescent proteins, with higher photostability and resistance to photobleaching as well as chemical degradation, which gave them flexible applications in a number of research areas.[4] Aside from cellular imaging and drug delivery, QDs have also been used in tracing infection, viral localization[5] and in single molecule tracking.[6]

In order to increase the functionality and water solubility of QDs, to increase its ability to enter cell membranes and unhampered its intracellular and molecular imaging

uses,[7] surface modification and functionalization have been introduced[8] using various antibodies, DNA,[9] proteins,[10] peptides,[11] and carbohydrates.[12] These modifications in effect increase its cellular uptake, specificity, and efficiency.[13] However, the cytoplasmic delivery of QDs follows either facilitated or non-facilitated delivery to the cytoplasm, in which both mechanisms utilized the typical endocytic pathway that usually results to encapsulation of QDs within the endolysosomal vesicles.[14] Endolysosomal sequestration represents another obstacle for drug delivery with nanoparticle-based vehicles. Sequestration of nanoparticles within the endosome and its subsequent degradation in lysosome can significantly reduce or completely prevent the delivery of active drugs or therapeutic agents to intracellular space making endosomal escape mechanism an integral and substantial constituent in nanoparticle-based drug delivery and tracking.[15]

In the past years, studies to solve trans-membrane delivery and lysosomal sequestration have also been conducted venturing on the use of cell penetrating peptides (CPPs)[7b,16] to facilitate QDs intracellular delivery and endolysosomal escape. CPPs are a group of short amphipathic, hydrophobic or cationic peptide that has the ability to penetrate cell membrane. They have been considered as candidates for mediating intracellular drug delivery[17] and are able to deliver macromolecules into cells of various species,[18] although internalization mechanisms used by QD conjugated CPPs are still not completely understood. Consideration on the type of molecules used for surface modification, particle size, charge, and cell type must also be taken into account since they influence the routes of entry and intracellular transport, which in effect will influence the destination and biological efficacy of the intracellularly delivered load or therapeutic agents.[19]

The poly-histidine sequence, a positive charge polypeptide, is being used as affinity tags ("His Tags"), especially hexa-histidine (His_6), to facilitate protein

purification[20] and as pH-sensitive moiety tag for a specific cargo/protein to be delivered inside the cell upon encountering pH drops inside intracellular space.[21] It is reportedly used during transfection, together with arginine, after encapsulating plasmid DNA (pDNA) using chitosan and formation of a nanoparticle based on the electrostatic interaction between the negative charged pDNA and the positive charge chitosan backbone.[22] Arginine was used to mediate nanoparticle internalization while histidine was used as pH-responsive moieties that enhance buffering capacity in the pH range of lysosome.[23-24] Poly-histidine sequences were also reportedly used to append longer CPP type sequences, either they are attached and buried or displayed in the QDs surface, such as those in Palm-1, NLS and CPP histidine-tagged peptides.[14b] However, these CPPs have longer peptide sequences and concentration-dependent cytotoxicities,[25] thus posed a great threat and unsuitability in terms of longer time cellular imaging for small bio-molecules such as short-chain peptides, glycopeptides and carbohydrates in intracellular delivery.

The presence of these huge and long sequence CPPs, in QD-based intracellular delivery and tracking of small molecules, may affect and influence the recognition of these small molecules and could prevent them from reaching and localizing into the exact cellular compartment where they supposed to localize. Therefore, developing an efficient, robust, non-cytotoxic, short, and facile CPP sequence, that could facilitate faster endolysosomal escape of QDs in a wide variety of cells, is indispensable.

Unlike poly-ariginine, the use of the homopolymer of histidine as an endolysosomal escape molecule has not been deeply ventured in QD- and nanoparticle-based intracellular delivery. In this study the ability of short chain ketone-functionalized hexahistidine (*k*-His_6) and ketone-functionalized hexaarginine (*k*-Arg_6) in mediating endolysosomal escape of QDs displaying glycopeptide on its surface were examined and compared. QDs were first surface-modified by self-assembled monolayers (SAMs) of

11,11'-dithio bis[undec-11-yl 12-(aminooxyacetyl)amino hexa(ethyleneglycol)] (AOSH) linker[12c,25] and 11-mercaptoundecylphosphorylcholine (PCSH) ligand[12c,26] to generate aminooxy/phosphorylcholine self-assembled monolayer-coated QDs (AO/PCSAM-QDs). AOSH contains the aminooxy group to which the ketone-functionalized peptides and glycopeptide can be easily attached. PCSH on the other hand, provided QDs with non-fouling surface characteristics to prevent non specific protein adsorption during intracellular delivery and allows spatial control between peptides and glycopeptide on QD's surface.[12c] The glycopeptide sequence used in this study was a hexamer serglycin-like synthetic peptide[27,28] ketone-functionalized by appending 5-oxohexanoic acid. The monomer of this seglycin-like peptide is a tetrapeptide composed of Ser^1-Gly^2-Ser^3-Gly^4 with Galβ(1-4)Xylβ1-, where the sugar moiety was attached to the third amino acid Ser^3. Ketone-functionalization was done on both peptides and glycopeptide N-termini, while the C-termini were blocked with an amide group after coupling of the last amino acid residue.

2.2 Results and Discussion

The peptides and the serglycine-like glycopeptide (Figure 2.1) were easily synthesized manually, following Solid-Phase Peptide Synthesis (SPPS)[24] method (Schemes 2.1a & 2.1b). They were all characterized using high resolution MALDI-TOFMS and RP-HPLC (Figure 2.2-2.4). The attachment of 5-oxohexanoic acid on the *N*-terminal made it easier to attach them to the aminooxy-functionalized molecule AOSH, through oxime bond formation.[20]

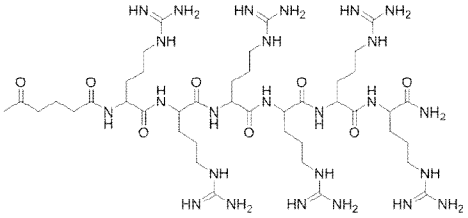

***k*-Arg$_6$**

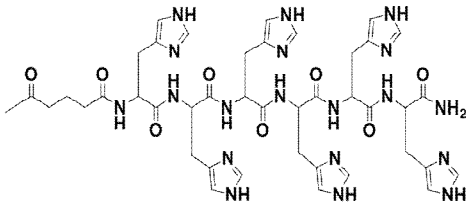

***k*-His$_6$**

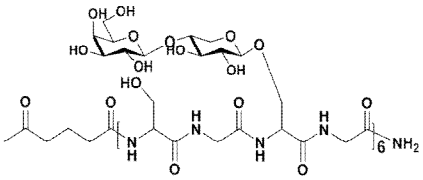

ketone-functionalized glycopeptide

Figure 2.1. Peptides and glycopeptide structures.

This concept of displaying peptides and glycopeptide on QD's surface was taken from the chemoselective ligation of compounds bearing aldehyde/ketone group by the use of amonooxy-functionalized materials like in the glycoblotting process.[25]

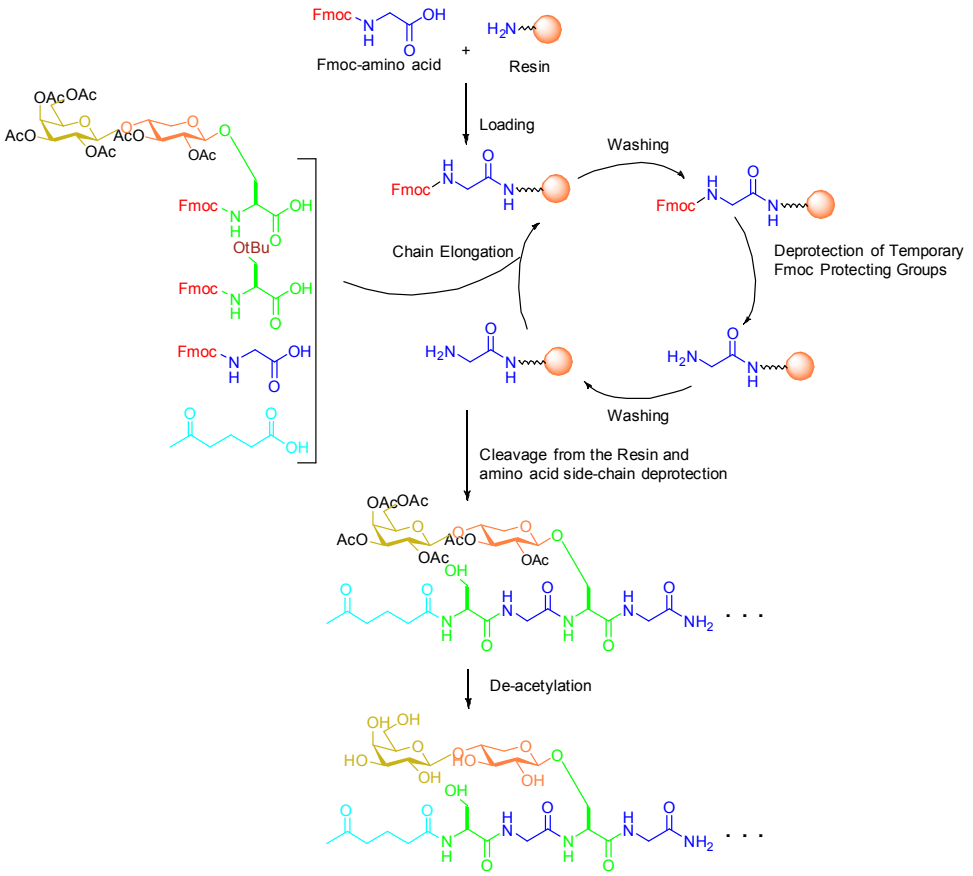

Scheme 2.1a. Diagram for SPPS of ketone-functionalized glycopeptide.

Table 2.1. High resolution masses of peptides and glycopeptide taken using MALDI-TOFMS.

Compound	Calculated *m/z*	Measured *m/z*	Δ *m/z*	Abundant ion	Error (ppm)
k-Arg$_6$	1066.694	1066.695	0.00096	$[M+H]^+$	0.899977
k-His$_6$	952.4405	952.4401	-0.00035	$[M+H]^+$	0.367477
glycopeptide	3645.281	3645.275	-0.00615	$[M+Na]^+$	1.686838

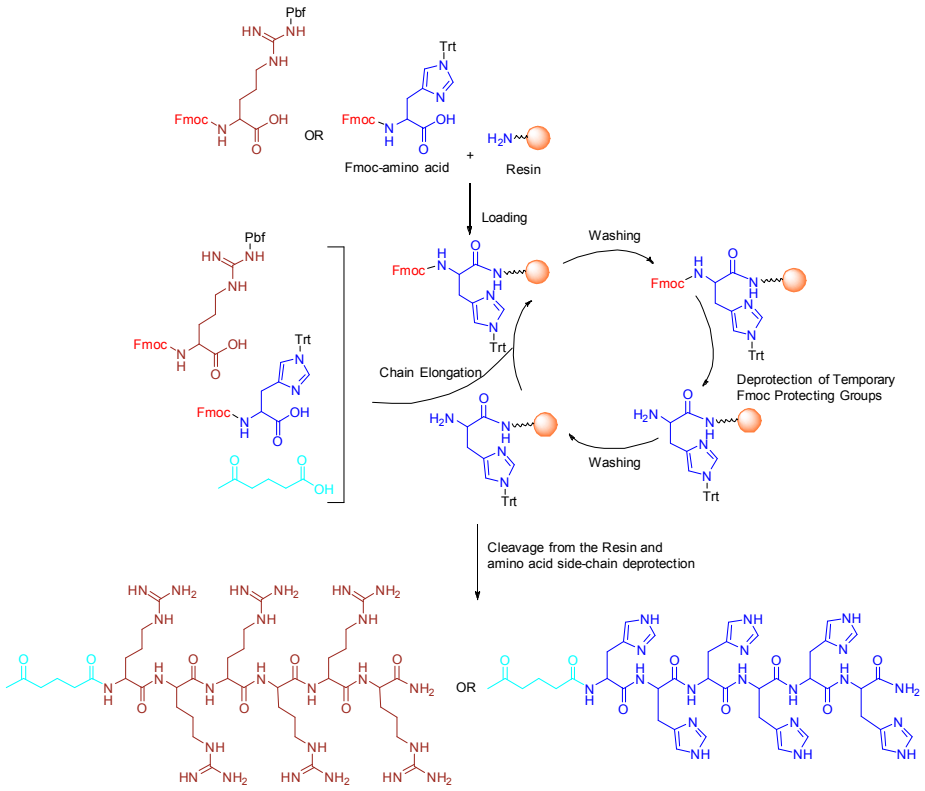

Scheme 2.1b. Diagram for SPPS of *k*-His_6 and *k*-Arg_6.

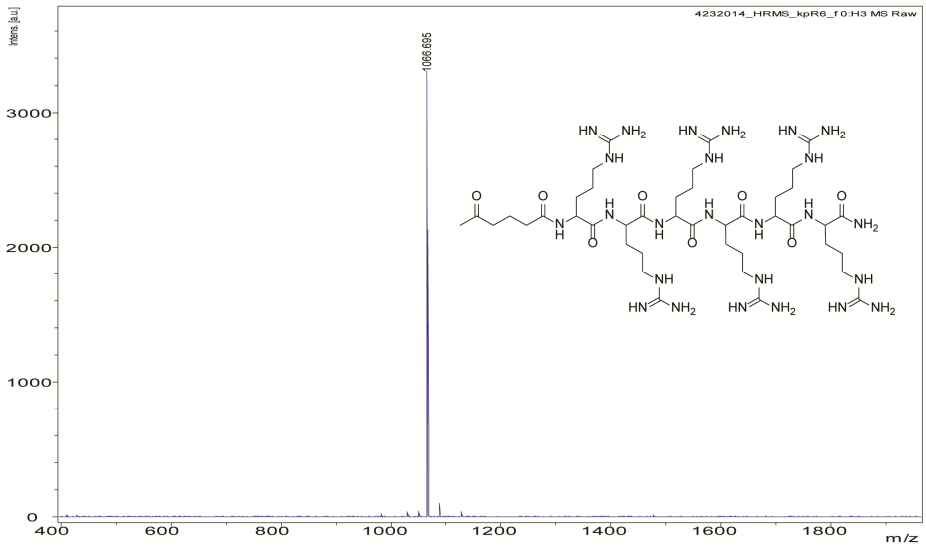

Figure 2.2a. Structure and high resolution mass spectrum of *k*-Arg_6.

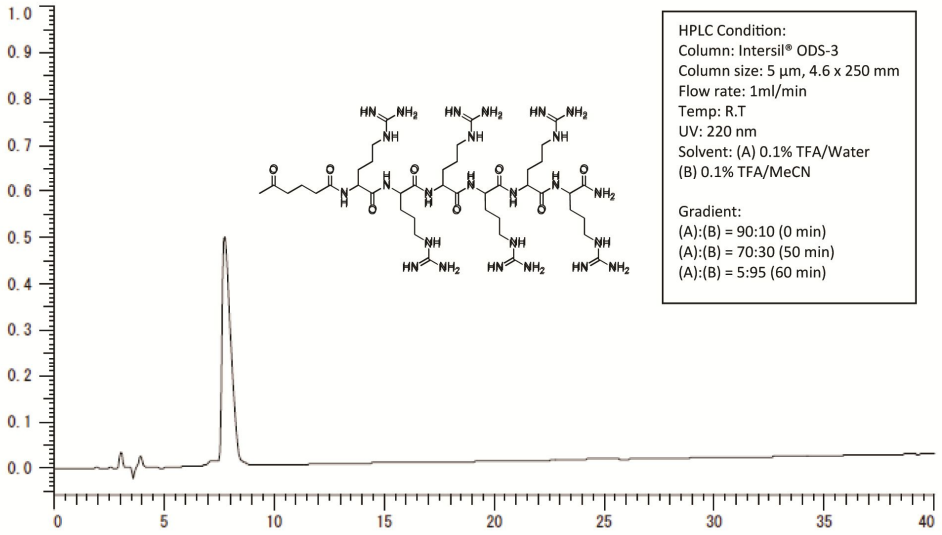

Figure 2.2b. Structure and RP-HPLC chromatogram of *k*-Arg$_6$.

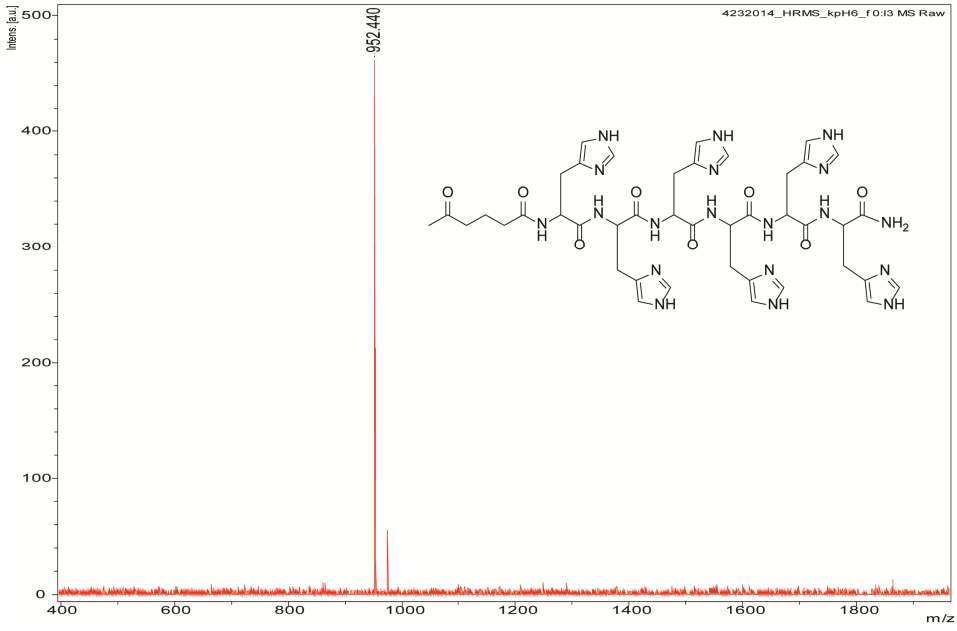

Figure 2.3a. Structure and high resolution mass spectrum of *k*-His$_6$.

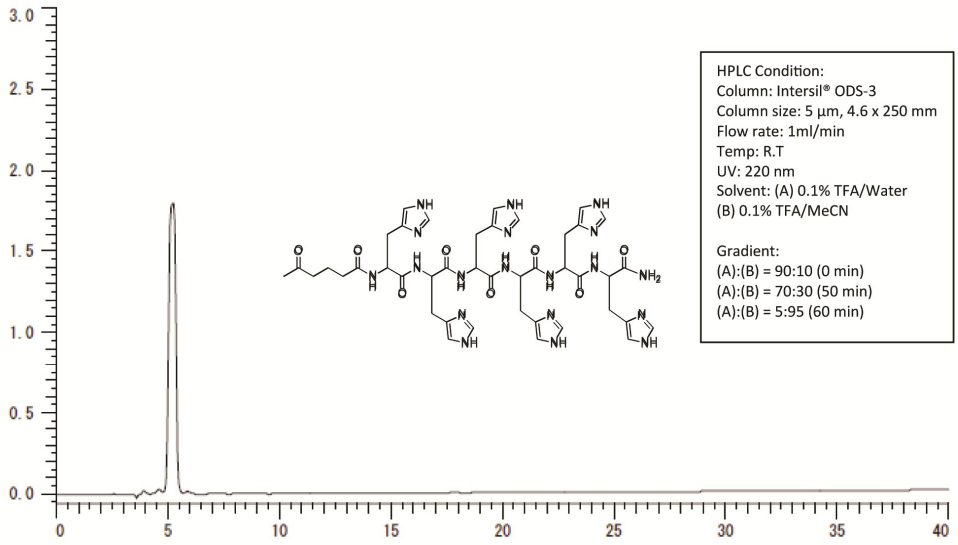

Figure 2.3b. Structure and RP-HPLC chromatogram of *k*-His_6.

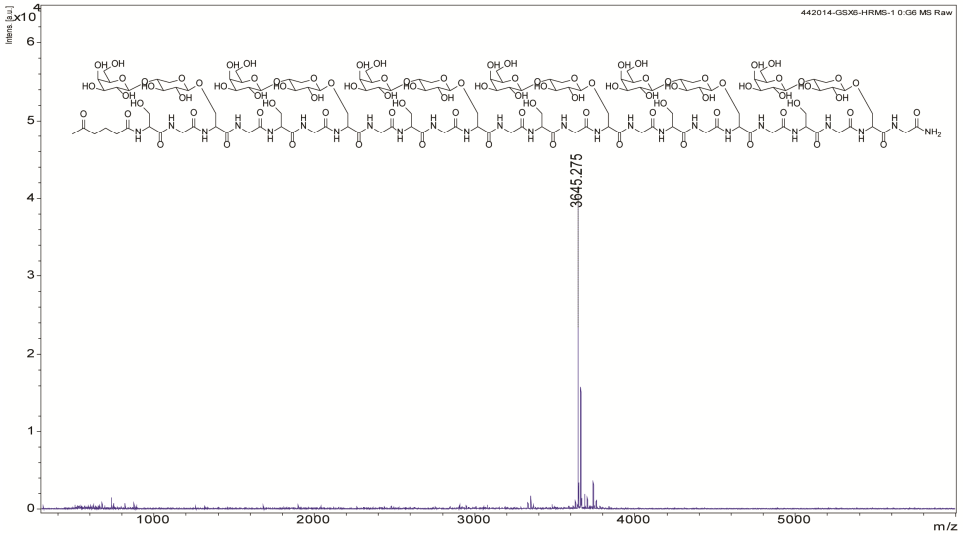

Figure 2.4a. Structure and high resolution mass spectrum of ketone-functionalized glycopeptide.

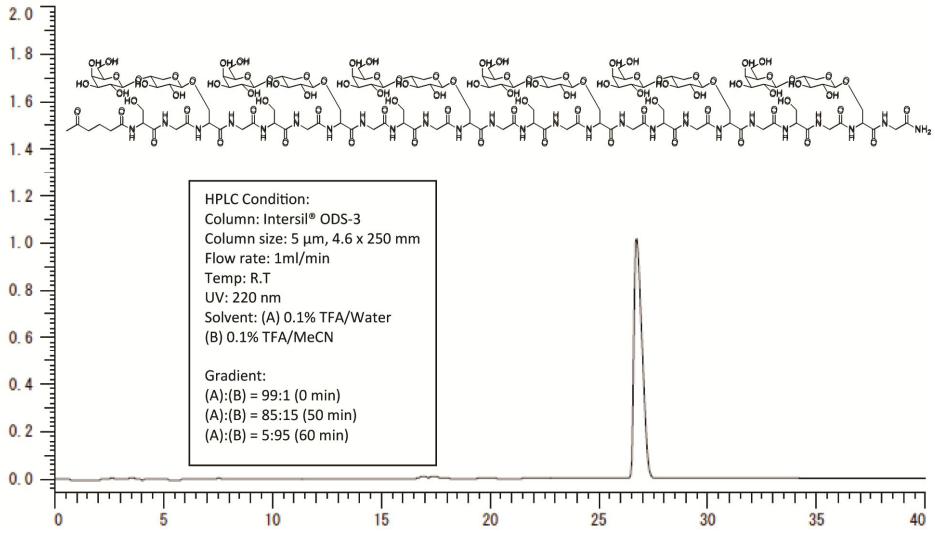

Figure 2.4b. Structure and RP-HPLC chromatogram of ketone-functionalized glycopeptide.

Preparation of AO/PCSAM-QDs

In order to solubilise the synthetic commercially available TOPO-coated QDs (CdSe/ZnS, λ_{em} = 545 nm) in water, QD surface was modified by AOSH and PCSH[12c,21,22] (Figure 2.5a). The surface modification, using thiol tethered SAMs, was directly confirmed by MALDI-TOFMS.

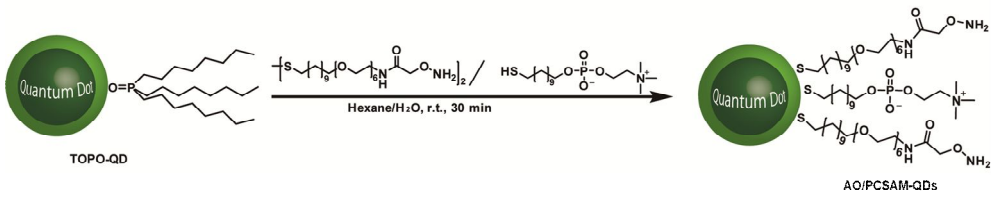

Figure 2.5. General protocol for preparation of AO/PCSAM-QDs.

The MALDI-TOFMS spectrum of AO/PCSAM-QDs showed 908 *m/z* indicated the presence of a heterodimer of AOS-SPC connected via disulfide linkage, while the 737

m/z indicated the homodimer of PCS-SPC also connected via disulfide linkage (Figure 2.6).

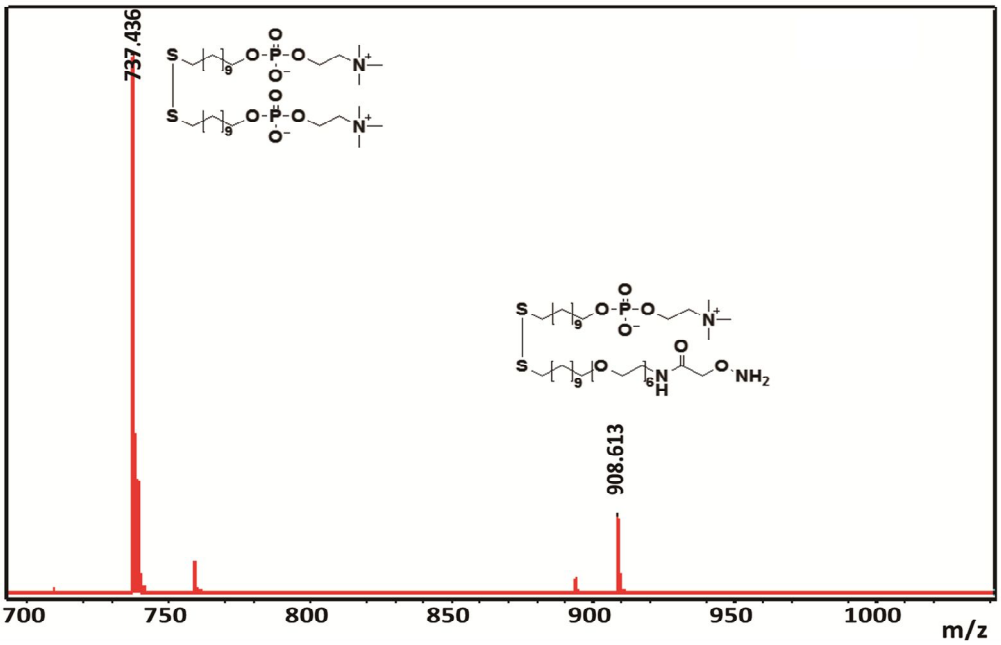

Figure 2.6. Direct MALDI-TOFMS of AO/PCSAM-QDs.

This modification yielded an appropriate molecular packing of SAMs in the surface of QDs making it remarkably soluble with excellent dispersion in water,[20] as confirmed by fluorescence correlation spectroscopy (FCS) analysis, showing a smooth curve of its rapid fluorescence fluctuations (Figure 2.7). Since the number of AOSH is directly proportional to the amount of displayed CPPs and ketone-functionalized glycopeptide, it is imperative to control the ratio of AOSH from PCSH in order to control the number of compounds to be displayed on the QD surface.

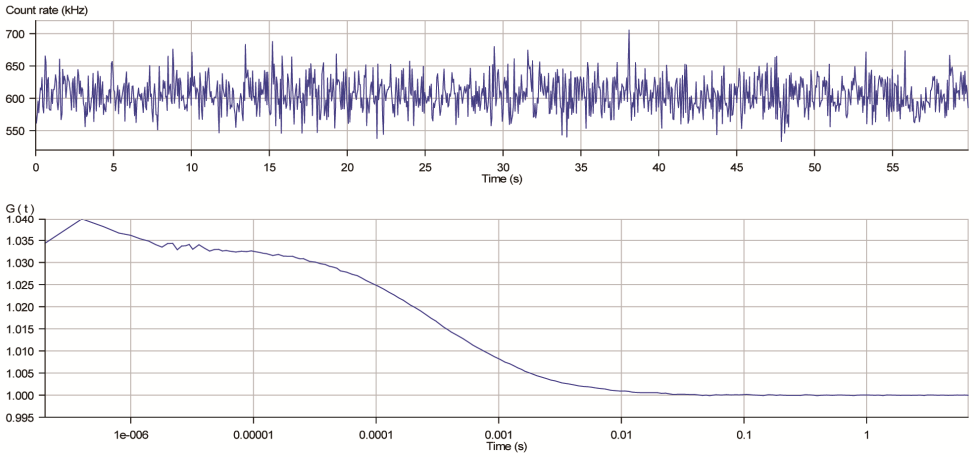

Figure 2.7. Fluorescence fluctuation profile of AO/PCSAM-QDs measured by Fluorescence Correlation Spectroscopy.

Preparation and Characterization of QD conjugates

After successful surface modification of QDs, *k*-His_6, *k*-Arg_6, and the ketone-functionalized glycopeptide (with or without *k*-His_6 and *k*-Arg_6) were conjugated on QD's surface between the amino-oxy groups of AOSH and the ketone group blocking the *N*-termini of CPPs and the glycopeptide (Figure 2.8). The reaction in an acetic acid buffer at room temperature afforded AO/PCSAM-QDs carrying His_6, AO/PCSAM-QDs carrying Arg_6, AO/PCSAM-QDs carrying the glycopeptide, and AO/PCSAM-QDs carrying His_6 and glycopeptide as confirmed by direct MALDI-TOF/MS (Figures 2.9-2.12). The density of the displayed samples can affect the dispersion of the modified QDs in water and even in the serum-containing cell culture medium during cellular delivery. It was frequently observed that higher density of surface-displayed CPPs and glycopeptide usually resulted to QDs aggregation, which could certainly affect the internalization and dispersion of the QDs.[26] The good ratio between AOSH and PCSH was found to be 1:20, with good water dispersion and no observed significant aggregation.

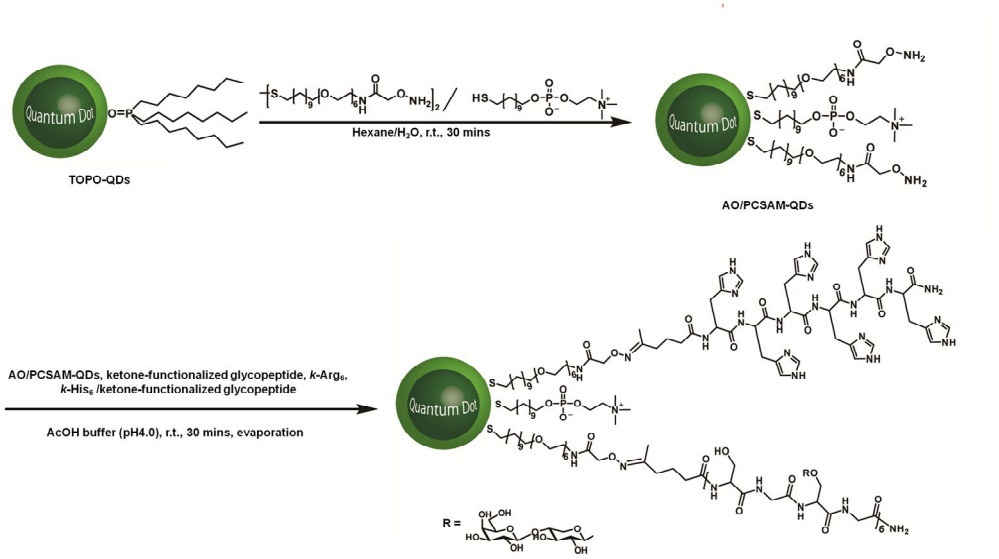

Figure 2.8. General protocol for preparation of QD conjugates.

This strategy is so robust that any aldehyde- or ketone-functionalized molecule could be attached to AOSH via this type of bond formation, which in principle, could be used as general strategy for facile QD surface modification using an array of desired molecules to be displayed on QD surface.

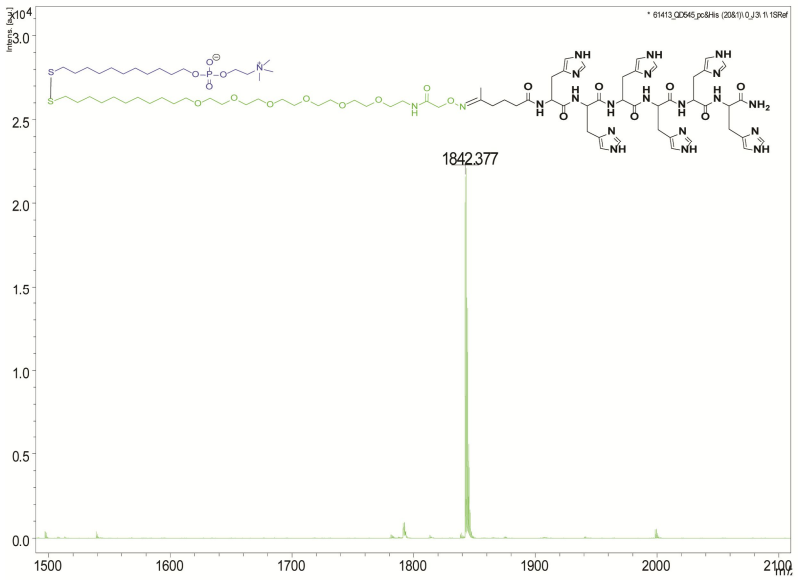

Figure 2.9. MALDI-TOF/MS Spectrum of AO/PCSAM-QD carrying His_6. Calculated mass [M]: 1840.961Da. Observed mass $[M+H]^+$: 1842.377 Da.

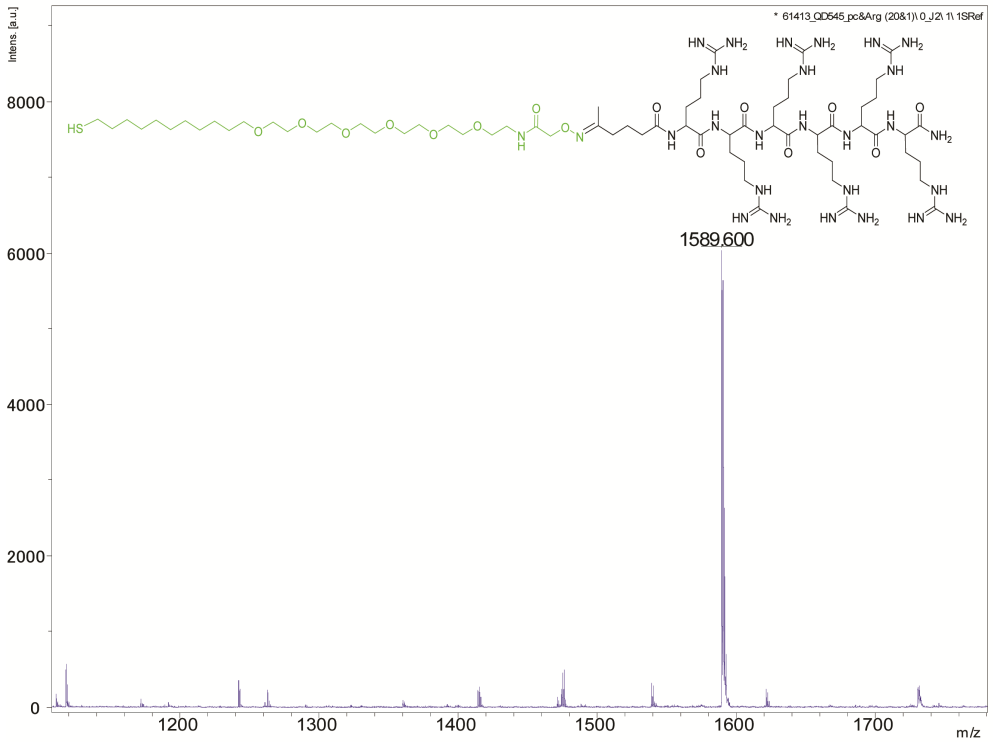

Figure 2.10. MALDI-TOF/MS Spectrum of AO/PCSAM-QD carrying Arg_6. Calculated mass [M]: 1588.020Da. Observed mass $[M+H]^+$: 1589.600 Da.

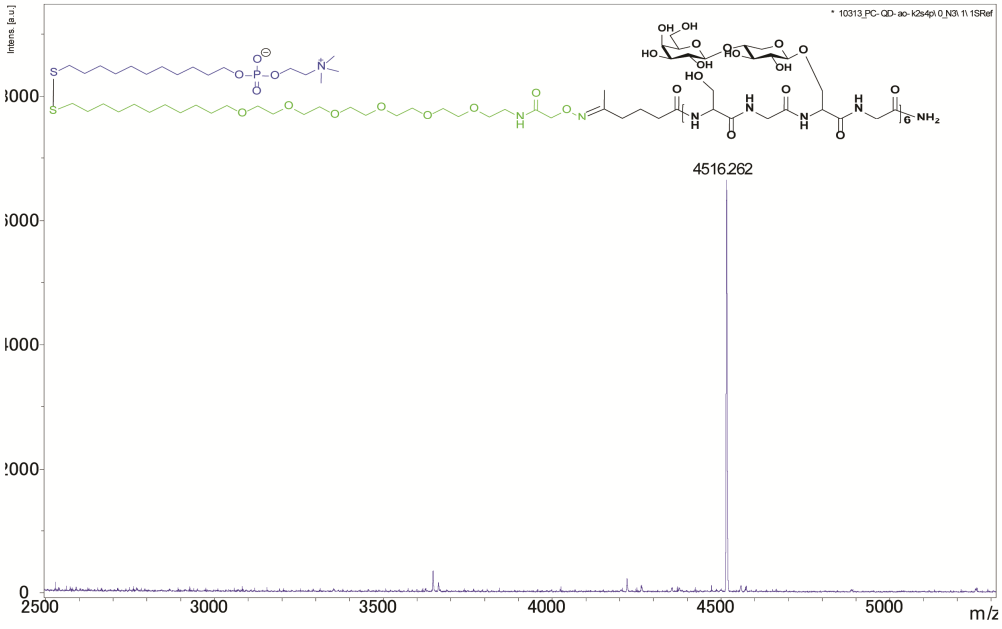

Figure 2.11. MALDI-TOF/MS Spectrum of AO/PCSAM-QD carrying glycopeptide. Calculated $[M+Na]^+$: 4514.48 Da. Observed mass: 4516.26 Da.

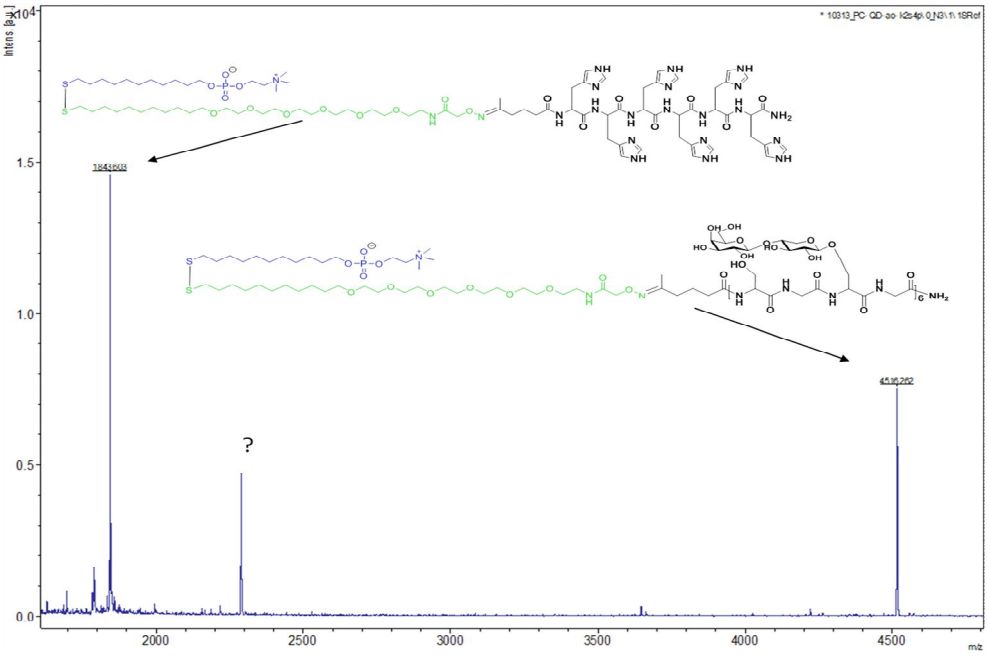

Figure 2.12. MALDI-TOF/MS Spectrum of AO/PCSAM-QD carrying His_6 and glycopeptide.

The conjugation resulted in the formation of highly dispersed QD conjugates (Figures 2.13-2.15) most likely similar in character to the AO/PCSAM-QD.

The QD conjugates' rapid fluorescence fluctuation shown as a smooth diffusion curve suggested that QD conjugates are well dispersed in water. After the coupling process, the resulting AO/PCSAM-QD carrying His_6 and glycopeptide showed no significant change in fluorescence intensity emitted per molecule of QD with respect to AO/PCSAM-QD suggesting stability of fluorescence intensity even after the conjugation process (Figure 2.16).

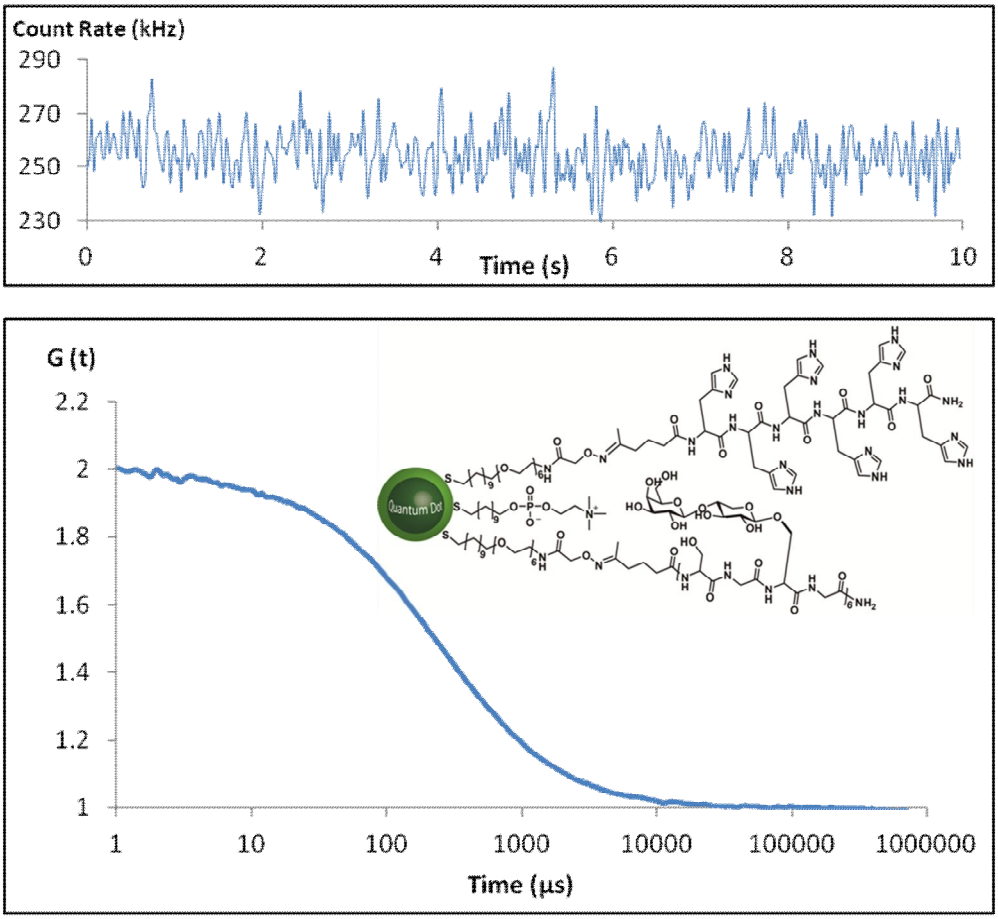

Figure 2.13. Cartoon structure representation and Fluorescence fluctuation profile of AO/PCSAM-QD carrying His_6 and glycopeptide measured by Fluorescence Correlation Spectroscopy.

Cellular Uptake and Lysosomal sequestration of QD conjugate

The cellular uptake of AO/PCSAM-QDs simply conjugated with glycopeptide was examined using normal human articular chondrocytes (NHAC-Kn), human lung adenocarcinoma (A549), human prostate adenocarcinoma (PC-3), human hepatoma(HepG2), human epithelial colon cancer cells (HT-29), and human normal lung tissue (OUS-11).

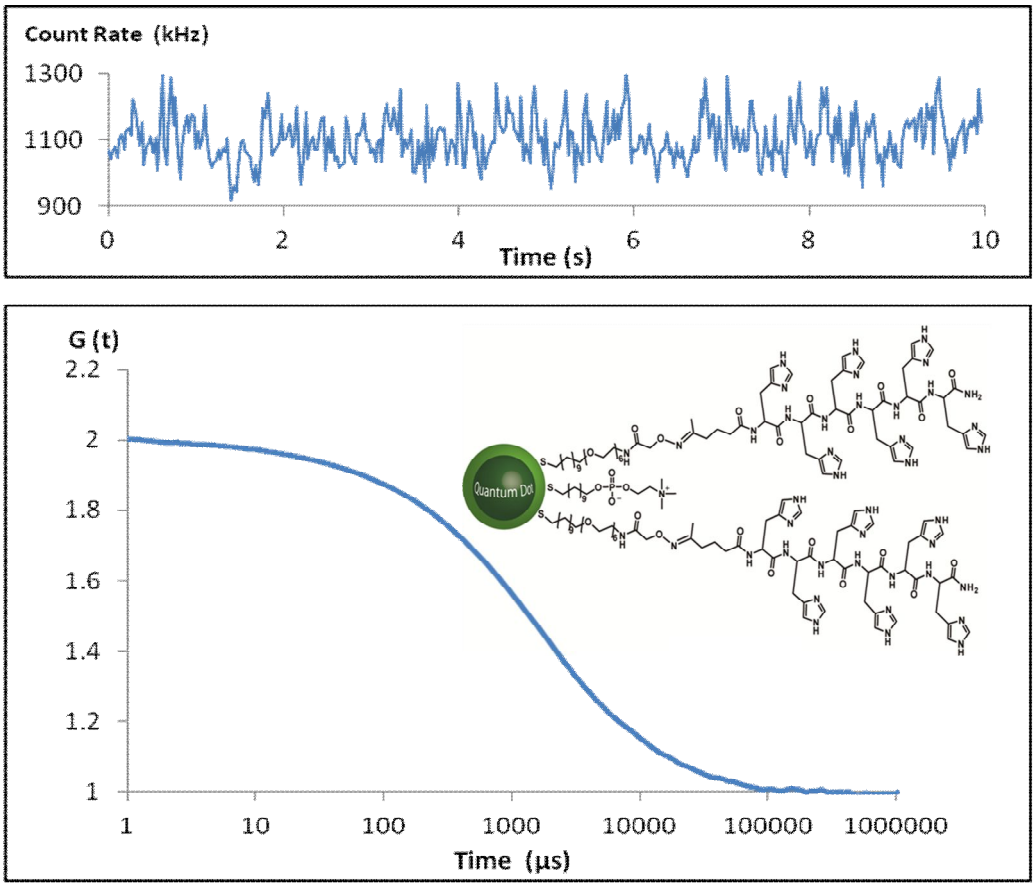

Figure 2.14. Cartoon structure representation and Fluorescence fluctuation profile of AO/PCSAM-QD carrying His_6 measured by Fluorescence Correlation Spectroscopy.

The prepared AO/PCSAM-QDs containing only the glycopeptide was co-incubated with the different cell lines and track the intracellular fate of the surface-displayed glycopeptide. Although it penetrated the cells, the QD conjugate had suffered greatly from endolysosomal sequestration after 2 hours, as showed in the merge image of colocalization (Figure 2.17) in a counter-labelled lysosome (LysoTracker Red DND-99). The most common and crucial fate of delivered nanoparticles and proteins is lysosomal entrapment. Failure of cellular delivery is usually caused by degradation of delivered molecules inside the lysosome upon sequestration, where high levels of lysosomal enzymes are present.[8] This result strongly suggested the need for an additional functional

motif for controlling cellular uptake efficiency and subsequent trafficking of this QD-based nanoparticle-vehicles.

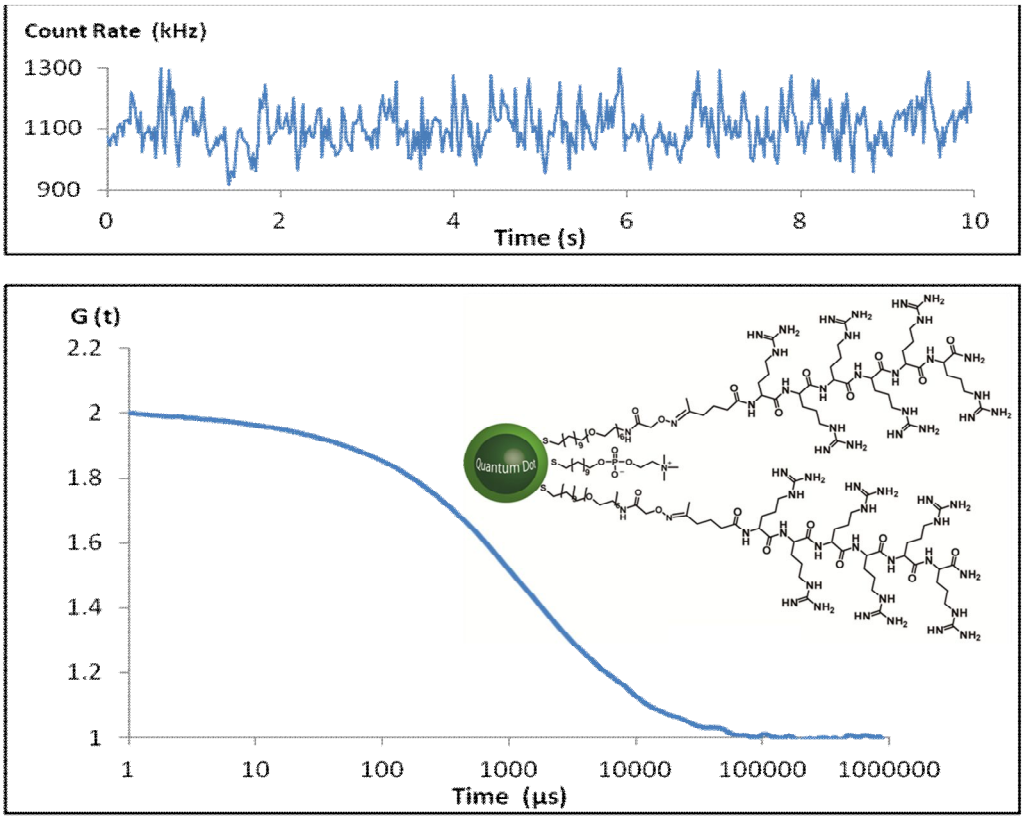

Figure 2.15. Cartoon structure representation and Fluorescence fluctuation profile of AO/PCSAM-QD carrying Arg_6 measured by Fluorescence Correlation Spectroscopy.

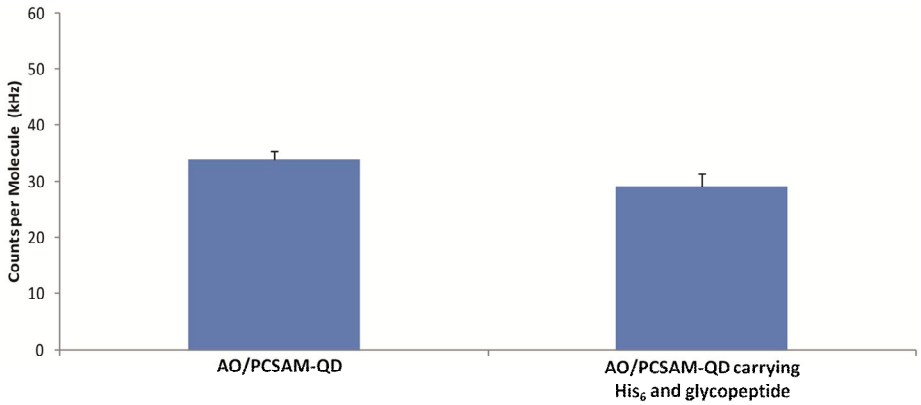

Figure 2.16. Fluorescence intensity per molecule of QD conjugates measured by FCS. Error bar represents standard error of the mean.

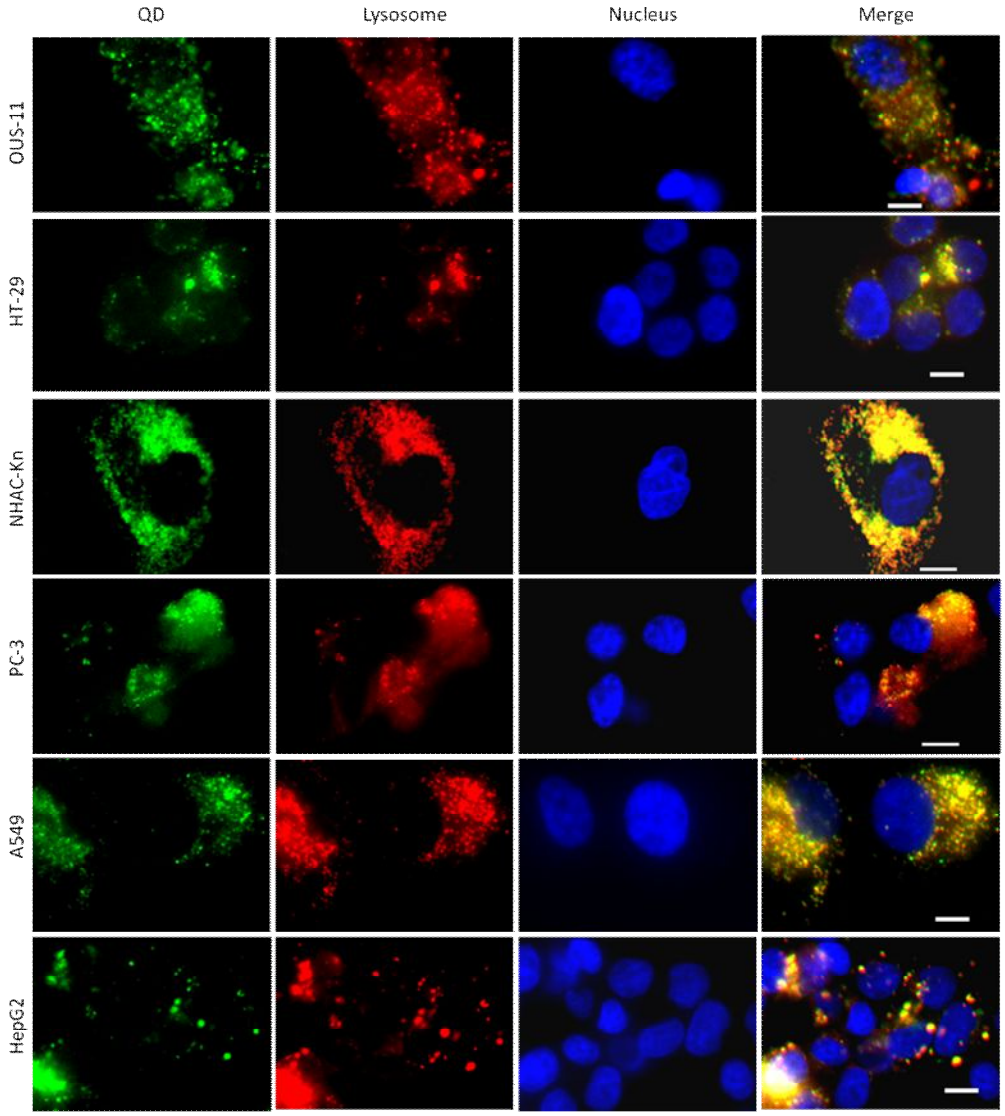

Figure 2.17. Representative images of different cell lines showing lysosomal entrapment of AO/PCSAM-QDs carrying glycopeptides after co-incubation for 2 h. Cells were co-incubated with QD conjugate (green) for 2 h and fixed. Lysosomes were stained with LysoTracker Red DND-99 (red), while the nuclei were stained with Hoechst (blue). Merged yellow color indicates that the QD conjugates were mostly accumulated and suffered endolysosomal sequestration after 2 hours. Scale bar is 10μm.

CPP conjugation to AO/PCSAM-QDs

The unique functions of CPPs in terms of their ability to assist cellular uptake and subsequent endolysosomal escape of cell surface mimetic QD conjugate were investigated

by designing and preparing AO/PCSAM-QDs carrying CPPs. The effect of the histidine-rich and arginine-rich peptide on the general property and efficacy of AO/PCSAM-QDs platform in cellular uptake were analyzed using different human cell lines.

The AO/PCSAM-QDs carrying Arg_6 were first examined during intracellular delivery of the QD conjugate. However, QD conjugate was observed to form large aggregates and locates mostly on the surface of cell membrane during intracellular delivery. On the contrary, AO/PCSAM-QDs carrying His_6 (Figure 2.18) has penetrated the cell in a dispersed fashion.

Poly-arginine CPP has been reported to be highly internalized in the cell, no cytotoxic effect, and no aggregation observed after cellular co-incubation. Generally, polyarginine conjugated compounds, like other cell penetrating peptide conjugated compounds, enter the cell through its interaction with the sulphate and carboxylate groups of cell-surface heparan sulphate proteoglycans (HSPGs).[34] Cell surface HSPGs are known to enter the cell by endocytosis and then being degraded in the lysosome as a major turnover route.[40] Binding between HSPGs and polyarginine induces aggregation and ligand clustering causing polyarginine-carrying compounds to concentrate on the cell surface and subsequently internalized.[41] In this case, Arg_6 displayed in the QD surface was observed to aggregate in the cell surface, even in the cell culture medium, upon intracellular delivery. This could be likely because at physiological pH, Arg (*pKa,* 12) is protonated and could interact with negatively charged sulphate and phosphate groups on the cell surface. The observed aggregation could be due to the electrostatic interaction with sulphate groups of HSPG and other glycosaminoglycans (GAGs) that are either majorly expressed on the cell surface or released in the extracellular environment. It is also likely that hydrogen bonding occurred, taking into account the ability of the guanidinium group of arginine to form hydrogen bonds with sulphate and carboxylate groups.[20,28-30] In many instances, the

difference in molecular display on modified QD surface as well as different QD material could also result in disparate outcomes, which could also be the reason why aggregation was observed.[18] This observation prompted us to discontinue the use of Arg_6 as CPP.

Poly-histidine, on the other hand, forms non-covalent metal-affinity interactions on the QD surface, which could also be a great strategy for direct QD surface modification without the use of AOSH linker. However, during the formation of the late endosome and lysosome, the pH of the vesicles inside the cell can drop to as low as ~5.0 to 5.5. Given the fact that the normal *pKa* of histidine residue is ~6.5, protonation of its imidazole side chain could result in dissociation of poly-histidine from QD surface.[18]

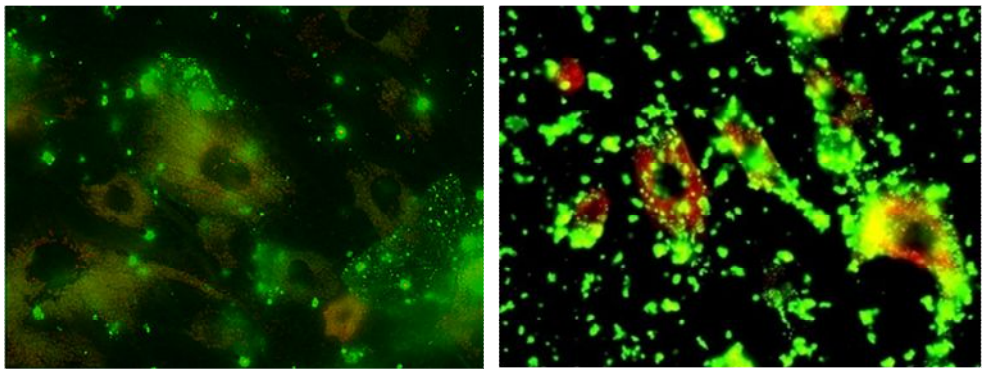

Figure 2.18. Representative fluorescent images after 2 h co-incubation of A549 cells in the presence of 5 nM AO/PCSAM-QDs carrying His_6 (Left) and Arg_6 (Right). Red color represents lysosomes stained with LysoTracker Red DND-99 and Green color represents the QD conjugates.

In this study, the experimental design ensures stable attachment of poly-histidine to the modified QD surface, which is of prime importance. This design also took advantage of the cell-membrane compatibility of PCSH coupled with the ability of the CPP to traverse the cell membrane and escape from endolysosomal sequestration, which we believed could enhance QD cellular incorporation.

Energy Independent Cellular Uptake

Endocytosis is an energy-dependent process that usually translocates extracellular material across cell membrane. This type of mechanism is usually the process involved in cellular entry of most QDs.[8] Endocytosis can be inhibited by conditions involving ATP depletion and low temperatures incubation.[31]

As shown in Figure 2.19, it was revealed that AO/PCSAM-QDs carrying His_6 were incorporated efficiently after 2 h into all cell lines used under physiological condition at 37ºC, while efficiency of uptake appeared to differ significantly between normal and cancer cells.

To understand more about the interaction of this new QD conjugates to the cells, possible uptake pathways utilized by AO/PCSAM-QDs carrying His_6 were determined. Low temperature incubation at 4ºC, although resulted in a slight reduction of cellular uptake of QD conjugates by OUS-11, HT-29, and NHAC-Kn cells compared with the normal physiological temperature at 37ºC, did not affect the uptake efficiency of most cells (Figure 2.19).

It is important to note that although membrane-bound QD fluorescent signal was greatly increased in HepG2 and A549 cells, it did not prevent QDs from entering the cells. These results indicated that QD conjugates, however slow, can still cross cellular membranes via energy-independent direct membrane translocation process even at rigidified lipid membrane. The increased membrane-bound fluorescence signal and reduced cellular uptake might have been due to slow uptake of QDs at this condition compared to the normal physiological temperature.

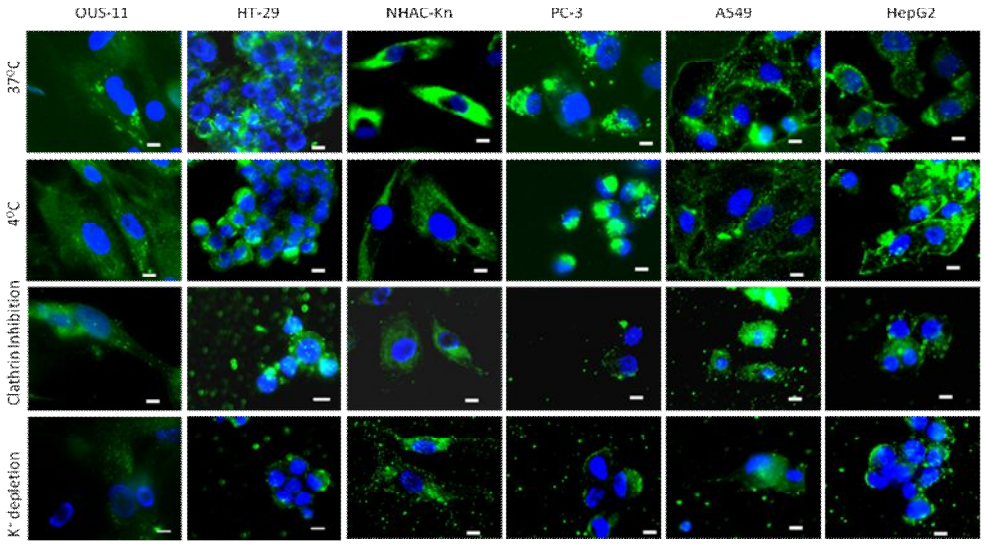

Figure 2.19. Representative cell images showing **c**ellular Uptake of AO/PCSAM-QDs carrying His_6 (green) at different endocytic inhibition conditions. Scale bar is 10 µm.

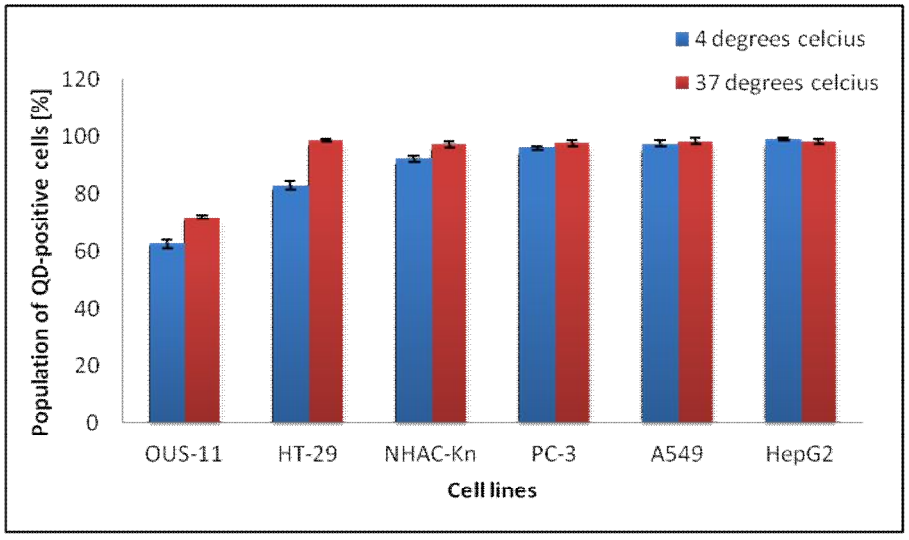

Figure 2.20. Effect of the different temperature incubation on the cellular uptake efficiency of QD conjugates carrying His_6. Error bars represent ± SEM of n = 500.

Inhibition of Clathrin-dependent Endocytosis

Non-phagocytic endocytosis can occur in most cells by several recognized mechanisms including; clathrin-mediated endocytosis, caveolin-mediated endocytosis,

clathrin- and caveolin-independent mechanisms, and actin-dependent macropinocytosis.[32] Several of these processes may be working together at the same time within a cell, and therefore, the mechanism of QD uptake may vary within and between different cell types.[32]

The endocytic pathway of this QD conjugate was examined through clathrin-dependent pathway. It occurs by formation of clathrin-coated pits that invaginate and pinch off from the membrane to form endocytic vesicles. Before the co-incubation, formation of these pits were inhibited by depleting cell with K^+ through HEPES-K^+ and hypertonic treatments, these conditions were known to disrupt the formation of clathrin-coated pits.[31,33] The results showed that K^+ depletion and hypertonic treatment of cells, however reduced the QD uptake, did not inhibit QDs from entering the cell in all of the cell lines (Figure 2.19). This suggested that clathrin-mediated endocytosis may be acting as one of the endocytic pathways but may not be the main endocytic pathway utilized by QDs. This narrowed down the investigation to caveolin-mediated endocytosis and macropinocytosis. One mechanism of lipid raft-mediated endocytosis is through caveolae-involved slow transcellular vesicle trafficking.[34] Since QD conjugates, at all conditions, were able to penetrate on HepG2 cells, a caveolae-deficient cells that do not express caveolins endogenously,[35] suggested that caveolin-dependent uptake may not also be the main endocytic pathway utilized by QDs.

Macropinocytosis is a clathrin- and caveolin-independent pathway that involves the formation of large vesicles called macropinosomes, which occur through actin filament driven plasma membrane protrution. However, the QDs also managed to enter the cell at low temperature incubation that rigidified the membrane, which could prevent plasma membrane protrution, and thus doubted the major participation of macropinocytosis.

Another CPP internalization pathway was proposed recently called the self-induced endocytosis or physical endocytosis, an energy-independent pathway that involves direct translocation and induction of endocytic-like membrane invagination[32] that defined the capacity of a peptide to induce their cellular entry and produce endosome-like invaginations without participation of metabolic energy. This pathway relied on the interaction of peptide with GAGs and phospholipids that resulted in normal endocytosis. This pathway might explain the entry of QDs in the cell even at low temperature energy-independent condition.

GAG-mediated Cellular Uptake.

Polycationic CPP internalization and translocation mechanisms across biological membranes likely involved a direct electrostatic interaction with the negatively charged phospholipids[36] and GAGs.[37] It has been reported that CPP internalisation either via passive diffusion or via endocytosis seems to be initially in contact with membrane constituent proteoglycans that act as receptors for extracellular CPPs leading to peptide uptake at the multiple sites of cell surface.[20]

To verify the possible involvement of GAGs in mediating the QD conjugate cellular internalization, the interaction of His_6 and the glycopeptide with heparin was investigated using microarray. Figure 2.21 showed the fluorescence intensity of interaction between glycopeptide and His_6 with heparin. The results showed that both have interaction with heparin and suggested that the fast internalization might be partly or fully driven by their interactions with cell surface GAGs.

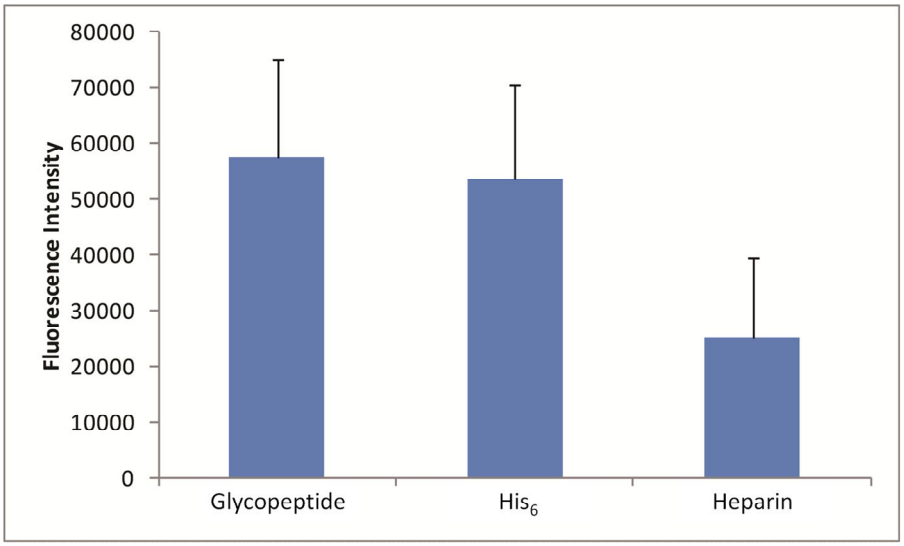

Figure 2.21. Interaction of His_6 and glycopeptide with heparin (n = 3) using microarray. Error bar represents standard error of the mean (SEM).

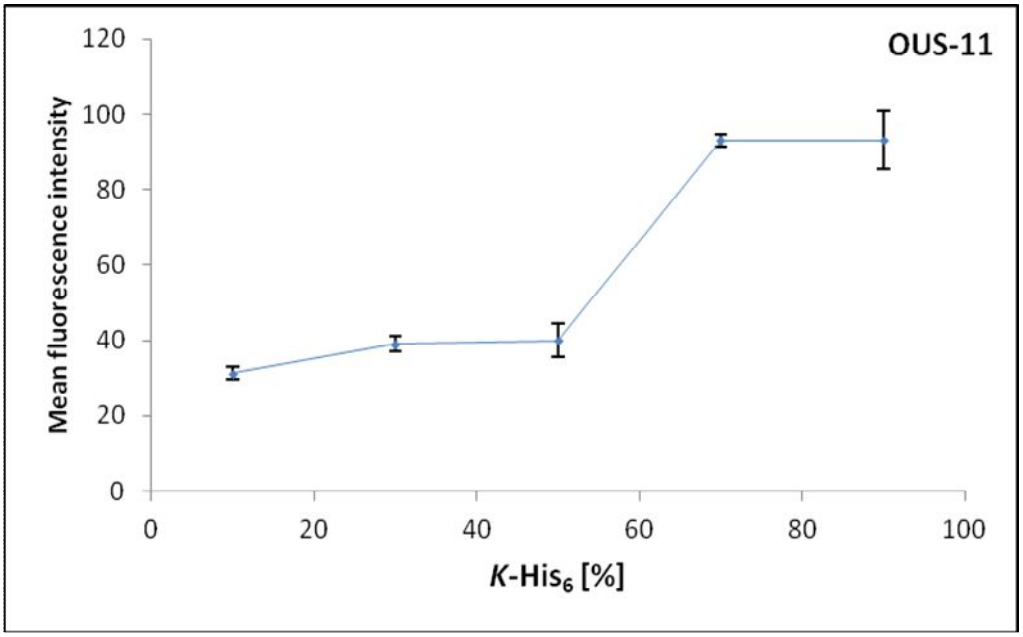

Figure 2.22. Plot showing cellular uptake of AO/PCSAMQDs displaying different ratios of His_6 in OUS-11. At least 15 cells were scored per data point. Error bars represent ±SEM.

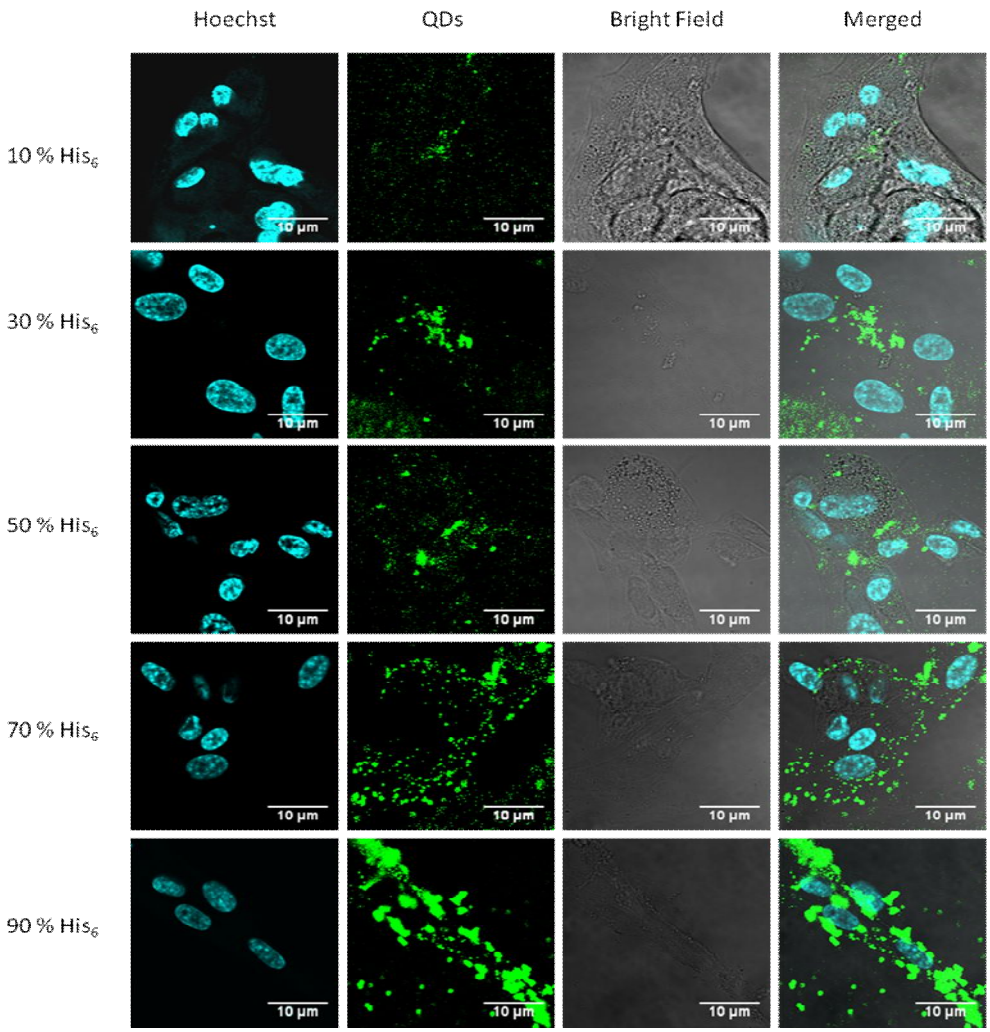

Figure 2.23. Representative images showing cellular uptake of AO/PCSAMQDs displaying different ratios of His_6 in OUS-11.

Optimization of Glycopeptide-His_6 ratio for efficient QD delivery

In order to determine the optimal glycopeptide-His_6 ratio on the QD surface that could efficiently deliver QD conjugate intracellularly, the concentration of His_6 displayed on the QD surface was varied ranging from 10% up to 90%.

After the delivery of the varying the concentrations of serglycine-like glycopeptide and His_6 ratio on the QD surface, the result showed that higher concentration of His_6 on the QD surface induced aggregation of QD conjugates both in the extracellular and intracellular spaces (Figure 2.22-2.33) suggesting that generally, 30% to 50% is the optimum range to get the cellular uptake of higher efficiency. Although OUS-11, NHAC-Kn, and HepG2 cell lines showed an increasing trend in the intracellular fluorescence intensity as the ratio of His_6 increased, nasty aggregation has been observed on QD conjugates containing more than 50% of His_6.

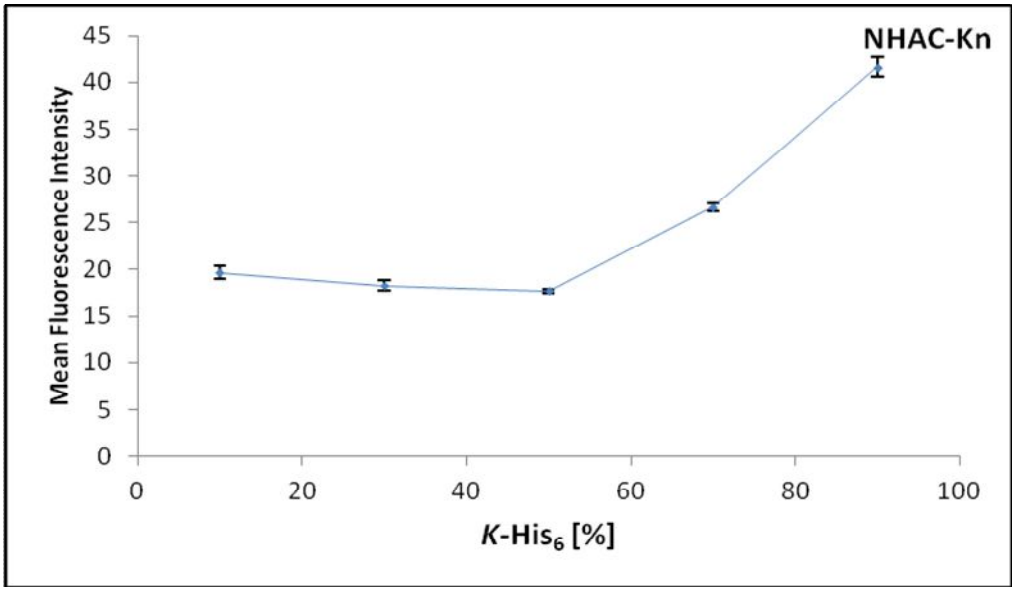

Figure 2.24. Plot showing cellular uptake of AO/PCSAMQDs displaying different ratios of His_6 in NHAC-Kn. At least 15 cells were scored per data point. Error bars represent ±SEM.

The increased fluorescence intensity was highly due to the intracellular aggregation of the QDs giving off very bright fluorescence intensity, which is not a non-ideal condition for intracellular delivery. The rapid aggregation could potentially harm the cells and could induce cytotoxicity. The A549, PC-3, and HT-29 cells lines, on the other hand, showed different trends in intracellular QD fluorescence. A decrease in fluorescence intensity after

50% His_6 was observed in all of these cell lines. However, detailed observation of the cells after co-incubation showed that QD conjugates have the same aggregation plight with increasing His_6 ratio. This time QD conjugates were highly aggregated outside the cell and in the plasma membrane. The golgi accumulation is predicated by the endolysosomal escape of QDs.

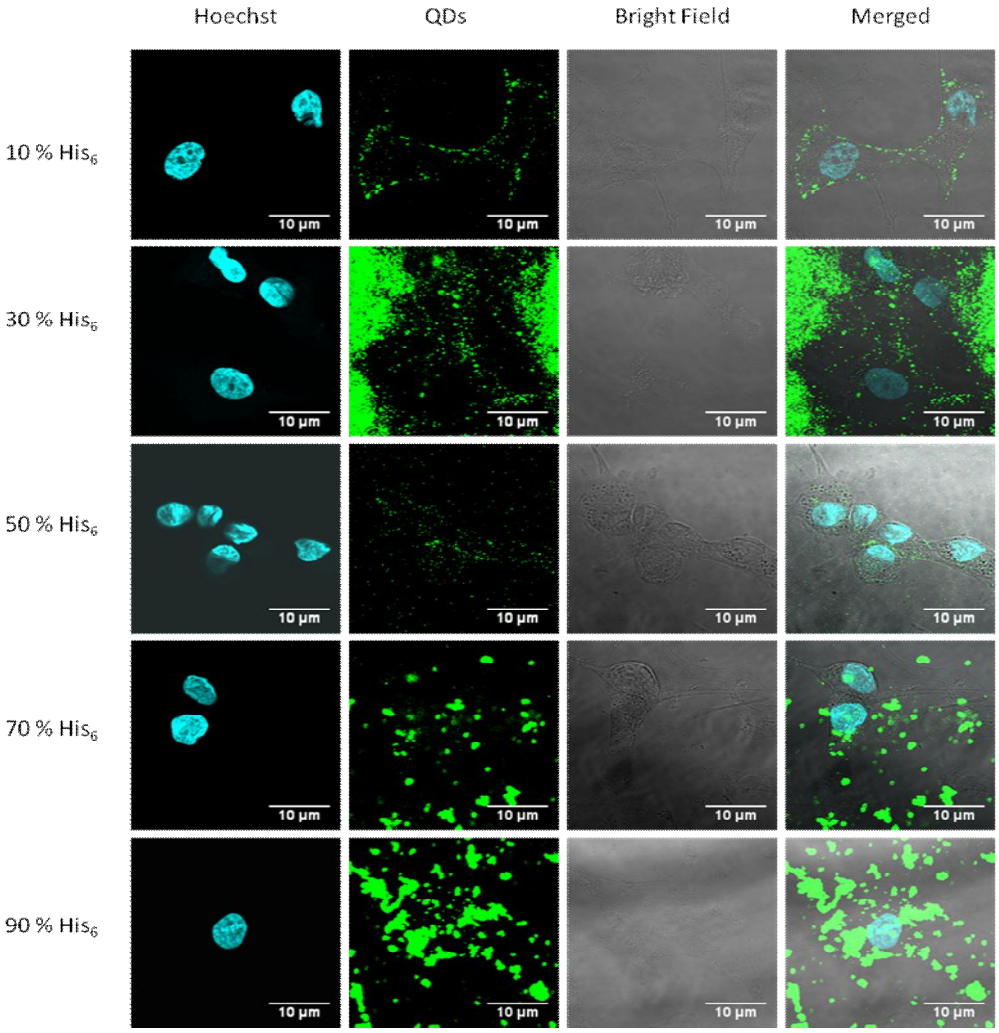

Figure 2.25. Representative images showing cellular uptake of AO/PCSAMQDs displaying different ratios of His_6 in NHAC-Kn.

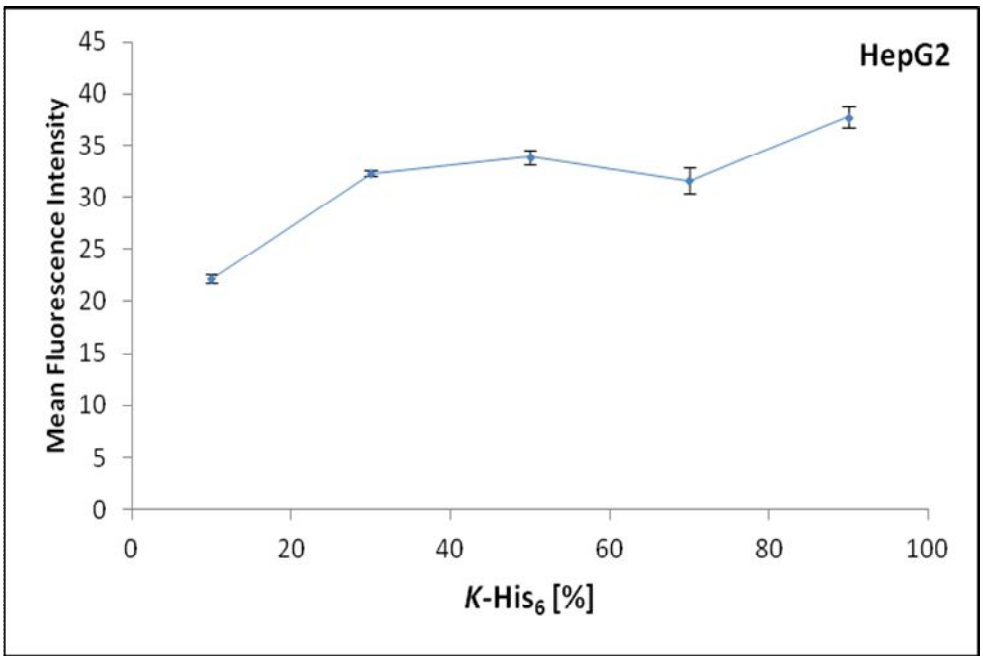

Figure 2.26. Plot showing cellular uptake of AO/PCSAMQDs displaying different ratios of His_6 in HepG2. At least 15 cells were scored per data point. Error bars represent ±SEM.

As observed in this experiment, at His_6 ratio over 50% can cause QDs to aggregate both extra- and intra-cellular spaces, which is not ideal for intracellular delivery. This aggregation could be due to a possible cross-linking of His_6 as a result of their interaction with cell surface HSPG. Therefore, considering the ideal condition for intracellular delivery, 30% - 50% was considered an ideal ratio that could elicit highest endolysosomal escape and consequent golgi accumulation.

Endolysosomal Escape of AO/PCSAM-QDs by His_6 Conjugation

To verify that cell uptake and intracellular traffic of AO/PCSAM-QDs carrying glycopeptide can be mediated specifically by the presence of His_6, cells were co-incubated with AO/PCSAM-QDs co-displaying glycopeptide and His_6 (Figure 2.34a).

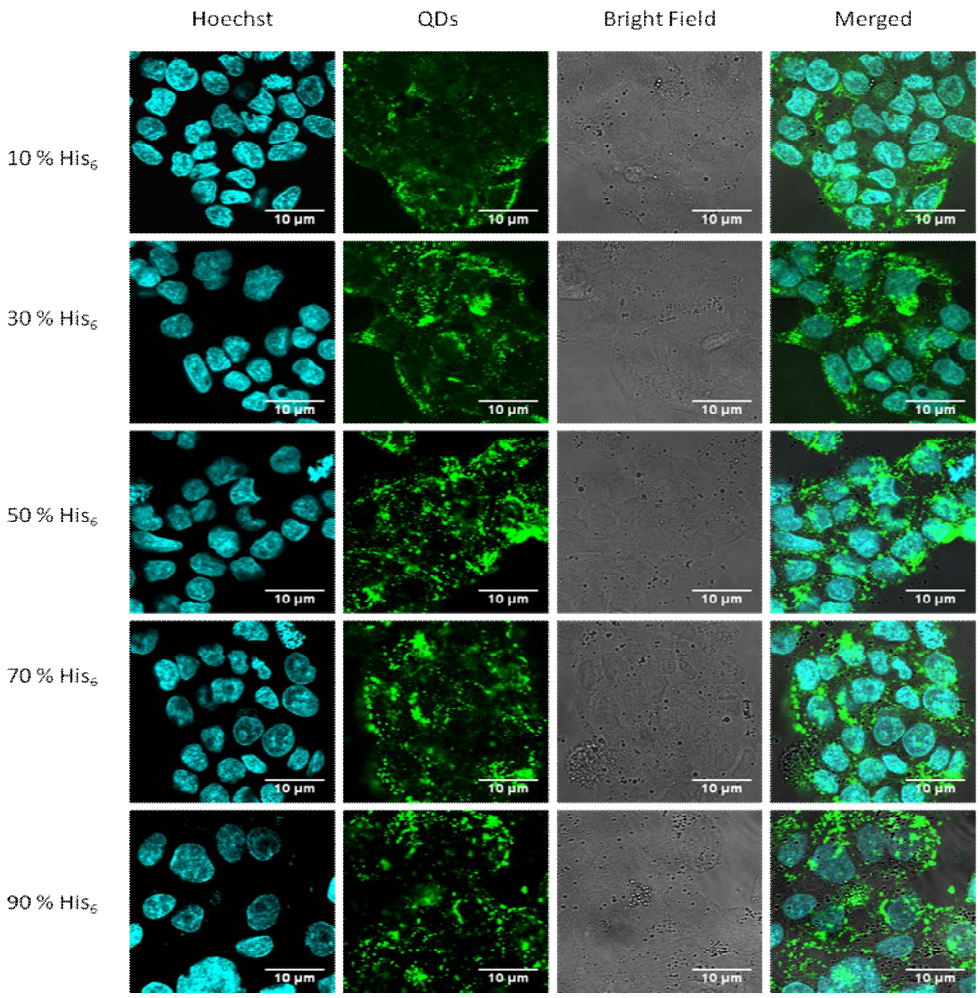

Figure 2.27. Representative images showing cellular uptake of AO/PCSAMQDs displaying different ratios of His_6 in HepG2.

Attachment of ketone-functionalized His_6 allowed for enhanced uptake and subsequent endosomal escaping of QD conjugates as clearly shown in an intracellular QD fluorescence signal that appeared to be unmerged (pointed by white arrows) with the endolysosomal red fluorescence signal, while some are gradually escaping from the endoysosomal entrapment (pointed by yellow arrows).

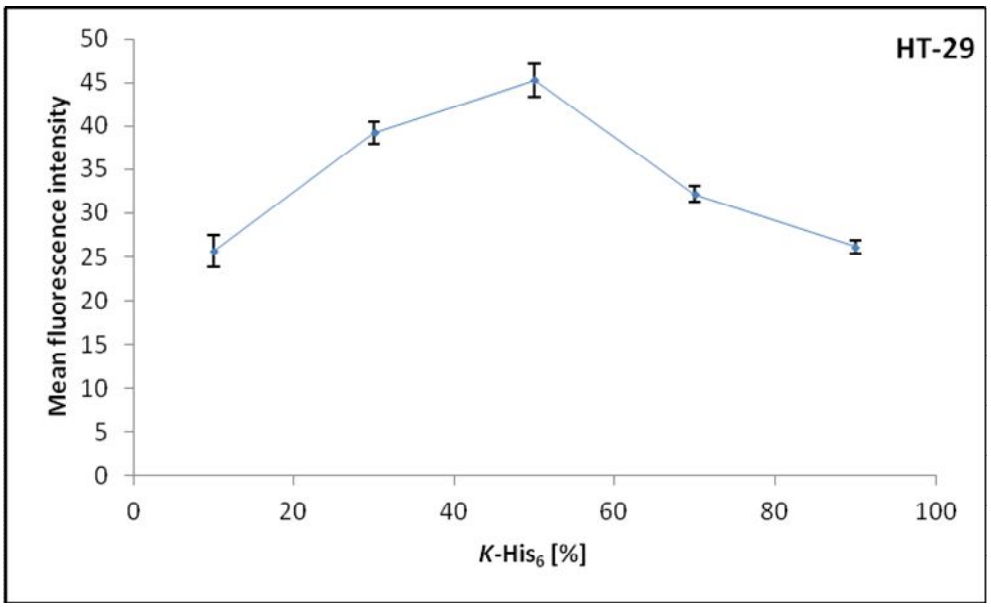

Figure 2.28. Plot showing cellular uptake of AO/PCSAMQDs displaying different ratios of His_6 in HT-29. At least 15 cells were scored per data point. Error bars represent ±SEM.

QD conjugates that managed to escape from sequestration were also observed being channelled and accumulated to a specific cellular space adjacent to the nuclear membrane (area inside white broken lines). The semi quantitative analysis of the QD-positive cells that contain QD conjugate escaping from lysosomal sequestration is shown in Figure 2.34b.

In a detailed analysis of this phenomenon, a representative fluorescence images were taken and analyzed. As shown in Figure 2.35a, QD conjugate (green) sequestered inside the endolysosome complex (represented as yellow merged color) shown to gradually managed to escape from the entrapment and were being delivered into a confined specific intracellular space adjacent to the nuclear membrane (area inside white broken lines).

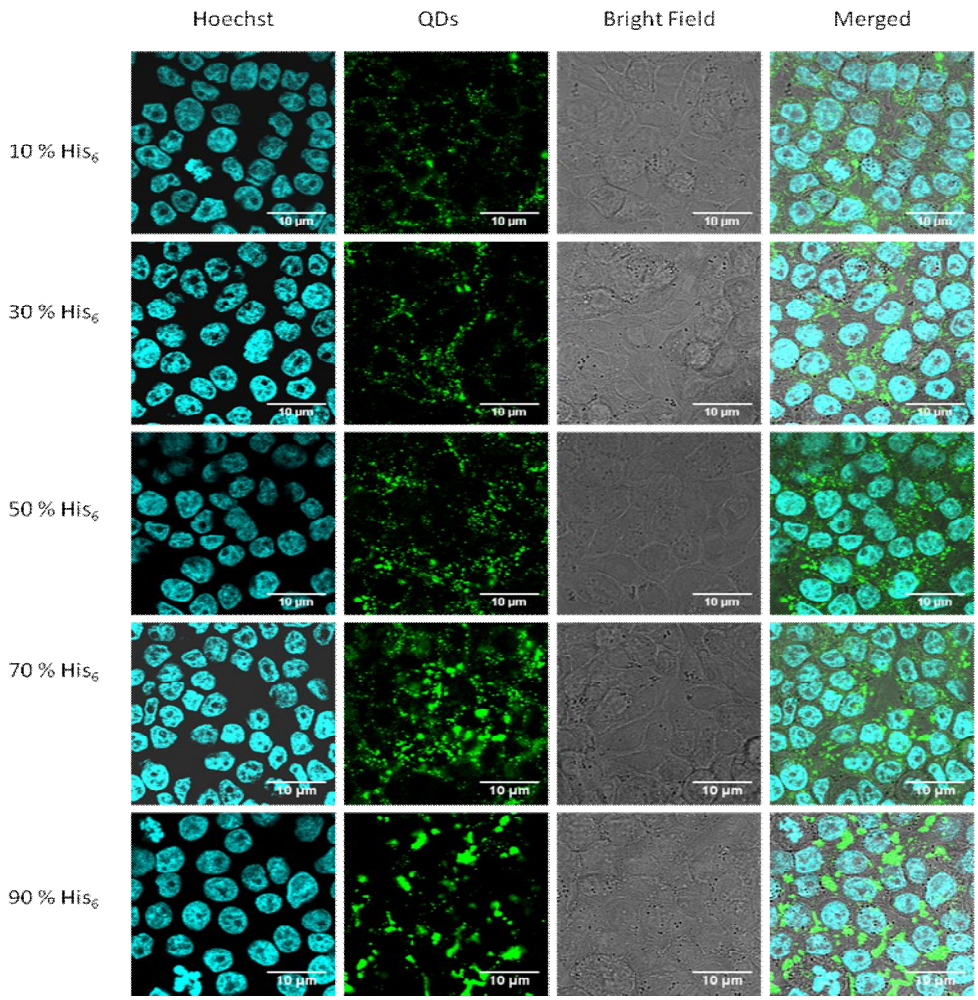

Figure 2.29. Representative images showing cellular uptake of AO/PCSAMQDs displaying different ratios of His_6 in HT-29.

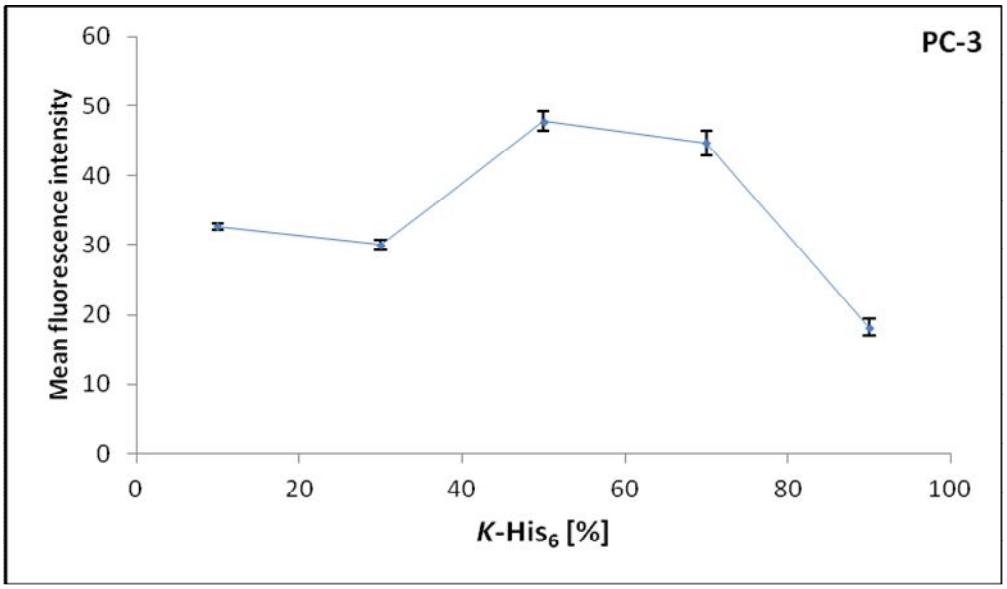

Figure 2.30. Plot showing cellular uptake of AO/PCSAMQDs displaying different ratios of His_6 in PC-3. At least 15 cells were scored per data point. Error bars represent ±SEM.

The escaping mechanism was so efficient that most of the QD conjugates have managed to escape. This specific intracellular space appeared to be the golgi apparatus (red) as confirmed by marking the golgi with golgi marker anti-giantin IgG and detected with secondary antibody (Figure 2.35b), this suggested that QD conjugates were being delivered into the golgi apparatus after an escape from sequestration.

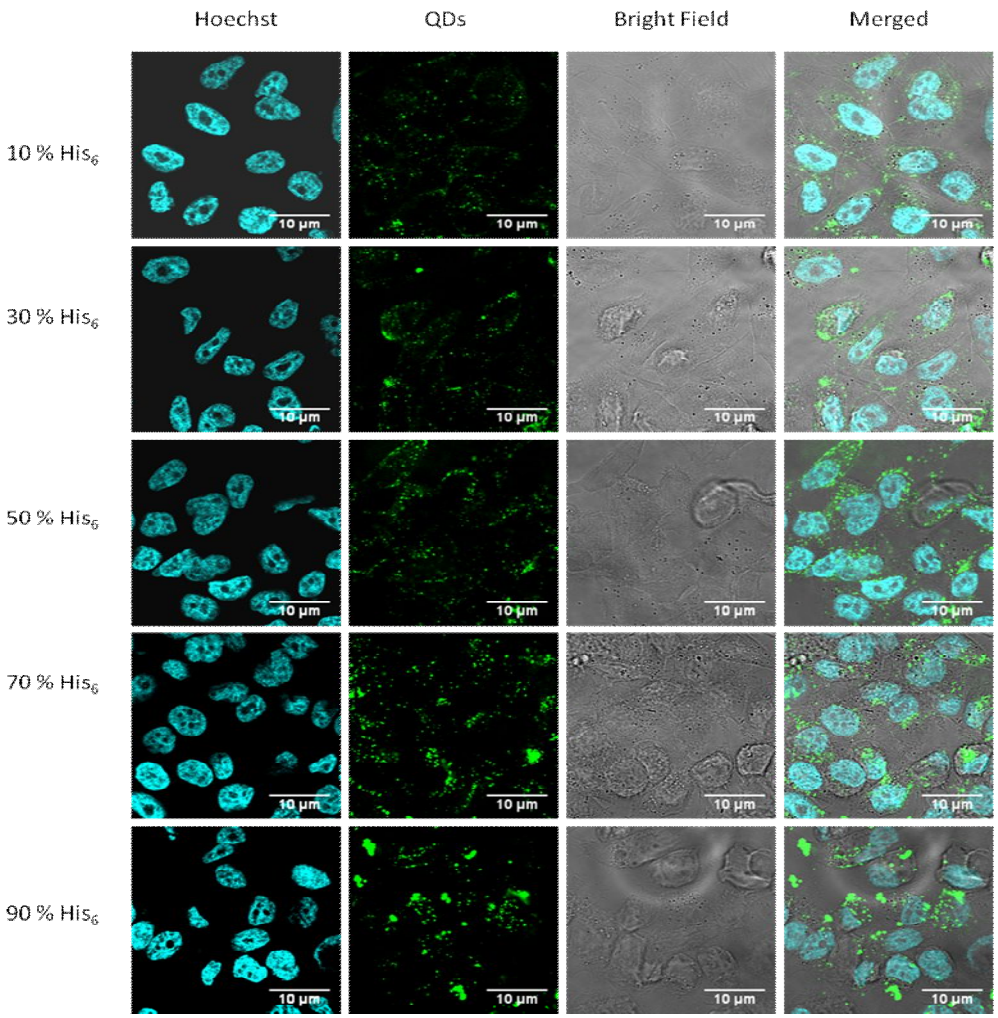

Figure 2.31. Representative images showing cellular uptake of AO/PCSAMQDs displaying different ratios of His_6 in PC-3.

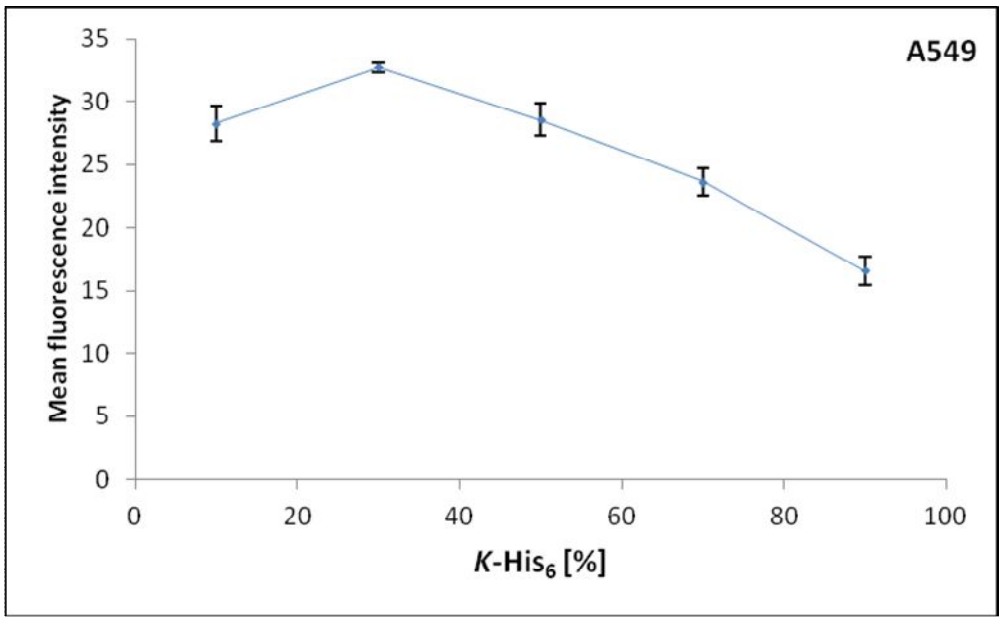

Figure 2.32. Plot showing cellular uptake of AO/PCSAMQDs displaying different ratios of His_6 in A549. At least 15 cells were scored per data point. Error bars represent ±SEM.

Since the aim is to track the fate of these QD conjugates inside the cell, the visualization of the routes and movement of QD conjugates provide a means to better understand protein trafficking processes inside the cell. As shown in Figure 2.35a, the QD journey was started by a cellular entry, which resulted into endolysosomal sequestration. The sequestered QDs then escape from the endolysosomal system following lysosomal membrane permeabilization (LMP) mediated by His_6 and then delivered to the golgi apparatus and Endoplasmic reticulum (Figure 2.35b).

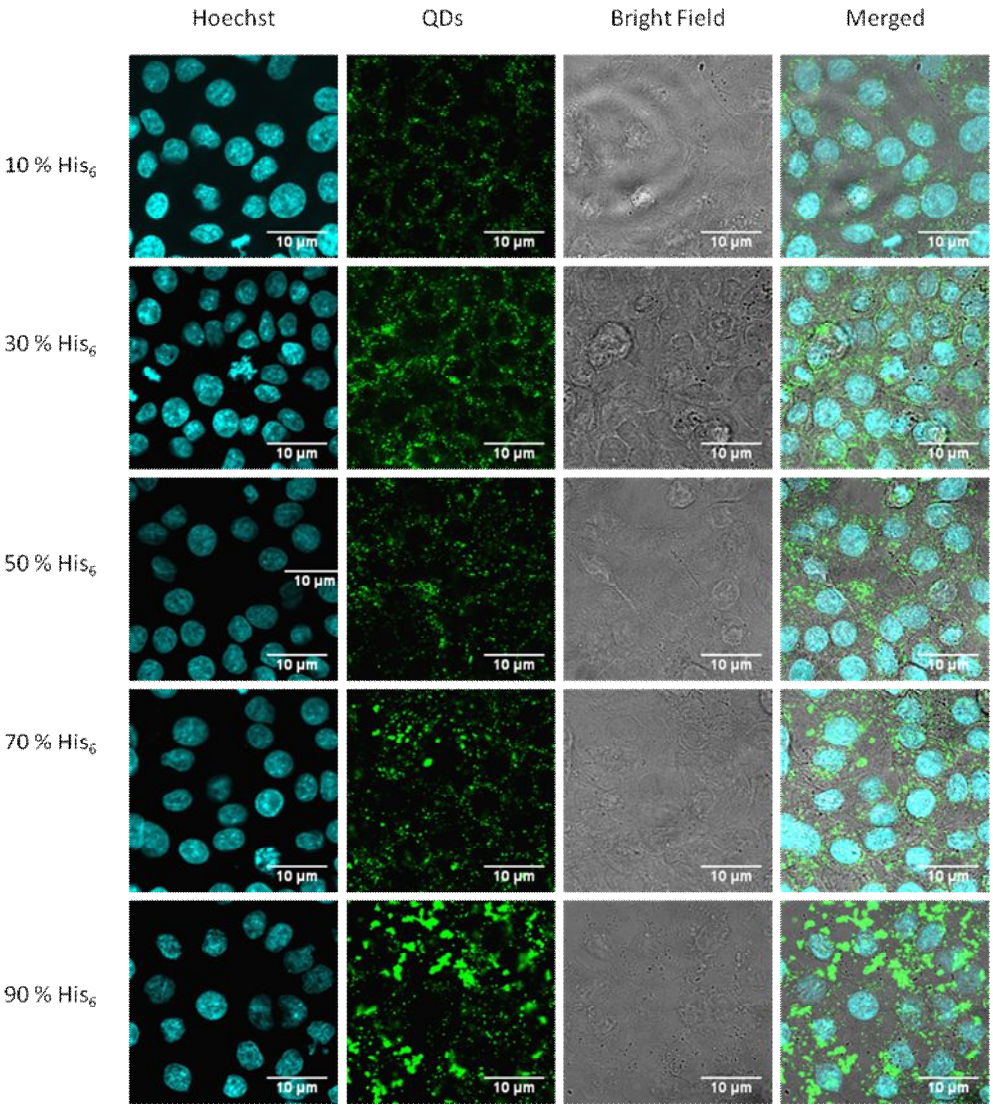

Figure 2.33. Representative images showing cellular uptake of AO/PCSAMQDs displaying different ratios of His_6 in A549.

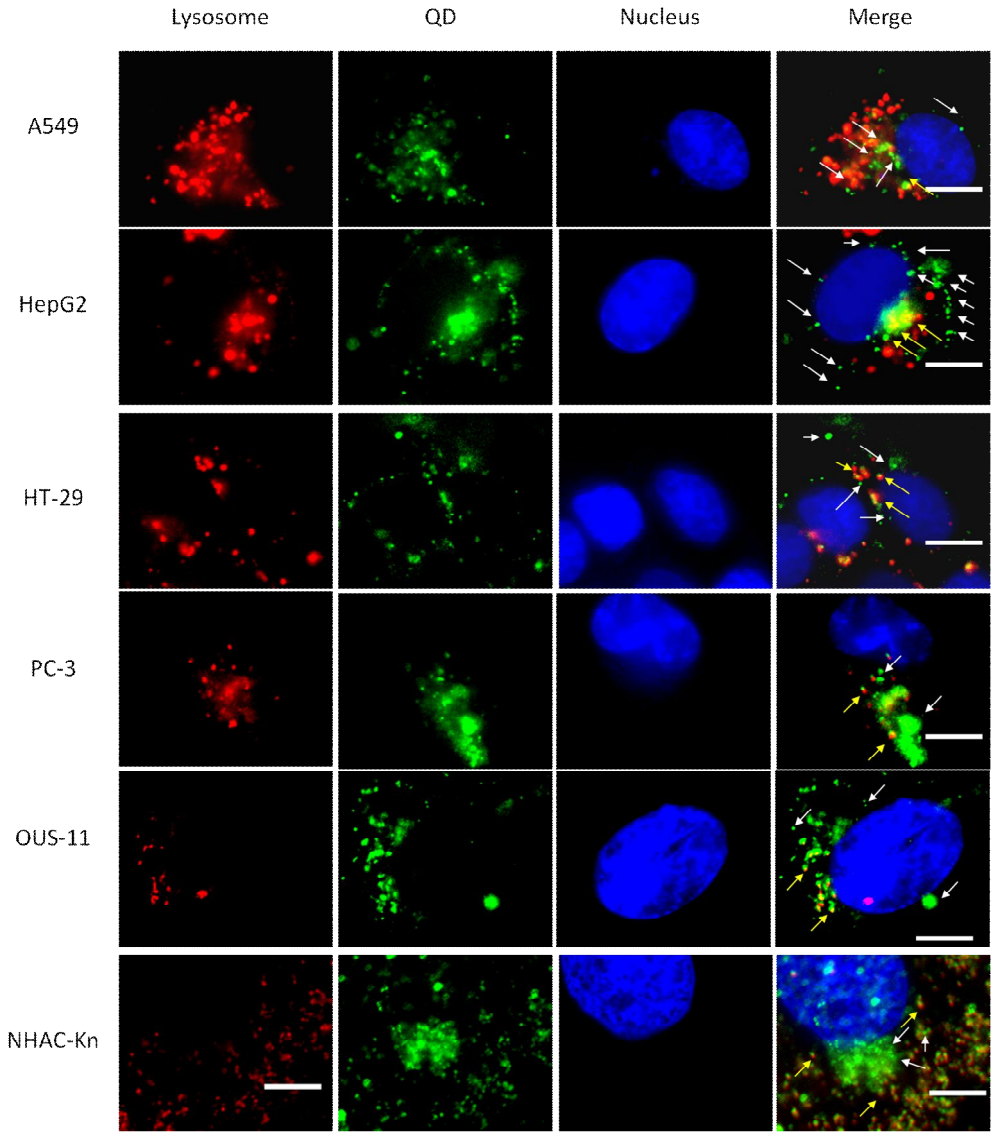

Figure 2.34a. Representative cell images showing intracellular distribution of QD conjugates (green) when co-incubated with different human cell lines for 2 h. Lysosomes were stained with LysoTracker Red DND-99 (red); nuclei were stained with Hoechst 33342 (blue). White arrows indicate QD conjugates excluded from lysosome. Yellow arrows indicate areas of colocalization. Scale bar is 10 μm.

This observation has been confirmed by tracking the fate of QD conjugate in real-time. The real-time tracking observation revealed that aside from golgi delivery, the QD conjugates were also excreted outside the cell (Figure 2.36). The observed excretion of QD conjugates was made apparent by the appearance of a punctate-shaped green fluorescent dot coming out of the cell membrane (pointed by blue arrow) and disappeared once it

reaches the extracellular space while, the entry of QD conjugate was observe by the presence of a punctuate-shaped fluorescence coming inside the cell forming a bright green dot in the cytoplasm (pointed by white arrow).

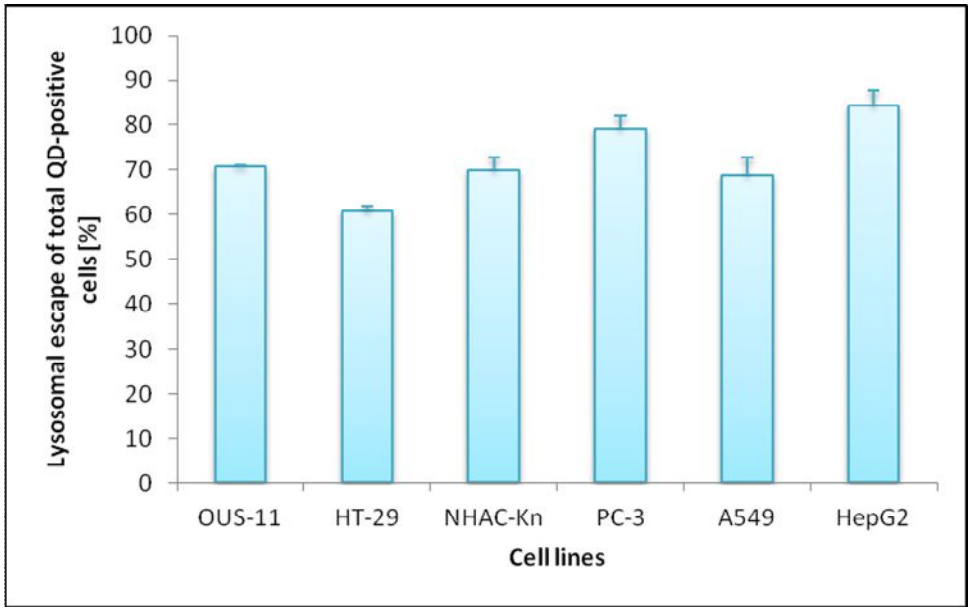

Figure 2.34b. Semi-quantitative scoring of lysosomal escape in different human cell lines. Error bar represents SEM for n = 300.

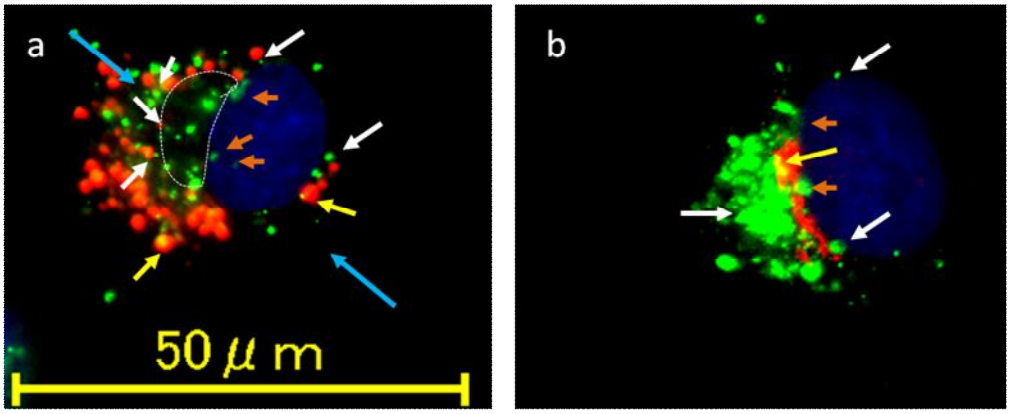

Figure 2.35. Representative cell images showing dynamic intracellular escape of QD-conjugates from lysosomal sequestration and subsequent trafficking of QD conjugates when co-incubated with A549 cells for 2 h. White arrows indicate QD conjugates excluded from lysosome. Yellow arrows indicate areas of co-localization and orange arrows indicate nuclear localization. a) QD conjugates (green) escaping from lysosome (red) sequestration and moving towards the center. Blue arrows indicate the direction of movement of QDs. b) QD conjugates being channelled and moving towards the golgi stained by anti-giantin IgG and secondary anti-body (red) following endolysosomal escape.

The bright green dot traversed the cytoplasm and disappeared, which believed to have entered other cellular compartment. On the other hand, QD conjugates that have already entered previously inside the cytoplasm have been sorted inside in which we believed to be the sorting endosome (area inside red broken lines) and then delivered and disappeared into the larger intracellular area where QDs were mostly accumulated. This area was expected to be the golgi apparatus based from the observed accumulation of most QDs into the golgi from the previous results (as pointed by red arrow).

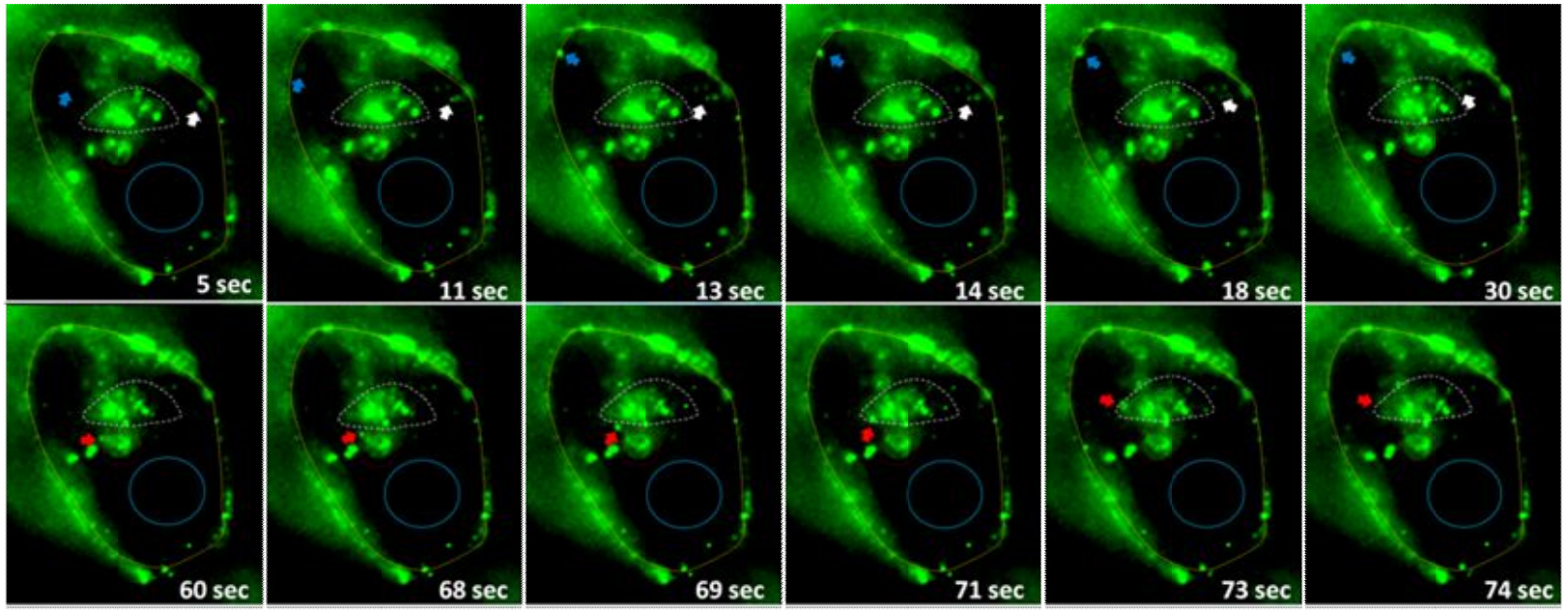

Figure 2.36. Selected frames from the real-time imaging of AO/PCSAM-QDs co-displaying glycopeptide and His_6. Yellow lines indicate plasma membrane. Blue circle indicated area where nucleus could possibly situated. Area inside the broken white lines marked the expected location of golgi apparatus. Area inside red broken lines indicates what is believed to be a sorting endosome. Ble arrows point the movement of exocytosed QDs. White arrows point the endocytosed QDs. Red arrows point the movement of sorted QDs from the sorting endosome to the golgi apparatus.

Cytotoxicity of His_6, glycopeptide and QD-conjugates

The problem with most of the delivering agents is their cytotoxicity. Aside from the core metal, molecules conjugated in the surface of QDs also likely to contribute to the cytotoxicity of QDs. To demonstrate that the cells are not adversely affected by QD conjugates, cytotoxicity assay performed for QD conjugates. Results showed that QD conjugates have no significant cytotoxicity in all cell lines used (Figures 2.37-2.40), although a decrease in cell viability is observed in a concentration-dependent manner in some cell lines. As shown in the figures, compounds were individually non-cytotoxic and even mitogenic to some cell lines.

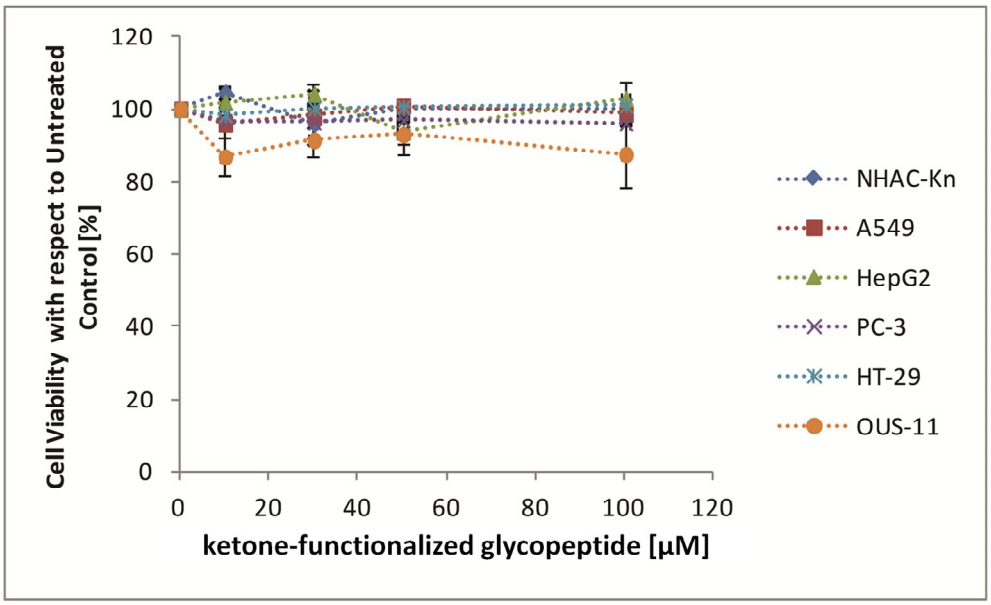

Figure 2.37. Cytotoxicity of ketone-functionalized glycopeptide on different human cell lines after 24 h treatment. Each data point represents average percent viability. Error bars represent ±SEM of n = 3.

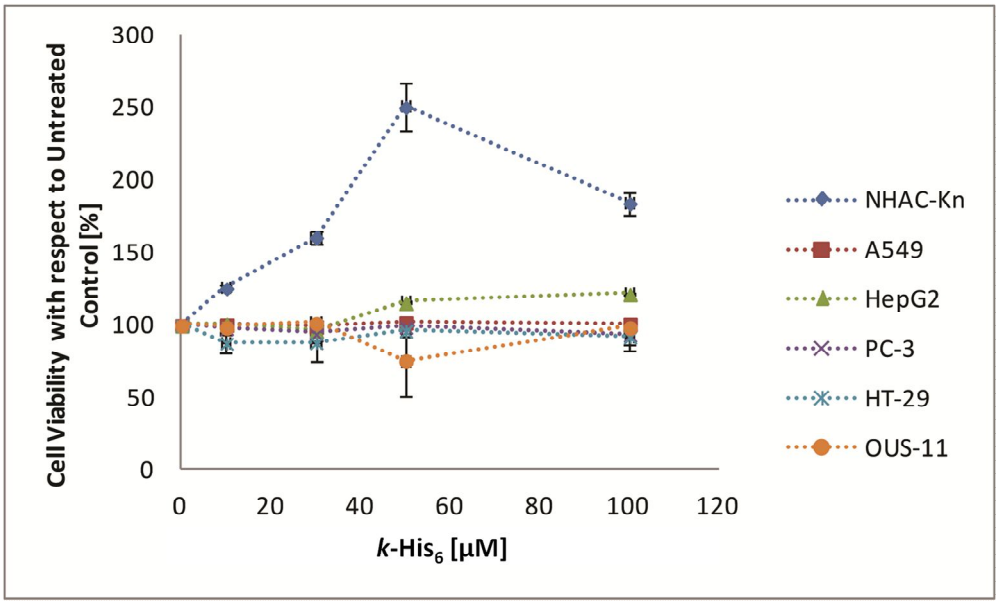

Figure 2.38. Cytotoxicity of *k*-His_6 on different human cell lines after 24 h treatment. Each data point represents average percent viability. Error bars represent ±SEM of n = 3.

The observed concentration-dependent cytotoxicity of AOPCSAM-QDs carrying glycopeptides and His_6, on PC-3, could not be attributed to the surface-displayed compounds but rather to the entirety of the QD conjugates and its behaviour once inside the cell. The escaping mechanism of this QD conjugates once inside the cell could be like a "proton sponge effect".[38] At acidic condition inside the lysosome, this QD conjugate can elicit a "proton sponge effect" response resulting to LMP. This permeabilizaion caused the QDs to penetrate its way out of the lysosome. Consequently, this will caused the release of hydrolases and all other lysosomal load to the cytosol that could result in an increased intracellular pH, which will eventually damage mitochondria and other intracellular compartments. The intense intracellular damage incurred due to lysosomal dysfunction can trigger cellular death.[34,39] Therefore, since this QD conjugates have a remarkable endolysosomal escaping capability; cytotoxicity can likely be induced once inside the cell.

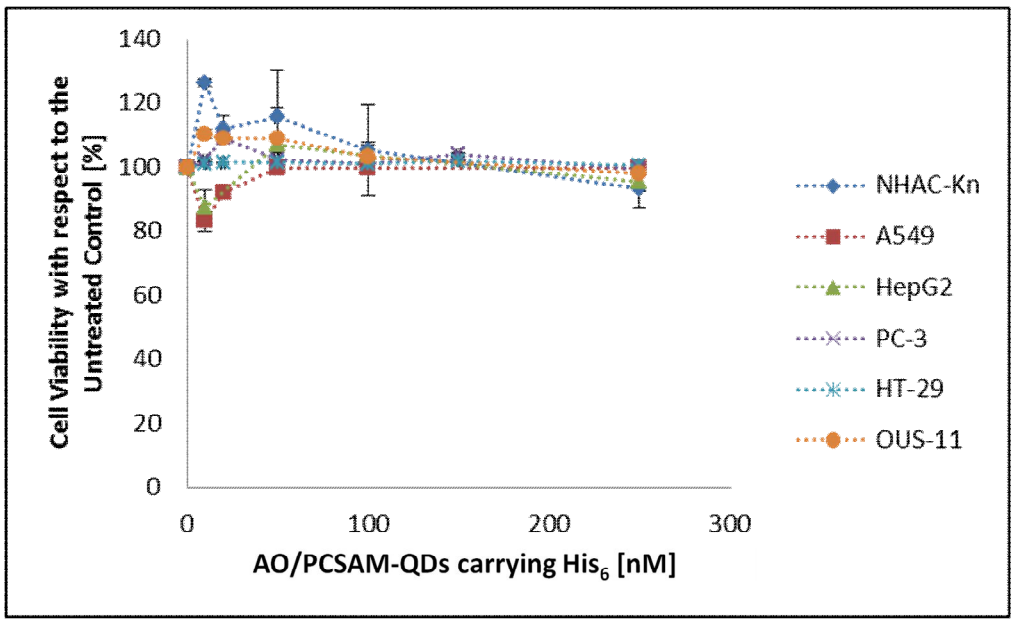

Figure 2.39. Cytotoxicity of AOPCSAM-QDs carrying His_6 on different human cell lines after 24 h treatment. Each data point represents average percent viability. Error bars represent ±SEM of n = 3.

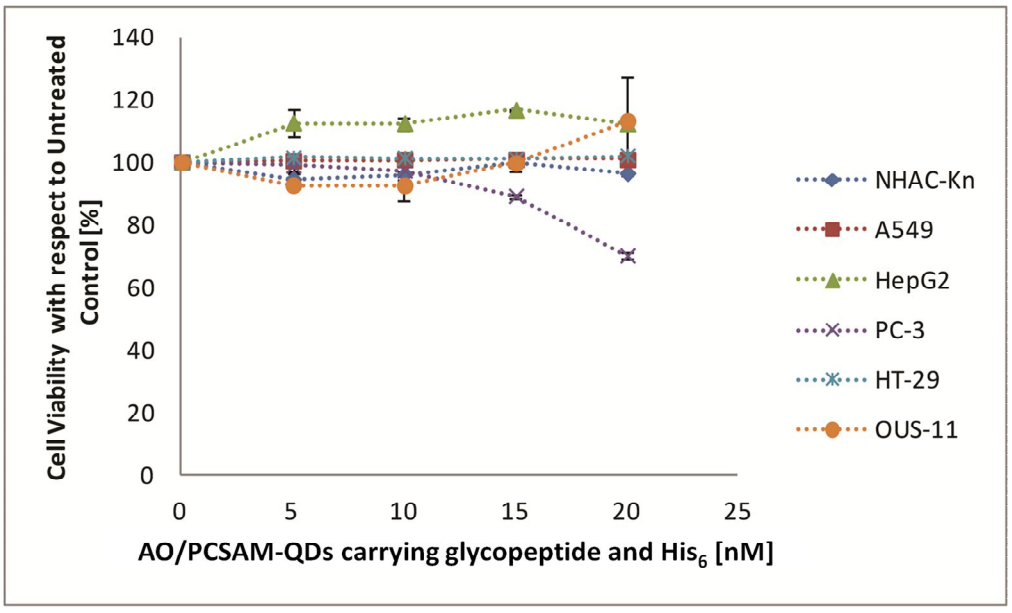

Figure 2.40. Cytotoxicity of AOPCSAM-QDs carrying glycopeptides and His_6 on different human cell lines after 24 h treatment. Each data point represents average percent viability. Error bars represent ±SEM of n = 3.

This study demonstrated that AOPCSAM-QDs carrying His_6 has a strong endolysosomal escaping ability on various human cell lines. The His_6 type CPP confirms a promising cell penetrating ability and non-cytotoxic in intracellular delivery of QD-anchored glycopeptide at shorter time incubation period. The remarkable cell penetrating and endolysosomal escaping abilities of this QD conjugate may have been due to the clustering effect of His_6 on the QD surface. Its cell penetrating mechanism might have involved direct membrane translocation, which was believed to have a good efficiency and broad spectrum cell penetrating and endolysosomal escaping abilities that could be used in many applications.

From the observed evidences presented above, the intracellular fate of AO/PCSAM-QDs co-displaying glycopeptides and His_6, was clearly observed. Intracellular trafficking of this QD conjugate was elucidated following a series of complex events as proposed in Figure 2.41.

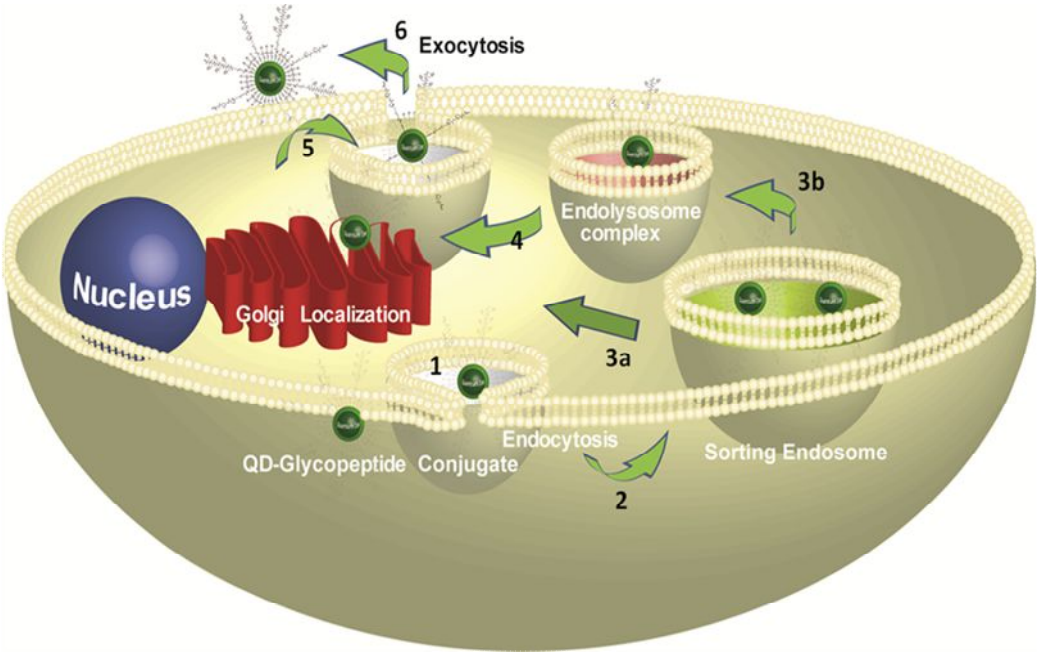

Figure 2.41. Cartoon model of observed cellular fate of AO/PCSAM-QD with co-displayed glycopeptide and His_6. QD conjugates were internalized by the cell through direct membrane penetration mediated by GAGs and the phosphate group of tha phospholipids in the plasma membrane [1]. The QD conjugates can then be delivered to the golgi [3a] (depending on the displayed moeity on the QD suface and the type of cell line used) or fused with lysosome [3b] following sorting in the sorting endosome [2]. Upon lysosomal sequestration, QD conjugates can elicit an escape mechanism mediated by the hexahistidine. Depending on the displayed moeity and the cell line used, the QD conjugates can either be delivered into the golgi [4] (QD conjugates with co-displayed serglycin-like glycopeptides in normal cell lines or QD conjugates with either co-displayed serglycin-like glycopeptides or peptides in cancer cell lines) or will remain in the cytoplasmic space (QD conjugates with co-displayed serglycin-like peptides in normal cell lines). The golgi-delivered QD conjugates bearing the glycopeptides can then exit the intracellular space though exosomes [5] followed by exocytosis [6].

2.3 Experimental

Materials. All Fmoc-protected amino acids and PyBOP were purchased from Novabiochem, HBTU was from Peptide Institute Inc., HOBT from Kokusan Kagaku Corp., HOAt was from GenScript, Rink-Amide-ChemMatrix resin was from Biotage. *N*-(9-Fluorenylmethoxycarbonyl)-*O*-[2,3-di-*O*-acetyl-4-*O*-(2,3,4,6-tetra-*O*-acetyl-β-D-galactopyranosyl)-β-D-xylopyranosyl]-L-Serine was purchased from Medicinal Chemistry Pharmaceutical Ltd., Japan (http://soyaku.co.jp/). Coating reagents, 11,11'-dothio bis[undec-11-yl 12-(aminooxyacetyl)amino hexa(ethyleneglycol)] (AOSH) and a phosphoryl derivative, 11-mercaptoundecylphosphorylcholine (PCSH) were synthesized by the procedures reported previously and available from MCP Co. Ltd., Qdot 545 ITK™, Lysotracker Red DND-99, and Hoechst 33342 were from Invitrogen. DCM, DMF, DIEA and TFA were purchased from Watanabe Chem. IND., LTD. Ultrafiltration membranes were supplied from Milipore, Carrigtwohill, Co. Cork, Ireland. Unless otherwise noted, solvents and other reagents were purchased from Aldrich Chemical Co. (Milwaukee, WI), Tokyo Chemical Industry (Tokyo, Japan), and Wako Pure Chemical Industries Ltd. (Tokyo, Japan).

General synthetic protocol for ketone-functionalized peptides and glycopeptide. Peptides and glycopeptide were synthesized manually following Fmoc-solid-phase synthesis protocol previously described[29]. Briefly, 0.24 mmol/g of Rink-amide-ChemMatrix resin was washed with DMF and DCM followed by DCM swelling for 30 minutes. The swollen resin was washed with DMF. All washing steps were performed three times. Fmoc-amino acid (4 equivalents) was pre-activated using 4 equivalents of HBTU, 4 equivalents of HOBt in DMF and 3 equivalents of DIEA for 30 seconds. The pre-activated Fmoc-amino acid was then added to the resin and allowed to couple for 15 minutes at 50°C under microwave irradiation. The resin was then washed subsequently

with DMF, DCM and then DMF. To block the unreacted/uncoupled animo groups in the resin, acetyl capping was performed using DMF:Ac_2O:DIEA (8.5:1.0:0.5) for 5 minutes at room temperature, washed with DMF, DCM and then DMF, then Fmoc deprotection using 20% piperidine in DMF followed by washing with DMF, DCM and then DMF and the cycle repeated for subsequent iterative synthesis. For the glycopeptide, same steps were applied except for the coupling reagents used and the number of coupling times. Instead of Fmoc-protected amino acid, 1.2 equivalents of *N*-(9-Fluorenylmethoxycarbonyl)-*O*-[2,3-di-*O*-acetyl-4-*O*-(2,3,4,6-tetra-*O*-acetyl-β-D-galactopyranosyl)-β-D-xylopyranosyl]-L-Serine (MCP Co., Ltd, Japan) was used in the coupling process with 1.2 equivalents of PyBOP, 1.2 equivalents of HOAt in DMF and 3 equivalents of DIEA as the coupling cocktail. After coupling for 15 minutes at 50°C under microwave irradiation, the same coupling cocktail without Fmoc-glycoamino acid was added, for a "double activation-like" approach, for 15 minutes at 50°C under microwave irradiation. After coupling and deprotection of the last amino acid, the N-terminai of peptides and glycopeptide were functionalized with 5-oxohexanoic acid, washed, cleaved from the resin and deprotected using TFA:EDT:H2O (95:2.5:2.5) for peptides (1 hour) and TFA:H_2O for glycopeptides (2 hours) at room temperature. The samples were purified using RP-HPLC with acetonitrile and water both with 0.1% TFA and lyophilized. The purified glycopeptide was de-*O*-acetylated by dissolving in trifluoroethanol and added with sodium hydroxide to pH 10.5-11.0 for 30 minutes. The removal of the acetyl groups from the sugar moiety was monitored using MALDI-TOF/MS. After the complete deacetylation process, the solvent was removed either under reduced pressure or air-drying. The de-*O*-acetylated glycopeptide was purified by RP-HPLC and lyophilized.

Synthesis of ketone-functionalized hexaArginine (*k*-Arg_6)

A 0.24 mmol/g of Rink-amide-ChemMatrix resin, Fmoc-Arg(pbf)-OH (96 μmol, 4.0 equivalents), and 5-oxohexanoic acid (4.0 equivalents) were used. Briefly, 0.24 mmol/g of

Rink-amide-ChemMatrix resin was placed in a 5 mL Libra tube, washed sequentially with DMF and DCM followed by DCM swelling for 30 minutes. The swollen resin was washed with DMF. Fmoc-Arg(pbf)-OH amino acid was pre-activated using 4 equivalents of HBTU, 4 equivalents of HOBt in DMF and 3 equivalents of DIEA for 30 seconds. The pre-activated Fmoc-Arg(pbf)-OH was then added to the resin and allowed to couple for 15 minutes at 50°C under microwave irradiation. The resin was then washed subsequently with DMF, DCM and then DMF. To block the unreacted/uncoupled animo groups in the resin, acetyl capping was performed using DMF:Ac_2O:DIEA (8.5:1.0:0.5) for 5 minutes at room temperature, washed with DMF, DCM and then DMF, then Fmoc deprotection using 20% piperidine in DMF followed by washing with DMF, DCM and then DMF and the cycle repeated for six (6) times. After Fmoc deprotection of the last Fmoc-Arg(pbf)-OH, 5-oxohexanoic acid was pre-activated using 4 equivalents of HBTU, 4 equivalents of HOBt in DMF and 3 equivalents of DIEA for 30 seconds. The pre-activated 5-oxohexanoic acid was then added to the peptide-resin mixture and allowed to couple for 15 minutes at 50°C under microwave irradiation. The mixture was washed subsequently with DMF, DCM and then DMF. Deprotection and cleavage of the peptide from the resin was done by adding TFA:EDT:H2O (95:2.5:2.5) cocktail to the washed resin in ice for 30 minutes with shaking and then the shaking was continued at room temperature for additional 1 hour. The deprotection and cleavage processes were monitored using MALDI-TOF/MS. The solution containing the synthesized peptide was drained. The resin was flushed subsequently with the same cocktail solution, acetic acid, and methanol. The filtrates were combined and concentrated by air drying, dissolved in 50% acetonitrile and lyophilized. The peptide was then purified using RP-HPLC with acetonitrile (B) and water (A) both with 0.1% TFA using Intersil® ODS-3 (5 μm, 4.6 x 250 mm) column at room temperature, 1 ml/min flow rate, 220 nm wavelength for detection, and solvent gradient (A:B) of 90:10 (0 min), 70:30 (50 mins), and 5:95 (60 mins) to give k-Arg_6 (t = 7.8 mins) and then lyophilized. HRMS (MALDI): *m/z* calcd for $C_{42}H_{84}N_{25}O_8^+$, $[M+H]^+$ 1066.6936, found 1066.6946.

Synthesis of ketone-functionalized hexaHistidine (*k*-His_6)

A 0.24 mmol/g of Rink-amide-ChemMatrix resin, Fmoc-His(trt)-OH (96 µmol, 4.0 equivalents), and 5-oxohexanoic acid (4.0 equivalents) were used. Briefly, 0.24 mmol/g of Rink-amide-ChemMatrix resin was placed in a 5 mL Libra tube, washed sequentially with DMF and DCM followed by DCM swelling for 30 minutes. The swollen resin was washed with DMF. Fmoc-His(trt)-OH amino acid was pre-activated using 4 equivalents of HBTU, 4 equivalents of HOBt in DMF and 3 equivalents of DIEA for 30 seconds. The pre-activated Fmoc-His(trt)-OH was then added to the resin and allowed to couple for 15 minutes at 50°C under microwave irradiation. The resin was then washed subsequently with DMF, DCM and then DMF. To block the unreacted/uncoupled animo groups in the resin, acetyl capping was performed using DMF:Ac_2O:DIEA (8.5:1.0:0.5) for 5 minutes at room temperature, washed with DMF, DCM and then DMF, then Fmoc deprotection using 20% piperidine in DMF followed by washing with DMF, DCM and then DMF and the cycle repeated for six (6) times. After Fmoc deprotection of the last Fmoc-His(trt)-OH, 5-oxohexanoic acid was pre-activated using 4 equivalents of HBTU, 4 equivalents of HOBt in DMF and 3 equivalents of DIEA for 30 seconds. The pre-activated 5-oxohexanoic acid was then added to the peptide-resin mixture and allowed to couple for 15 minutes at 50°C under microwave irradiation. The mixture was washed subsequently with DMF, DCM and then DMF. Deprotection and cleavage of the peptide from the resin was done by adding TFA:EDT:H_2O (95:2.5:2.5) cocktail to the washed resin in ice for 30 minutes with shaking and then the shaking was continued at room temperature for additional 1 hour. The deprotection and cleavage processes were monitored using MALDI-TOF/MS. The solution containing the synthesized peptide was drained. The resin was flushed subsequently with the same cocktail solution, acetic acid, and methanol. The filtrates were combined and concentrated by air drying, dissolved in 50% acetonitrile and lyophilized. The peptide was then purified using RP-HPLC with acetonitrile (B) and water (A) both with 0.1% TFA using Intersil® ODS-3 (5 µm, 4.6 x 250 mm) column at room temperature, 1 ml/min flow

rate, 220 nm wavelength for detection, and solvent gradient (A:B) of 90:10 (0 min), 70:30 (50 mins), and 5:95 (60 mins) to get k-His_6 (t = 5.4 mins) and then lyophilized. HRMS (MALDI): *m/z* calcd for $C_{42}H_{54}N_{19}O_8^+$, $[M+H]^+$ 952.4405, found 952.4401.

Preparation of AO/PCSAM-QDs. To the 50 μL of 1 μM TOPO-QDs were added Isopropanol:Methanol (100 μL:50 μL), then centrifuged at 15,000 g for 3 minutes. The solvent was removed and the pelleted TOPO-QDs were re-suspended in 50 μL *n*-hexane and homogenized by sonication. TOPO-QDs/*n*-hexane solution was added with 30 μL of Milli Q water, 1 μL of $NaBH_4$ (12 wt % in 14 N NaOH), 5 μL of 5 mM 11,11'-dothio bis[undec-11-yl 12-(aminooxyacetyl)amino hexa(ethyleneglycol)] (HS-ao)[12c] and 10 μL of 50 mM 11-mercaptoundecylphosphorylcholine (HS-PC). The mixture was mixed for 30 minutes at room temperature. The *n*-hexane layer containing TOPO were removed, and washed three times with hexane. The water layer containing AO/PCSAM-QDs was purified using ultra filtration (YM 10) and washed with ultrapure water (400 μL) three times. The AO/PCSAM-QDs solution was directly analyzed by MALDI-TOFMS (Bruker Daltonics, Bremen, Germany) using DHB (1 μL, 10 mg/mL) as a matrix.

Conjugation of QDs with ketone-functionalized derivatives. To the 10 μL of AO/PCSAM-QDs solution was added 1 μL of 10 mM ketone-functionalized peptides/glycopeptides and 1 μL of 10 mM ketone-functionalized glycopeptide mixed thoroughly with 1 μL of 10 mM *k*-His_6. The mixture was added with 10 μL of 200 mM acetate buffer (pH 4.0), mixed for 15-30 minutes at room temperature and concentrated to dryness by centrifugal evaporator, to complete the oxime formation reaction, for 30 minutes at 40°C. The obtained solid was resuspended in Milli Q, purified using ultra filtration (YM 10) and washed with Milli Q (400 μL) three times. The products AO/PCSAM-QDs co-displaying the glycopeptide and His_6, AO/PCSAM-QDs carrying glycopeptides, AO/PCSAM-QDs carrying His_6 and AO/PCSAM-QDs carrying Arg_6 were

dissolved in Milli Q (10 μL) to obtain 1 μM solution. The samples were directly analyzed by MALDI-TOF/MS using DHB (1 μL, 10 mg/mL) as a matrix.[12c]

Cell Culture. NHAC-Kn (Kurabo Inc.), A549 (Health Science Research Resource Bank), HT-29 (American Type Culture Collection) and HepG2 (RIKEN cell bank) cell lines were grown in Dulbecco's Modified Eagle Medium (DMEM), PC-3 cells (Health Science Research Resource Bank) were grown in RPMI-1640 and OUS-11 (Health Science Research Resource Bank) were grown in MEM at 37°C with 5% CO_2. All media used were supplemented with 10% (v/v) FBS, Penicillin G (500 units/mL) and Streptomycin (500 unit/mL).

Cell Uptake Mechanism of QDs carrying His_6. Endocytic incorporation of AO/PCSAM-QDs carrying His_6 or Arg_6 were performed by incubating them with cells ($5x10^3$ cells/well) on an 8-well Nunc Lab-Teck II Chamber Slide System (ThermoScientific™). Images of cellular uptake after 2 h co-incubation with QD conjugates at different endocytic inhibition conditions were observed by fluorescence microscopy as follows: (a) Low temperature incubation: Cells were incubated with AO/PCSAM-QDs carrying His_6 in serum-free opti-MEM (Invitrogen) at 4ºC for 2 hours, followed by washing with PBS at 4ºC prior to fluorescence analysis. (b) Hypertonic incubation: The cells were pre-incubated with PBS supplemented with 0.45 M sucrose for 30 min at 37ºC prior to QDs co-incubation. (c) K^+ depletion treatment: K^+ depletion was achieved by pre-incubation of the cells in the K^+-free HEPES (HEPES-K^+) for 1 h and then rinsing in the hypotonic buffer (HEPES-K^+ diluted 1:1 with distilled water) for 5 min. The cells were then quickly washed with HEPES-K+ buffer three times and incubated in that buffer for 10 mins at 37ºC. After K^+ depletion treatment, the cells were incubated with QDs in HEPES-K^+.

Microarray. Boc-protected aminooxy coated slide was deprotected using 2M HCl for 2 hours at 37ºC, washed 3x with ultrapure water and centrifuged at 2000 rpm for 2 minutes to dry. Different concentrations of heparin, *k*-His_6 and ketone-functionalized glycopeptide, previously prepared using 50 mM AcOH reaction buffer, were machine platted onto the slide by BioChip-Arrayer machine (LASER TECHNO Co., Ltd.), incubated at 80ºC for 1 hour, washed with water 3 times, and dried using centrifuge. The unreacted aminooxy groups were capped with succinic anhydride for 2 hours at 37ºC, washed and dried. Heparin (Sigma-Aldrich) was added and allowed to interact at 37ºC for 2 hours. Slide was washed with washing buffer, containing 0.05 wt %Triton X-100, 3 times followed by water. Mouse anti-heparin/heparin sulphate IgG antibody (Millipore) was added, incubated for 2 hours at room temperature or at 4ºC overnight and washed subsequently with washing buffer and water 3 times. Secondary anti-body anti-IgG mouse Cy3 (Funakoshi, Japan) was added, allowed to react in the dark for 2 hours at room temperature or at 4ºC overnight and washed with washing buffer 3 times. The slide was analyzed using GE Typhoon $TRIO^+$ variable mode imager (Amersham Biosciences).

Intracellular trafficking of QD conjugates. All cellular internalization experiments were performed on an 8-well Nunc Lab-Tek II Chamber Slide System (Thermo Scientific™). Cells ($5x10^3$ cells/well) were seeded in the wells and cultured overnight. For the uptake and delivery experiments, QD-conjugates were diluted with the complete culture medium and incubated with cells at 37ºC with 5% CO_2 for 2 hours. For assessing lysosomal colocalization, the QD-conjugates were incubated with cells for 5 minutes or 2 hours and cells were stained with lysosomal marker LysoTracker Red DND-99 (Invitrogen). The nuclei were stained with Hoechst 33342 (Invitrogen) and observed under fluorescence microscope. For the golgi colocalization assessment, the incubation was only up to 2 hours. The excess QD-conjugates were removed by washing the cells with DPBS three times. The cells were then fixed with 4% paraformaldehyde for 10 minutes at 4ºC or

in ice, permeabilized with 0.4% Triton X-100 and washed. The cells were then incubated with the golgi marker anti-giantin antibody [9B6] mouse IgG1 (abcam), as the primary antibody, for 1 hour at room temperature or overnight at 4ºC, washed with DPBS three times and then incubated with secondary anti-body anti-IgG mouse Cy3 (Funakoshi, Japan) for 30 minutes to 1 hour at room temperature. The nuclei were stained with Hoechst 33342 (Invitrogen), as the final hybridization process, and observed under fluorescence microscope.

Fluorescence Microscopy and Imaging Study. The fluorescence microscope used for image acquisition and image analysis was an all-in-one fluorescence microscope BIOREVO BZ-9000 series generation II (Keyence, Japan) equipped with 4x, 20x, 40x, and 60x (oil immersion) lenses. Images were taken using standard filter set for DAPI (for Hoechst), FITC (for QD545) and TRITC (for anti-mouse IgG-Cy3). Merge images were generated and analyzed using BZ-II software. FCS measurement was performed by using LSM510 META Confocor 2 (Carl Zeiss Inc., Germany).

Cytotoxicity of QD conjugates. NHAC-Kn, HepG2, HT-29, A549, OUS-11 and PC-3 cells were seeded in a 96-well plate (Thermo Scientific), at $5.0x10^3$ cells/well, and incubated at 37ºC with 5% CO_2 for 24 hours. The cells were treated with *k*-His_6, ketone-functionalized glycopeptide, AO/PCSAM-QDs carrying His_6, and AO/PCSAM-QDs co-displaying glycopeptides and His_6 for 24 hours. Cell growth was determined by adding 10 µL of cell counting kit 8 (Dojindo, Kumamoto, JAPAN), incubated for 2-4 hours and optical density was measured using a model 550 Microplate reader (BioRad, Hercules, CA, USA). Data were reported in terms of percent viability with respect to the untreated control (± SEM) of the trials (n = 3).

2.4 References

1. Chang, Y.-P.; Pinaud, F.; Antelman J.; Weiss, S. *J. Biophoton.* **2008**, 1, 287-298.
2. (a) Brandenburg, B.; Zhuang, X. *Nat. Rev. Microbiol*. **2007**, 5, 197-208. (b) Wu, X.; Liu, H.; Liu, J.; Haley, K. N.; Treadway, J. A.; Larson, J. P.; Ge, N.; Peale, F.; Bruchez, M. P. *Nat. Biotechnol*. **2003**, 21, 41-46.
3. (a) Zhong, X.H.; Feng, Y. Y.; Knoll, W.; Han, M. Y. *J. Am. Chem. Soc.* **2003**,125, 13559–13563 (b) Bailey, R. E.; Nie, S. M. *J. Am. Chem. Soc*. **2003**, 125:7100–7106.
4. (a) Pinaud, F.; Clarke, S.; Sittner, A.; Dahan, M. *Nat. Methods* **2010**, 7, 275-285. (b)Alivisatos, A. P.; Gu, W.; Larabell, C. A. *Ann. Rev. Biomed. Eng*. **2005**, 7, 55-76. (c) Parak, W.; Pellegrino, T.; Plank, C. *Nanotechnology* **2005**, 16, R9-R25.
5. (a) Li, F.; Zhang, Z.; Peng, J.; Cui, Z.; Pang, D; Li, K.; Wei, H.; Zhou, Y.; Wen, J.; Zhang, X. *Small* **2009**, 5:718–726. (b) Joo, K-l.; Fang, Y.; Liu, Y.; Xiao, L.; Gu, Z.; Tai, A.; Lee, C-L.; Tang, Y.; Wang, P. *ACS Nano*. **2011**, 5, 3523-3535.
6. (a) Dahan, M.; Lévi, S.; Luccardini, C.; Rostaing, P.; Riveau, B.; Triller, A. *Science* **2003**, 302 (5644), 442-445. (b) Groc, L.; Lafourcade, M.; Heine, M.; Renner, M.; Racine, V.; Sibarita, J-B.; Lounis, B.; Choquet, D.; Cognet, L. *J. Neurosci.* **2007**, 27 (46), 12433-12437.
7. (a) Chen, X.; Kis, A.; Zettl, A.; Bertozzi, C. R. *Proc. Natl. Acad. Sci. U.S.A.* **2007**, *104*, 8218–8222. (b) Michalet, X.; Pinaud, F. F.; Bentolila, L. A.; Tsay, J. M.; Doose, S.; Li, J. J.; Sundaresan, G.; Wu, A. M.; Gambhir, S. S.; Weiss, S. *Science* **2005**, 307 (5709): 538-544. (c) Delehanty, J. B.; Mattoussi, H,; Medintz, I. L. *Anal. Bioanal. Chem.* **2009**, 393 (4): 1091-1105.

8. (a) Xue, F. L.; Chen, J. Y.; Guo, J.; Wang, C. C.; Yang, W. L.; Wang, P. N.; Lu, D. R. *J. Fluoresc.* **2007**, 17(2):149-154. (b) Koshman, Y. E.; Waters, S. B.; Walker, L. A.; Los, T.; de Tombe, P.; Goldspink, P. H.; Russell, B. *J. Mol. Cell Cardiol.* **2008**, 45, 853-856.

9. Gill, R.; Willner, I.; Shweky, I.; Banin, U. *J. Phys. Chem. B* **2005**, 109, 23715–23719.

10. Han, H.-S.; Devaraj, N. K.; Lee, J.; Hilderbrand, S. A.; Weissleder, R.; Bawendi, M. G. *J. Am. Chem. Soc*. **2010**, 132, 7838–7839.

11. (a) Cai, W.; Shin, D. W.; Chen, K.; Gheysens, O.; Cao, Q.; Wang, S. X.; Gambhir, S. S.; Chen, X. *Nano lett*. **2006**, 6, 669– 676. (b) Ruan, G.; Agrawal, A; Marcus, A. I.; Nie, S. *J. Am. Chem. Soc*. **2007**, 129, 14759–14766.

12. (a) De la Fuente, J. M.; Penades, S. *Tetrahedron Asymm*. **2005**, 16, 387–391. (b) Robinson, A.; Fang, J. M.; Chou, P. T.; Liao, K. W.; Chu., R. M.; Lee., S. *J. ChemBioChem.* **2005**, 6, 1899–1905. (c) Ohyanagi, T.; Nagahori, N.; Shimawaki, K.; Hinou, H.; Yamashita, T.; Sasaki, A.; Jin, T.; Iwanaga, T.; Kinjo, M.; Nishimura, S-I. *J. Am. Chem. Soc*. **2011**, 133, 12507–12517.

13. Smith, A.; Duan, H.; Mohs A.; Nie, S. *Adv. Drug Delivery Rev*. **2008**, 60, 1226–1240.

14. (a) Jaiswal, J. K.; Mattoussi, H.; Mauro J. M.; Simon, S. M. *Nat. Biotechnol*. **2003**, 21, 47–51. (b) Delehanty, J.B.; Bradburne, C.E.; Boeneman, K.; Susumu, K.; Farrell, D.; Mei, B. C.; Blanco-Canosa, J.B.; Dawson, G.; Dawson, P. E.; Mattoussi, H.; Medintz, I. L. *Integr. Biol*. **2010**, 2, 265-277.

15. (a) Probst, C. E.; Zrazhevskiy, P.; Bagalkot, V.; Gao, X. *Adv. Drug Deliver. Rev.* **2013**, 65, 703-718. (b) Jensen, K. D.; Nori, A.; Tijerina, M.; Kopeckova, P.; Kopecek, J. *J. Control. Release* **2003**, 87, 89-105. (c) Harush-Frenkel, O.;

Debotton, N.; Benita, S.; Altschuler, Y. *Bochem. Biophys. Res. Commun*. **2007**, 353, 26-32.

16. Chen, B.; Liu, Q.; Zhang, Y.; Xu, L.; Fang, X. *Langmuir* **2008**, 24, 11866-11871.
17. Stewart, K. M.; Horton, K. L.; Kelley, S. O. *Org. Biomol. Chem.* **2008**, 6, 2242-2255.
18. (a) Chen, C.P.; Chou, J.C.; Liu, B.R.; Chang, M.; Lee, H. J. *FEBS Lett.* **2007**, 58, 1891-1897. (b) Liu, B. R.; Li, J. F.; Lu, S. W.; Lee, H. J.; Huang, Y. W.; Shannon, K. B.; *et al*. *J. Nanosci. Nanotechnol.* **2010**, 10, 6534-6543.
19. (a) Jiao, C. Y.; Delaroche, D.; Burlina, F.; Alves, I. D.; Chassaing, G.; Sagan, S. *J. Biol. Chem.* **2009**, 284, 33957-33965. (b) Kawamura, K. S.; Sung, M.; Bolewska-Pedyczak, E.; Gariepy, J. *J. Biochemistry* **2006**, 45, 1116-1127. (c) Fervari, A.; Pellegrini, V.; Arcangeli, C.; Fittipaldi, A.; Giacca, M.; Beltram, F. *Mol. Ther.* **2003**, 8, 284-294. (d) Wadia, J. S.; Stan, R. V.; Dowdy, S. F. *Nat. Med.* **2004**, 10, 310-315. (e) Thurn, K. T.; Brown, E. M. B.; Wu, A.; Vogt, S.; Lai, B.; Maser, J.; Paunesku, T.; Woloschak, G. E. *Nanoscale Res. Lett*. **2007**, 2, 430-441.
20. Boonyarattanakalin, S.; Athavankar, S.; Sun, Q.; Peterson, B.R. *J. Am. Chem. Soc*. **2006**, 128, 386-387.
21. June, R.K.; Gogoi, K.; Eguchi, A.; Cui, X-S.; Dowdy, S.F. *J. Am. Chem. Soc*. **2010**, 132, 10680–10682.
22. Gaspar, V.M.; Marques, J.G.; Sousa, F.; Louro, R.O.; Queiroz, J.A.; Correia, I. J. *Nanotechnology* **2013**, 24, 275101 (16pp)
23. Chang, K-L.; Higuchi, Y.; Kawakami, S.; Yamashita, F.; Hashida, M. *Journal of Controlled Release* **2011**, *156*, 195–202.

24. Moreira, C.; Oliveira, H.; Pires, L.R.; Simões, S.; Barbosa, M.A.; Pêgo, A.P. *Acta Biomaterialia* **2009**, *5*, 2995–3006

25. (a) Gopal, V. *J. Control. Release* **2013**, 167, 323–332. (b) Pujals, S.; Fernandez-Carneado, J.; Lopez-Iglesias, C.; Kogan, M. J.; Giralt, E. *Biochim. Biophys. Acta* **2006**, 1758, 264-279.

26. Chen, S.; Zheng, J.; Li, L.; Jiang, S. *J. Am. Chem. Soc*. **2005**, 127, 14473-14478.

27. Hoshi, H.; Shimawaki, K.; Takegawa, Y.; Ohyanagi, T.; Amano, M.; Hinou, H.; Nishimura, S-I. *Biochim. Biophys. Acta* **2012**, 1820, 1391-1398.

28. Shimawaki, K.; Fujisawa, Y.; Sato, F.; Fujitani, N.; Kurogochi, M.; Hoshi, H.; Hinou, H.; Nishimura, S-I. *Angew. Chem. Int. Ed.* **2007**, 46, 3074-3079.

29. Garcia-Martin, F.; Hinou, H.; Matsushita, T.; Hayakawa, S.; Nishimura, S-I. *Org. Biomol. Chem*. **2012**, 10, 1612-1617.

30. Nagahori, N.; Abe, M.; Nishimura, S-I. *Biochemistry* **2009**, 48, 583-594.

31. Liu, B.R.; Huang, Y-W.; Winiarz, J. G.; Chiang, H. J.; Lee, H. J. *Biomaterials* **2011**, *32*, 3520-3537.

32. Sanchez-Quesada, J.; Seel, C.; Prados, P.; de Mendoza, J.; Dalcol, I.; Giralt, E. *J. Am. Chem. Soc*. **1996**, 118, 277–278.

33. Salvatella, X.; Martinell, M.; Gairi, M.; Mateu, M.G.; Feliz, M.; Hamilton, A.D.; de Mendoza, J.; Giralt, E. *Angew. Chem. Int. Ed.* **2003**, 43, 196–198.

34. Fernandez-Carneado, J.; Van Gool, M.; Martos, V.; Castel, S.; Prados, P.; De Mendoza, J.; Giralt. E. *J. Am. Chem. Soc*. **2005**, 127, 869–874.

35. Kam, N. W. S.; Liu, Z.; Dai, H. *Angew. Chem. Int. Ed.* **2006**, 45, 577-581.

36. Maniti, O.; Blanchard, E.; Trugnan, G.; Lamaziére, A.; Ayala-Sanmartin, J. *Int. J. Biochem. Cell B.* **2012**, 44, 869-875.

37. Puri, V.; Watanabe, R.; Singh, R. D.; Dominguez, M.; Brown, J. C.; Wheatley, C. L.; Marks, D. L.; Pagano, R. E. *J. Cell Biol*. **2001**, 154, 535-547.

38. Stern, S.T.; Adiseshaiah, P. P.; Crist, R. M. *Part. Fiber Toxicol.* **2012**, 9:20.

39. Rinne, J.; Albarran, B.; Jylhävä, J.; Ihalainen, T. O.; Kankaanpää, P.; Hytönen, V. P.; Stayton, P. S.; Kulomaa, M. S.; Vihinen-Ranta, M. *BMC Biotechnol.* **2007**, 7, 1-14.

40. Luo, D.; Saltzman, W. M. *Nat. Biotechnol*. **2000**, 18, 33-37.

41. Alves, I. D.; Bechara, C.; Walrant, A.; Zaltsman, Y.; Jiao, C. Y.; Sagan, S. *PLoS ONE* **2011**, 6, e24096.

42. Mattoussi, H.; Mauro, J. M.; Goldman, E. R.; Anderson, G. P.; Sundar, V. C.; Mikulec, F. V.; Bawendi, M. G. *J. Am. Chem. Soc*. **2000**, 122, 12142–12150.

43. Kroemer, G.; Jaattela, M. *Nat. Rev. Cancer* **2005**, 5, 886-897.

44. Yanagishita, M.; Hascall, V.C. *J. Biol. Chem.* **1992**, 267, 9451-9454.

45. (a) Fuchs, S. M.; R. T. *Biochemistry* **2004**, 43, 2438-2444. (b) Gonçalves, E.; Kitas; Seelig, J.; *Biochemistry* **2005**, 44, 2692-2702.

Chapter 3

Effect of Glycosylation on Intracellular Trafficking of Synthetic Peptides

3.1 Introduction

Protein glycosylation is one of the most common post-translational modifications employed by biological systems to expand proteome diversity.[1-3] Glycosylation is evolutionarily found to occur in proteins through the main domains of life[4,5] and has been shown to influence a variety of critical biological processes such as protein folding, stability, trafficking, localization, and protein–protein binding, with important implications for cell-cell interactions, intracellular signalling and intracellular targeting.[6,7] The specific conformational changes in the protein backbone as a consequence of protein glycosylation,[8-12] could alter the overall structure of protein and potentially change the functions, intracellular route, and recognition of proteins that are either exogenously incorporated or endogenously expressed in cells. Therefore, it is not surprising that a substantial fraction of the approved protein pharmaceuticals need to be properly glycosylated to exhibit optimal therapeutic efficacy.[13,14]

Glycans associated with cell surface receptors and proteins not only alter the dynamics of glycoprotein endocytosis but also their cell surface half-life through binding to multivalent lectins.[15] Glycan structures on newly synthesized proteins are crucial for protein secretion, as they influence protein folding, provide ligands for lectin chaperones, contribute to quality control surveillance in the endoplasmic reticulum (ER) and mediate transit, trafficking, and selective protein targeting throughout the secretory pathway.[16,17] Hence, in the presence of glycans, a therapeutic molecule or protein could potentially be trafficked inside the cell differently.

Cells sort biological molecules and regulate their entry, production, and release, depending on the cell's microenvironment demands, through intracellular trafficking. Reliable intracellular traffic is a prerequisite of a successful cellular processes.[18] Biological molecules are trafficked to distinct cellular compartments through both biosynthetic and endocytic pathways. Delivering pharmacological agents to cells via this endocytic pathway requires

knowledge and understanding of the trafficking itinerary and the molecular dynamics of the organelles concerned.[19-22] These pathways are vital to pave the way in understanding intracellular drug delivery and give insights into the real-time dynamics of exogenous molecules, including nanoparticle-based delivery of therapeutic agents, as they are delivered into and traffic within single cell.[23,24]

Despite emerging importance of quantum dot (QD)-based delivery of peptides[25,26] and glycans,[27-29] which are promising tools both in general cell biology and discovery research for diagnostic/therapeutic agents, there are no direct, systematic, and substantial studies on the direct evidence of intracellular sorting/trafficking mechanisms between peptides and glycopeptides, as well as the differences in their intracellular incorporation on both normal and cancer human cell lines.

In this study, differences in intracellular localization and trafficking of serglycin-like peptides and glycopeptides in both normal and cancer human cell lines were investigated. QD-based delivery of serglycin-like peptides and glycopeptides were performed to observe the differences in intracellular localization mechanism.

3.2 Results and Discussion

Both peptides and glycopeptides sequences used in this study were serglycin-like synthetic peptides and glycopeptides (Figure 3.1).[18,30] These were tetrapeptide composed of H-Ser[1]-Gly[2]-Ser[3]-Gly[4] (compound **1**) and tetrapeptide with Galβ(1-4)Xylβ1- (compound **2**), where the sugar moieties were attached to the third amino acid serine, as well as the corresponding hexamer of tetrapetide (compound **3**), and hexamer of tetrapeptide with Galβ(1-4)Xylβ1- (compound **4**, same glycopeptides in Chapter 2). This sequence was based from its reported acceptability as a new class of synthetic proteoglycan initiator (PGI).[18,23]

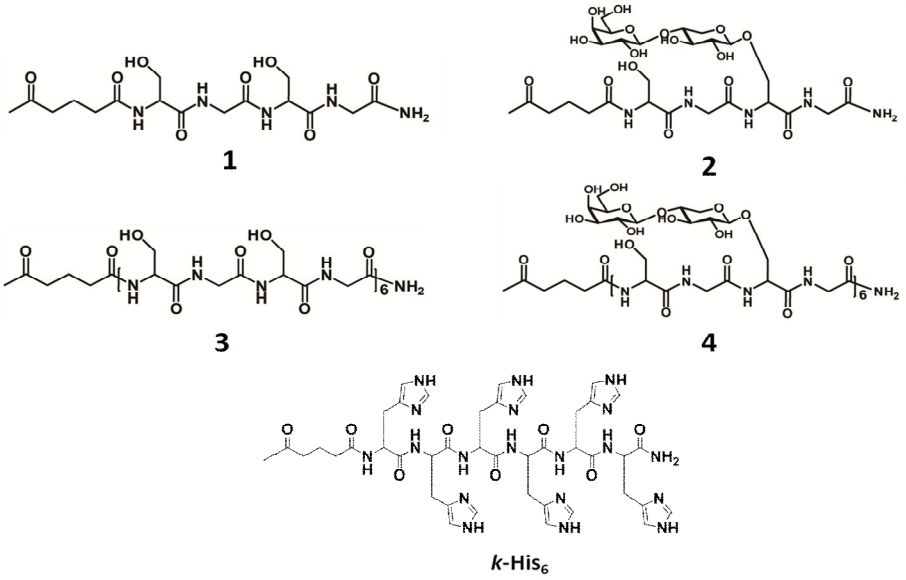

Figure 3.1. Peptides and glycopeptides sequences and structures.

The list of their high resolution masses, from MALDI-TOF/MS spectra of the synthesized peptides and glycopeptides shown in Figures 3.2-3.5, were summarized in Table 3.1, while their HPLC chromatograms were on Figures 3.6-3.9.

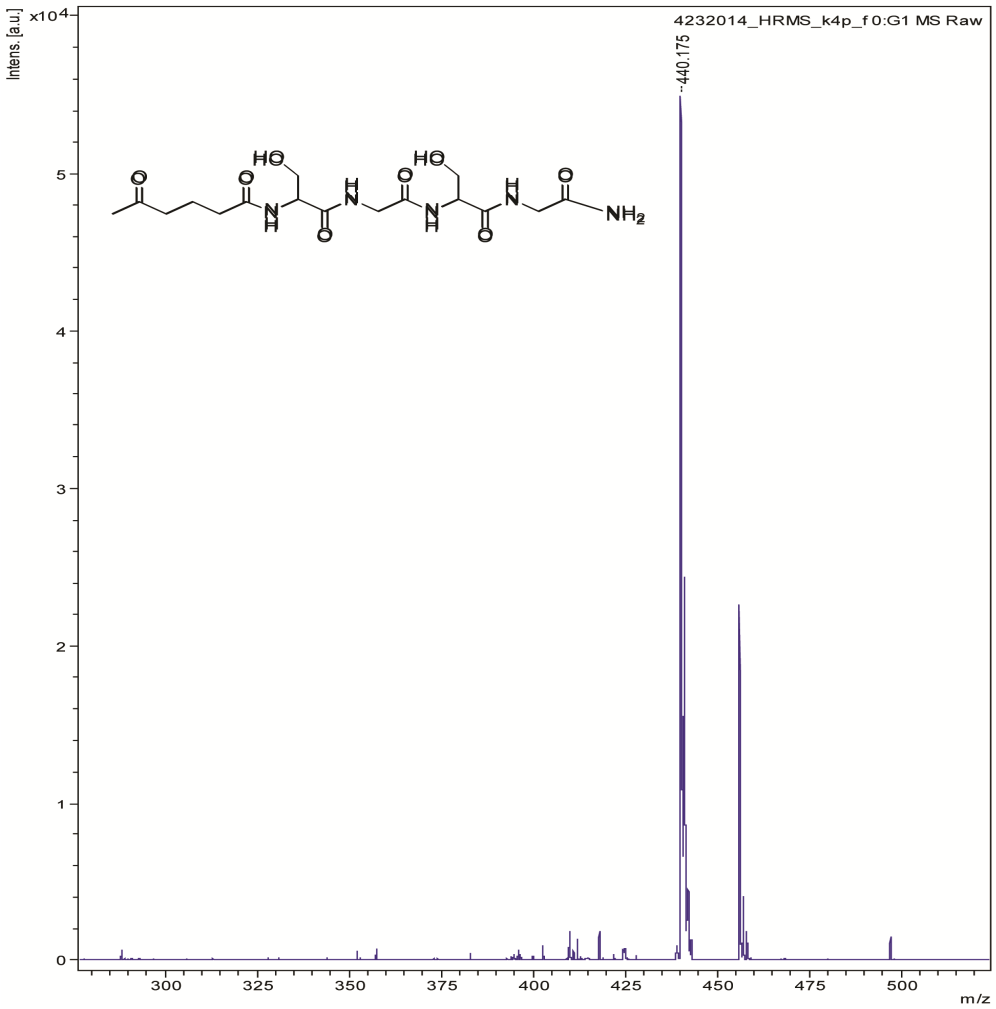

Figure 3.2. Structure and high resolution MALDI-TOFMS of compound **1**.

After the ketone-functionalized synthetic peptides or glycopeptides were successfully synthesized, isolated, and characterized, they were then co-displayed onto AO/PCSAM-QD surface together with *k*-His_6 (Figure 3.10, see Chapter 2 for *k*-His_6 and AO/PCSAM-QD characterizations). The resulting QD conjugates were characterized using MALDI-TOFMS (Figures 3.11-3.14) and Fluorescence Correlation Spectroscopy (FCS), shown in Figures 3.15-3.18, prior to intracellular delivery.

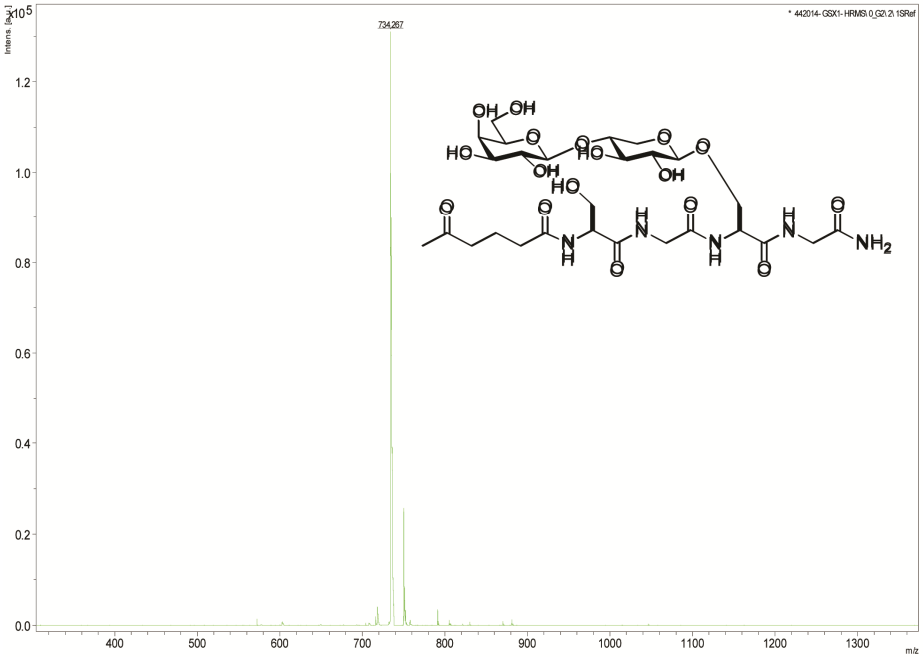

Figure 3.3. Structure and high resolution MALDI-TOFMS of compound **2**.

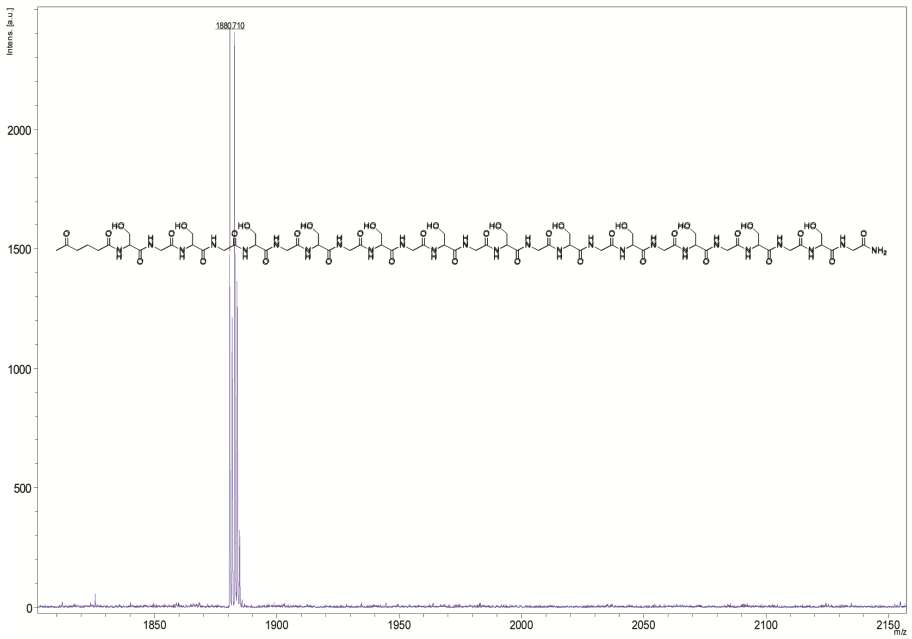

Figure 3.4. Structure and high resolution MALDI-TOFMS of compound **3**.

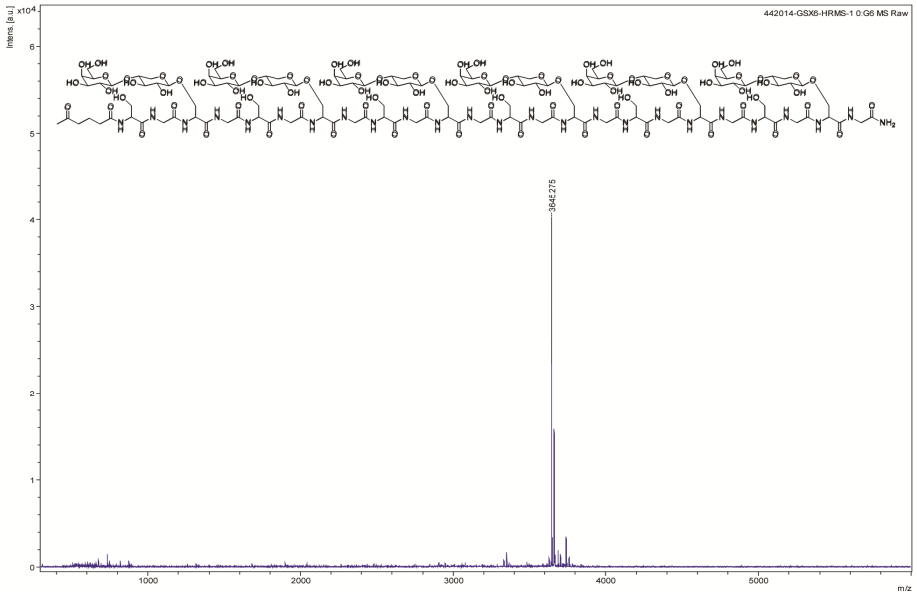

Figure 3.5. Structure and high resolution MALDI-TOFMS of compound **4**.

Table 3.1. List of high resolution masses of compounds **1-4** taken using MALDI-TOFMS.

Compound	Calculated m/z	Measured m/z	Δ m/z	Abundant ion	Error (ppm)
1	440.175729	440.175	0.000729	$[M+Na]^+$	1.65615674
2	734.270819	734.2672	0.003619	$[M+Na]^+$	4.9286992
3	1880.71065	1880.71	0.000649	$[M+Na]^+$	0.34508232
4	3645.28115	3645.275	0.006149	$[M+Na]^+$	1.68683834

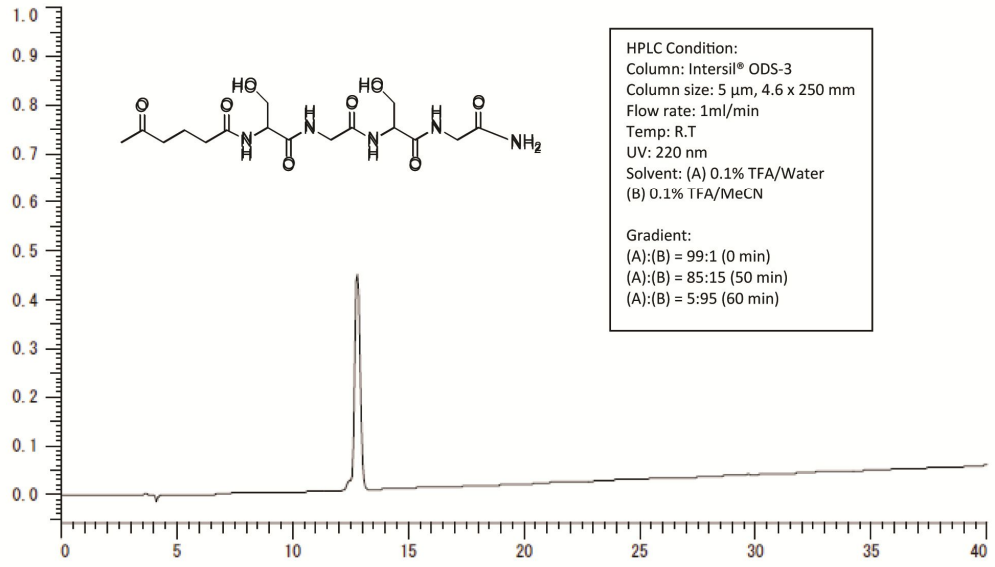

Figure 3.6. Structure and HPLC Chromatogram of compound **1**.

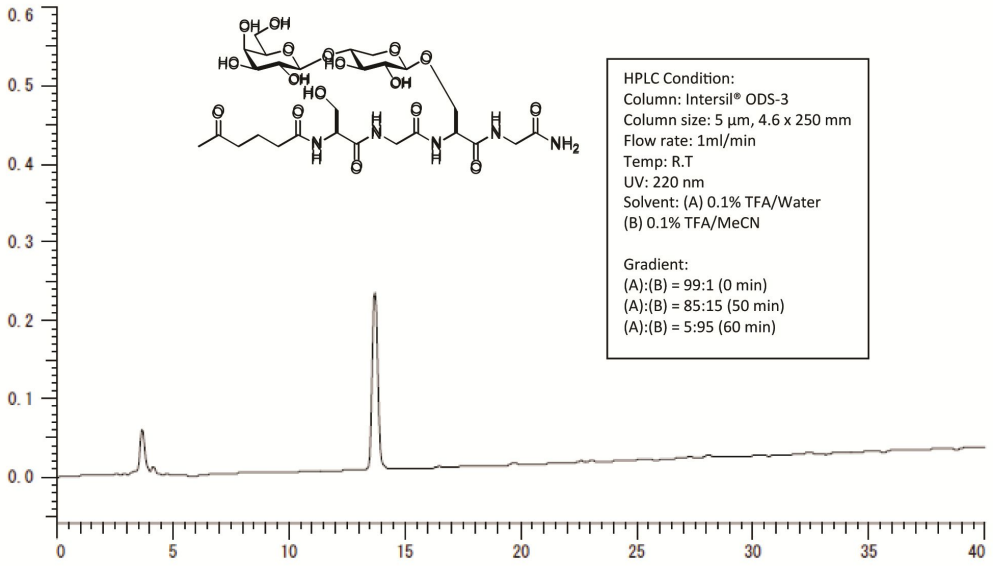

Figure 3.7. Structure and HPLC Chromatogram of compound **2**.

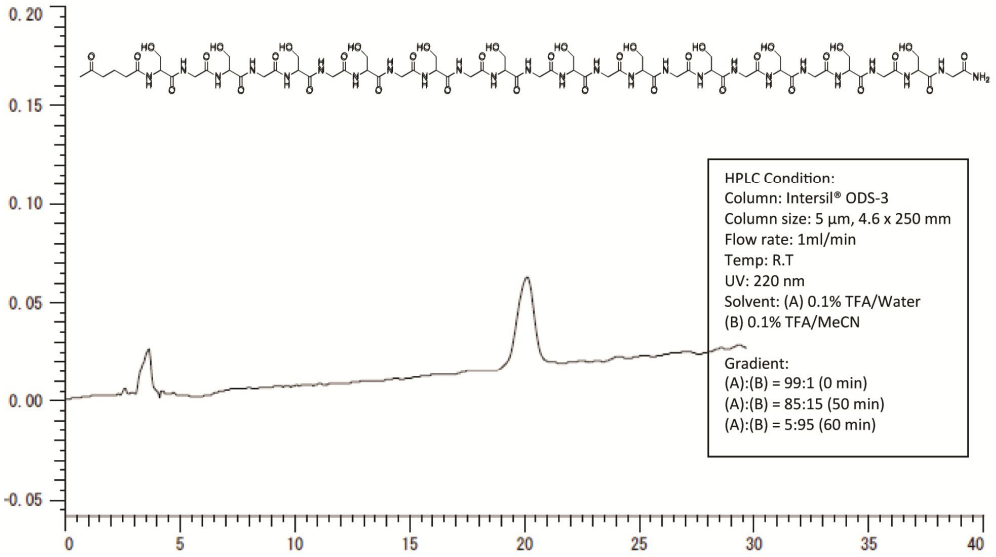

Figure 3.8. Structure and HPLC Chromatogram of compound **3**.

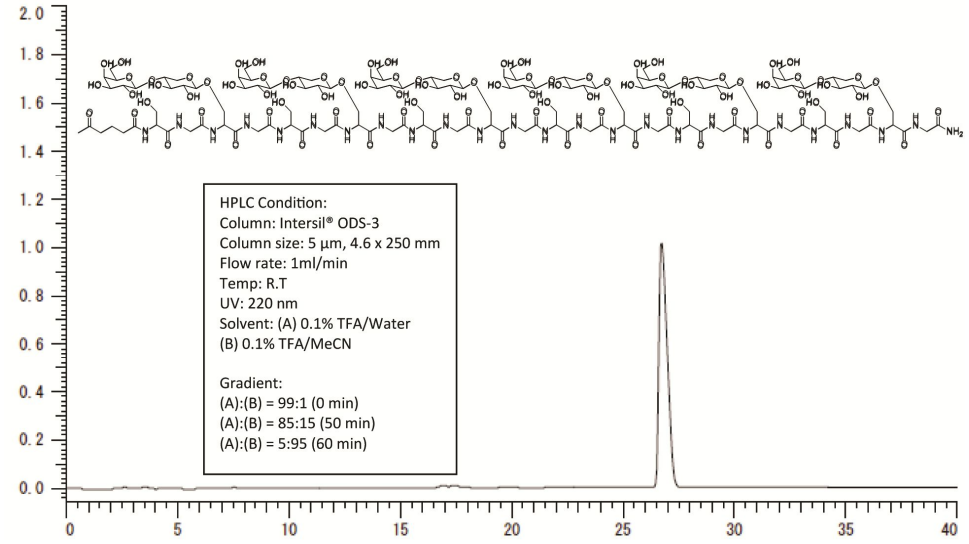

Figure 3.9. Structure and HPLC Chromatogram of compound **4**.

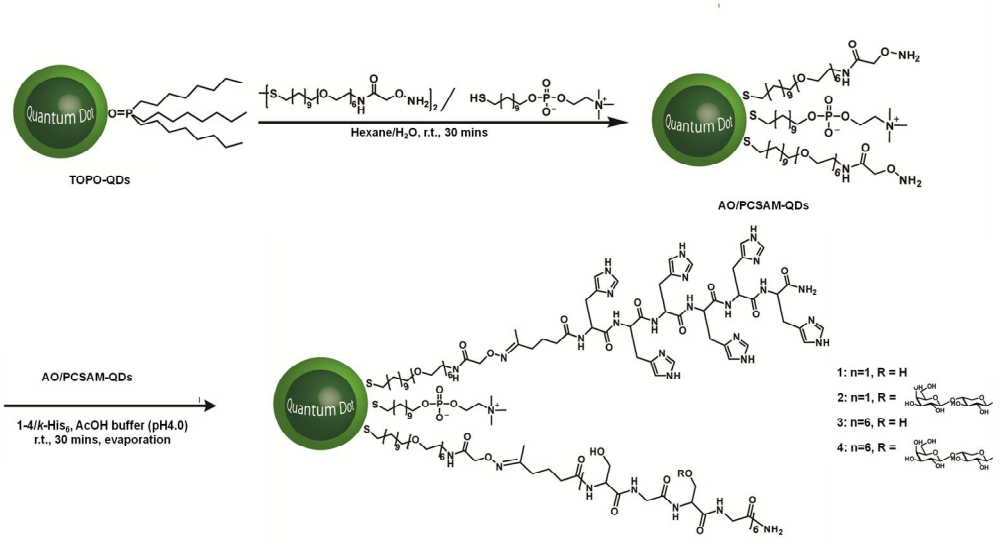

Figure 3.10. General Protocol for the preparation of QD conjugates AO/PCSAM-QD with *k*-His_6 and compounds **1-4**. See chapter 2 for complete characterization of *k*-His_6.

Results have shown that ketone-functionalized synthetic peptides and glycopeptides were successfully co-conjugated and displayed onto the surface of AO/PCSAM-QD as shown in their direct MALDI-TOF/MS spectra.

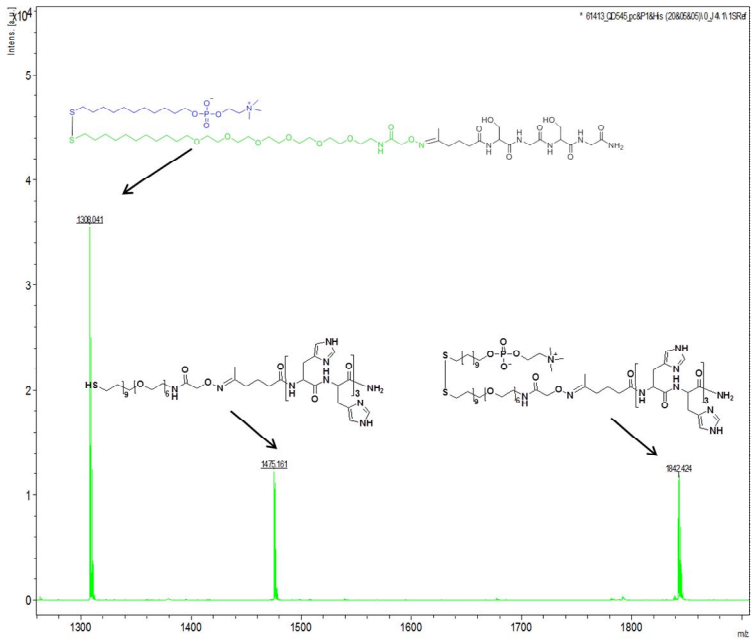

Figure 3.11. Direct MALDI-TOFMS spectra of AO/PCSAM-QD carrying *k*-His_6 and compound **1**.

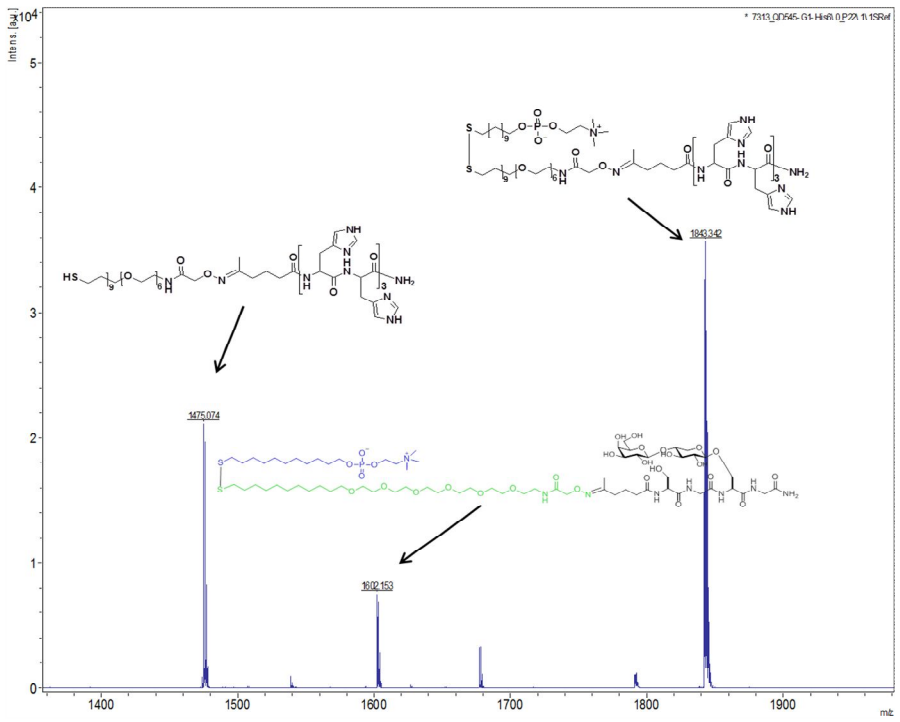

Figure 3.12. Direct MALDI-TOFMS spectra of AO/PCSAM-QD carrying *k*-His_6 and compound **2**.

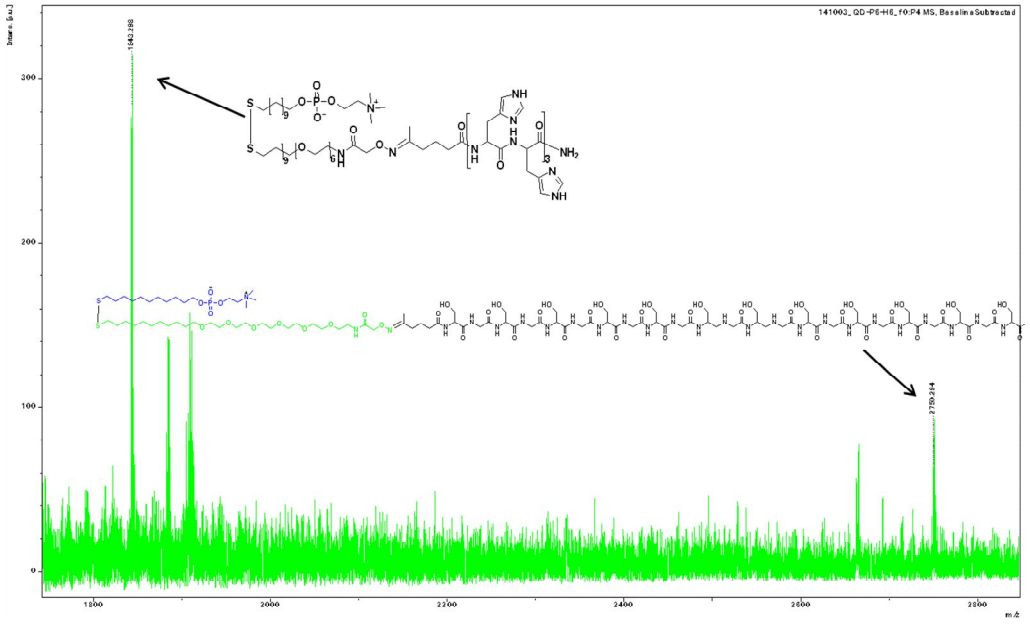

Figure 3.13. Direct MALDI-TOFMS spectra of AO/PCSAM-QD carrying *k*-His_6 and compound **3**.

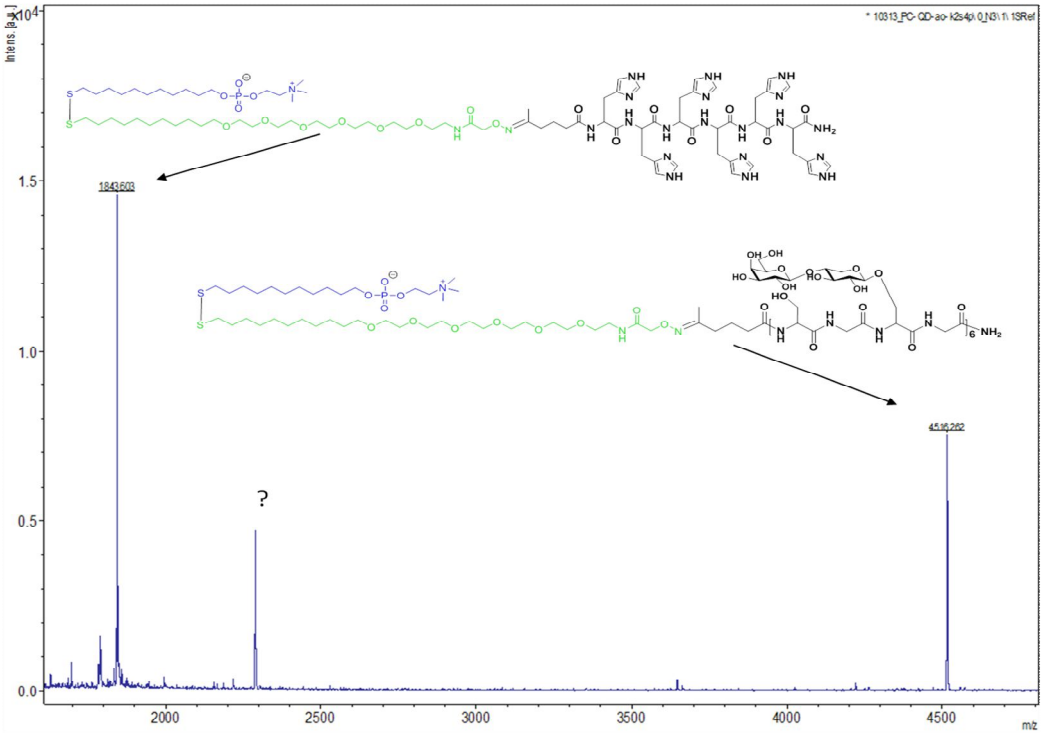

Figure 3.14. Direct MALDI-TOFMS spectra of AO/PCSAM-QD carrying *k*-His_6 and compound **4**.

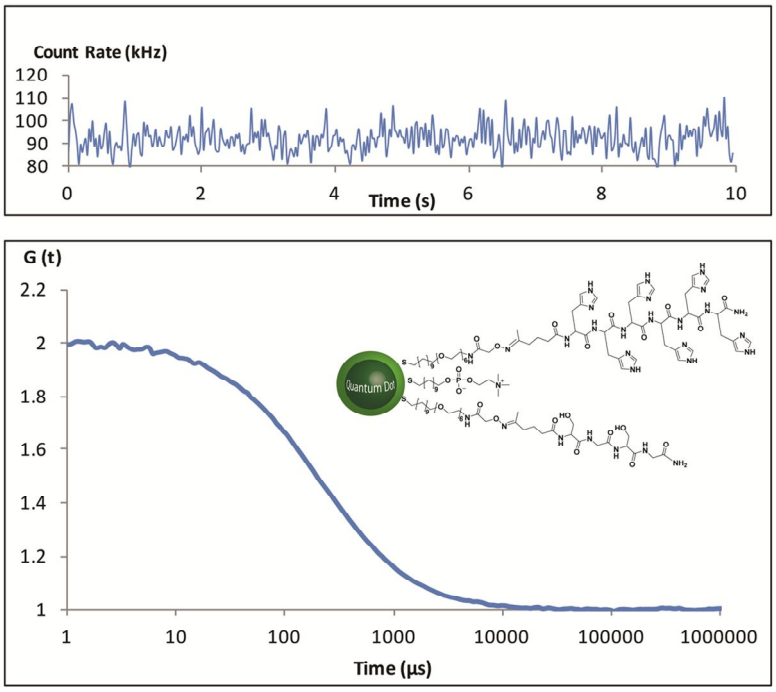

Figure 3.15. Fluorescence correlation profile using FCS of AO/PCSAM-QD carrying *k*-His_6 and compound **1**.

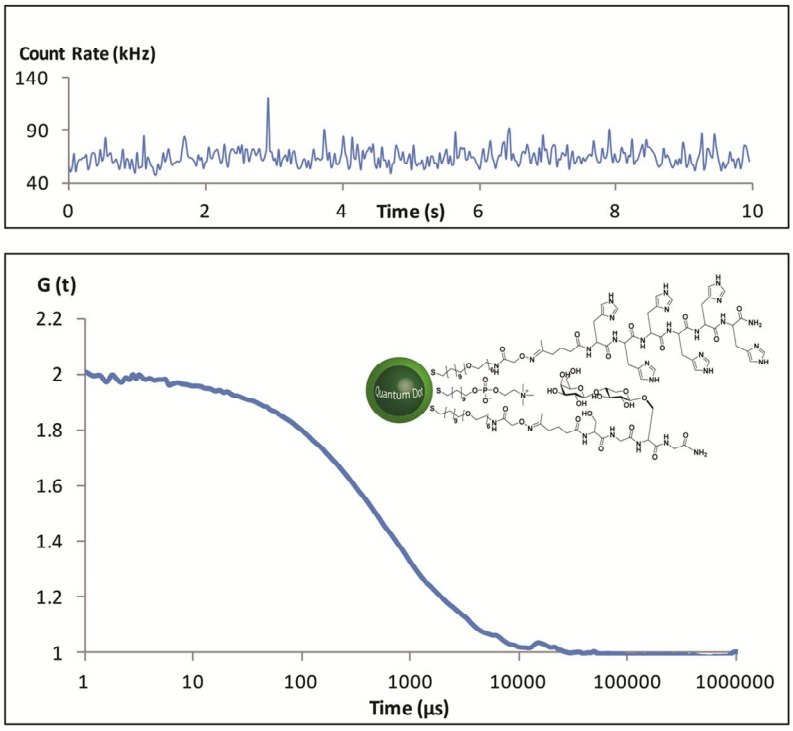

Figure 3.16. Fluorescence correlation profile using FCS of AO/PCSAM-QD carrying *k*-His_6 and compound **2**.

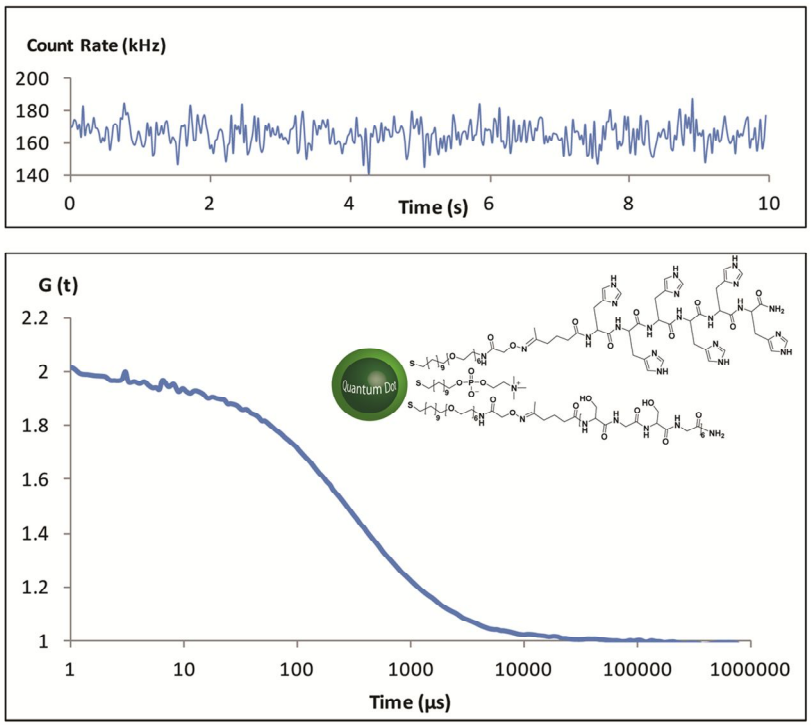

Figure 3.17. Fluorescence correlation profile using FCS of AO/PCSAM-QD carrying *k*-His_6 and compound **3**.

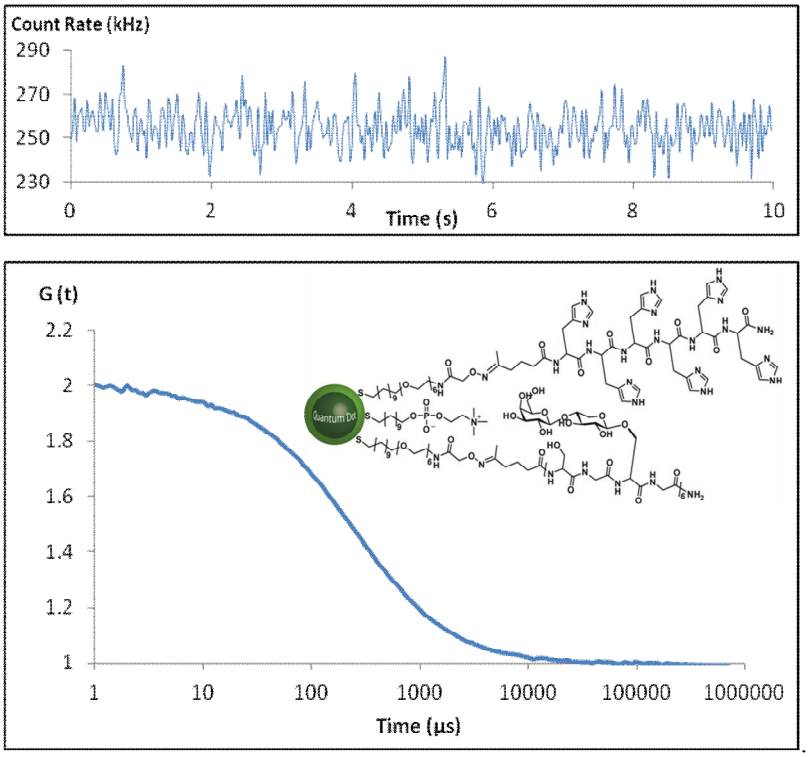

Figure 3.18. Fluorescence correlation profile using FCS of AO/PCSAM-QD carrying *k*-His_6 and compound **4**.

Individual fluorescence correlation spectrum also showed that QD conjugates were highly dispersed in aqueous solution with no observed aggregation, making it highly viable candidate for intracellular delivery experiments. The fluorescence signals of the QD conjugates were also not significantly affected after the conjugation process as shown in their individual fluorescence fluctuation per molecule (Figure 3.19). This unaffected fluorescence signal per molecule is advantageous during QD conjugate detection and tracking inside the cell due to its sustained intensity in fluorescence signal that could be easily detected and classified from the background fluorescence.

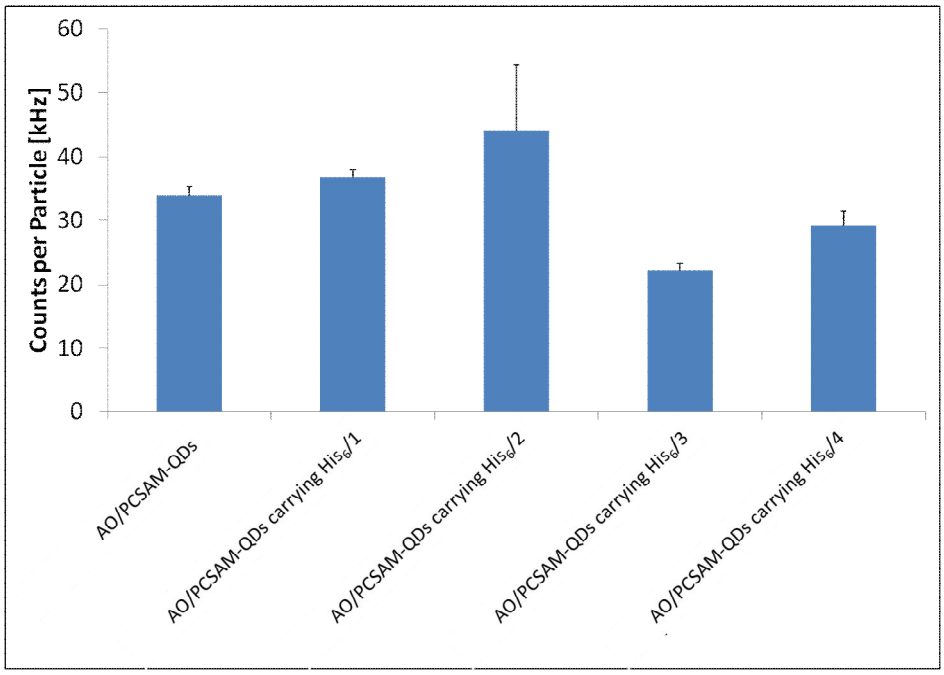

Figure 3.19. Fluorescence intensity per molecule of AO/PCSAM-QDs carrying His6 and compounds **1~4**. Error bar represents SEM.

The intracellular localization of QD conjugates were tracked during co-incubation with normal human articular chondrocyte (NHAC-Kn), normal human lung tissue (OUS-11), human lung adenocarcinoma (A549), human prostate adenocarcinoma (PC-3), human hepatoma (HepG2) and human epithelial colon cancer cells (HT-29). For immunocytochemistry, golgi and nuclear co-localizations were assessed by tagging the golgi apparatus with golgi marker anti-giantin and detected using secondary antibody, while the nuclei were stained with Hoechst.

Results revealed a different dynamics of QD conjugates between diseased (Figure 3.20a) and healthy (Figure 3.20b) human cell lines. In diseased cell lines, A549 cells showed golgi uptake (pointed by white arrows) of all the QD conjugates carrying compounds **1~4**. However, a membrane-bound fluorescence (pointed by red arrows) of QD conjugates carrying compound 2 was evidently observed but not on its naked counterpart (QD conjugates carrying compound **1**). The observation was also true in QD conjugates carrying the hexamer

counterparts of compound **2** (QD conjugates carrying compound **4**) but also not observed in its naked counterpart (QD conjugates carrying compound **3**). It is likely that the observed membrane-bound fluorescence could be due to the interaction of the glycopeptides with its complementary lectins highly expressed on this cell line[33] or through HSPG interaction. The QD conjugates carrying glycopeptides seem to have been directed specifically towards the golgi, while those QD conjugates carrying naked peptides were randomly distributed in the cytoplasm and the golgi. These observations suggested that although A549 cells directed all the QD conjugates to the golgi, they might have been delivered inside the cell differently. It seems that the QD conjugates carrying glycopeptides were not entering the cell all at once but rather in batches and that the remaining QD conjugates were hanging on the cell surface waiting for their cues to come-in, as indicated by the population of QD conjugates that are actually inside the cell, and thus their cellular delivery might have been driven by the presence of sugar moiety.

In HepG2 cells, QD conjugates were also channelled to the golgi apparatus. All QD conjugates carrying compounds **1** and **2** were observed to have higher golgi uptake compared to the ones carrying compounds **3** and **4**. However, QD conjugates carrying naked peptide (compound **3**) showed less golgi uptake compared to its glycosylated counterpart (QD conjugates carrying compound **4**). It is noteworthy, however, that the conjugates carrying the monomer compounds (compounds **1** and **2**) seem to have similar intracellular distribution patterns, whereas the conjugates with polymer counterparts have evident difference in intracellular localization. Most of the QD conjugates carrying compound **4** were localized in the golgi while those with compound **3** were largely distributed in the cytoplasm. It seems likely that although hepatocytes have galactose-specific binding receptor, that could potentially facilitate and influence the intracellular delivery of these QD conjugates,[34,35] compounds **1** and **2** are small tetrapeptides with only one glycosylation site difference. It might be that this difference was indistinguishable by HepG2 cells and were therefore be channelled intracellularly in similar manner. The presence of multiple glycosylation sites in compound **4**,

however, cannot be neglected and be disregarded by the cell. This apparent observable difference that differentiated each from the other could have driven a different intracellular trafficking. Intracellular uptake of compounds **1** and **2** in HT-29 cells showed similar phenomenon in terms of intracellular trafficking. The intracellular distribution and golgi uptake were quite comparable for both QD conjugates. Majority of the QDs were dispersed in cytoplasm while others are thinly localized in the golgi unlike in HepG2 cells. Cells co-incubated with conjugates carrying compounds **3** and **4**, on the other hand, have visibly higher QD uptake. Although both conjugates were channelled to the gogli, similar to HepG2 cells, significantly higher golgi co-localization was observed in cells co-incubated with QD conjugates carrying compound **4**. These results suggested that HT-29 cells, like HepG2, might be unable to differentiate between QD conjugates carrying compounds **1** and **2** in terms of their individual intracellular traffic. The presence of longer peptide sequence and multiple glycosylation, however, increased golgi colocalization compared to its naked counterpart. It seems that the presence of multiple glycosylation drew the conjugates more towards the golgi.

Like HepG2, PC-3 cells, on the other hand, showed similar intracellular distribution patterns on conjugates carrying the monomer compounds. Conjugates with polymer counterparts, however, have evident difference in intracellular localization. QD conjugates carrying compound **4**, unlike its observed behaviour when co-incubated with HepG2 and HT-29 cells, showed less golgi co-localization compared to the naked compound **3**. Judging from the result, it seemed that the glycosylated compound **4** were delivered and trafficked intracellularly in a very controlled fashion compared to the compound **3**, which seemed to have been distributed randomly in cytoplasm and golgi. The controlled delivery of compound **4** in the golgi could apparently be observed by their non-random and unsaturated presence of QD conjugates in the golgi.

In healthy cell lines, the intracellular localization of QD conjugates greatly differed from the diseased cell lines. The endocytosis of all QD conjugates in the diseased cell lines was of higher rate[36] as indicated by the densely QD conjugate populated cytoplasm, compared to

the scarcely QD conjugate populated cytoplasm of healthy normal cell lines (Figure 3.20b). Although these QD conjugates also displayed His_6 in their surface, this phenomenon was strikingly different from the observed localization of the QD conjugate carrying only His_6 (see chapter 2). This could suggest that the intracellular delivery of these QD conjugates was driven greatly by the serglycin-like peptides and glycopeptides co-displayed onto the surface of QDs, and may be partly by the His_6.

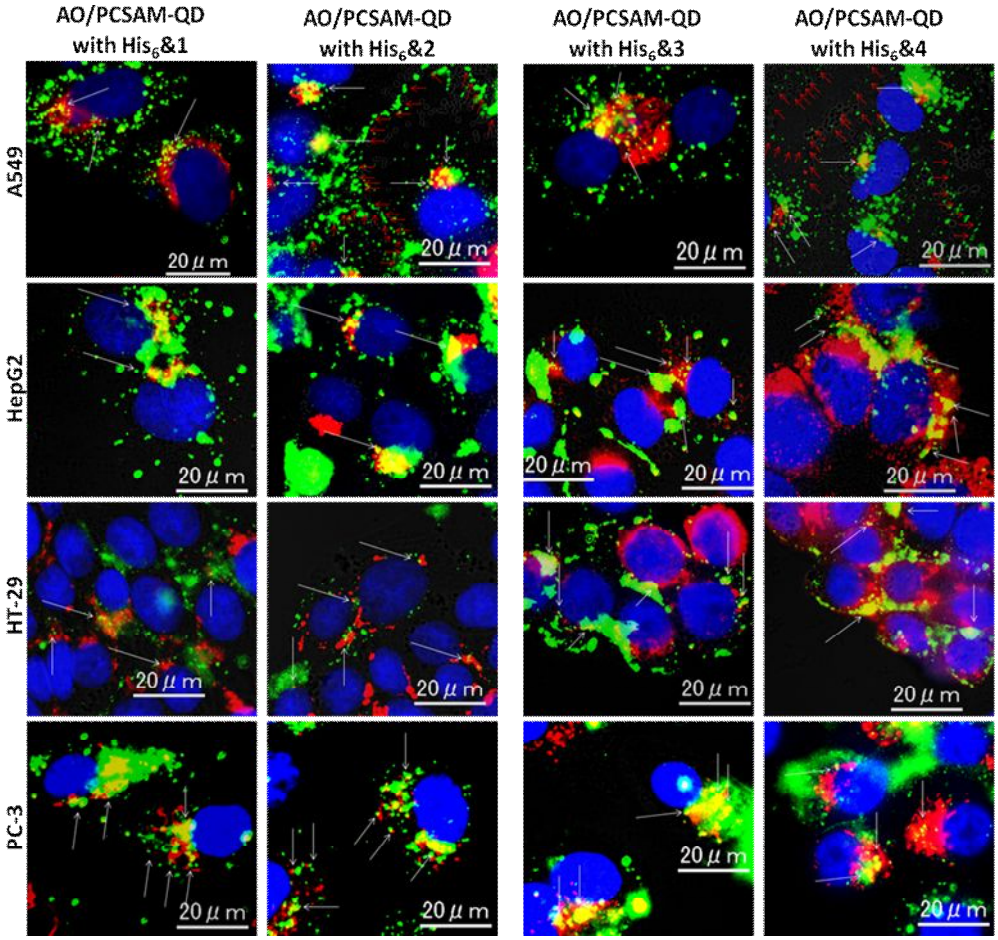

Figure 3.20a. Representative images showing different intracellular localization pattern of QD-conjugates (green) on different human cancer cell lines. Golgi was tagged by golgi marker anti-giantin and detected by the secondary anti-body (red), Nuclei were stained with Hoechst 33342 (blue), yellow color indicates QD conjugates co-localized in the golgi (also pointed by white arrows). Red arrows indicate cell surface-bound QD conjugates. Scale bar is 20 μm.

Interestingly, however, both NHAC-Kn and OUS-11 cells showed no localization of QD conjugates displaying naked peptides (compounds **1** and **3**) in the golgi, while those carrying glycopeptides **2** and **4** appeared to be distributed specifically in the golgi as shown by the yellow merged color (pointed by white arrows). It appeared that the presence of glycan moieties can drove the conjugates specifically to the golgi. The absence of glycosylation may have prevented the conjugates from localizing in the golgi, whereas the presence of sugar moieties, both monomer compound **2** and hexamer compound **4**, allowed golgi localization. It may seem that the minimum requirement for golgi localization, in these cells, was the presence of sugar moiety in the polypeptide chain. Interestingly, golgi localization behaviour on NHAC-Kn cells was similar and in agreement with the previously reported localization of this serglycin PGI monomer.[25] These observation exemplified the important role of glycosylation on intracellular compartmentalization.

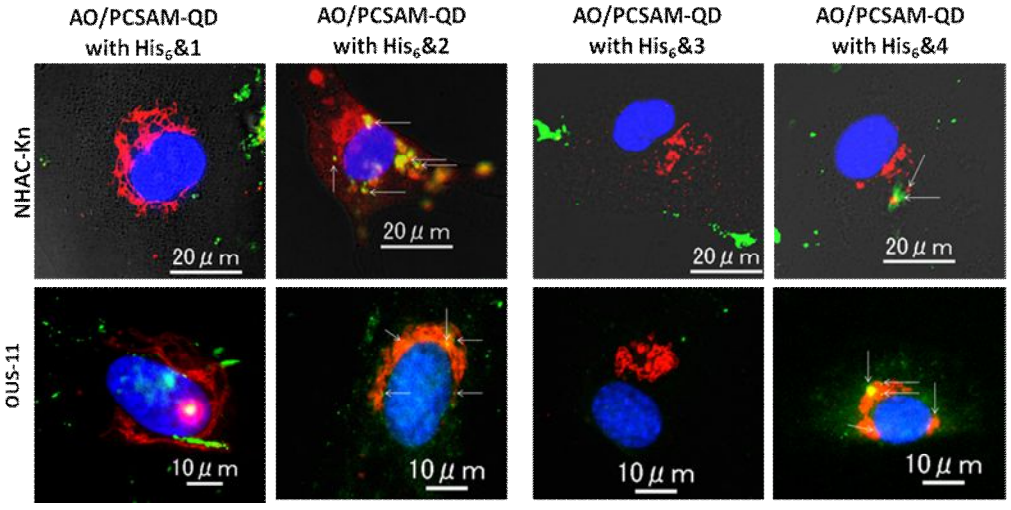

Figure 3.20b. Representative images showing different intracellular localization pattern of QD-conjugates (green) on different narmal healthy human cell lines. Golgi was tagged by golgi marker anti-giantin and detected by the secondary anti-body (red), Nuclei were stained with Hoechst 33342 (blue), yellow color indicates QD conjugates co-localized in the golgi (also pointed by white arrows). Scale bar is 20 μm.

There is no other concrete way to compare the effect of the presence and absence of glycosylation in terms of intracellular trafficking and compartmentalization than comparing its

effect on normal and cancer cells of same types. As shown in Figure 3.21, it was revealed that QD conjugates displaying naked peptides **1** or **3** did not localized in the golgi of normal human lung tissue while those carrying glycopeptides **2** or **4** appeared to distribute specifically in the golgi indicated by the yellow color resulted from the merged green and red color from QD conjugates and golgi, respectively. Surprisingly, in the case of human lung adenocarcinoma (A549), all QD conjugates, regardless of molecular size and presence or absence of glycan moieties, were delivered to the golgi compartment.

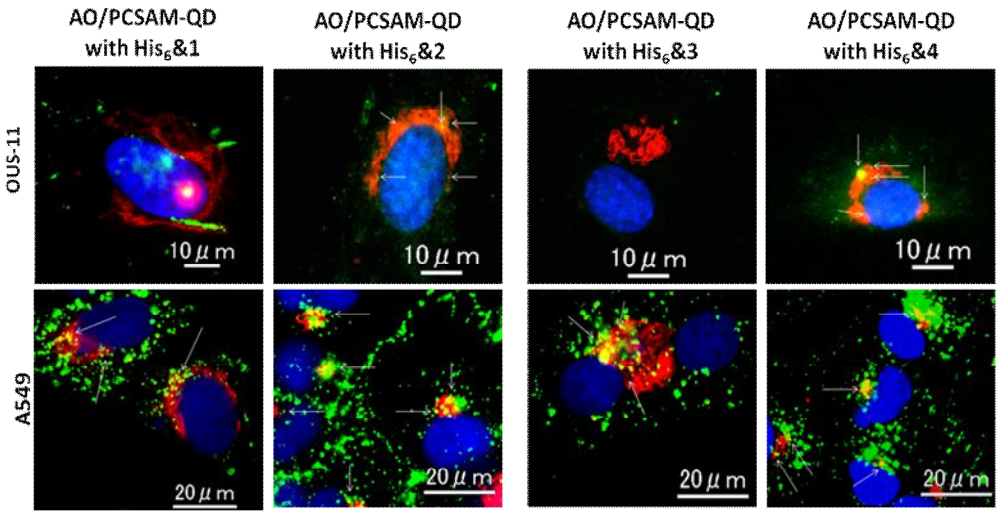

Figure 3.21. Representative images showing controlled intracellular delivery after 2 h of co-incubation with 5 nM AO/PCSAM-QDs carrying serglycine-like peptides/glycopeptides (green) in normal human lung tissue (OUS-11) and human lung adenocarcinoma (A549). Golgi was tagged by golgi marker anti-giantin and detected by the secondary anti-body (red), Nuclei were stained with Hoechst 33342 (blue), yellow color indicates QD conjugates co-localized in the golgi (also pointed by white arrows).

This observation warrants the specific effects of glycosylation of the serglycin-like peptides on the intracellular trafficking and localization of the His_6-modified QD conjugates. Although the mechanism remains unclear, normal human lung tissue cells can clearly discriminate glycosylated from non-glycosylated PGI peptides while human lung adenocarcinoma cannot.

Golgi localization efficiency

In order to assess the efficiency of *k*-His_6 in facilitating endolysosomal escape that subsequently enabled QDs to colocalize in the golgi apparatus, golgi localization of QD conjugates was examined (Figure 3.22-3.26) and quantify (Figure 3.27).

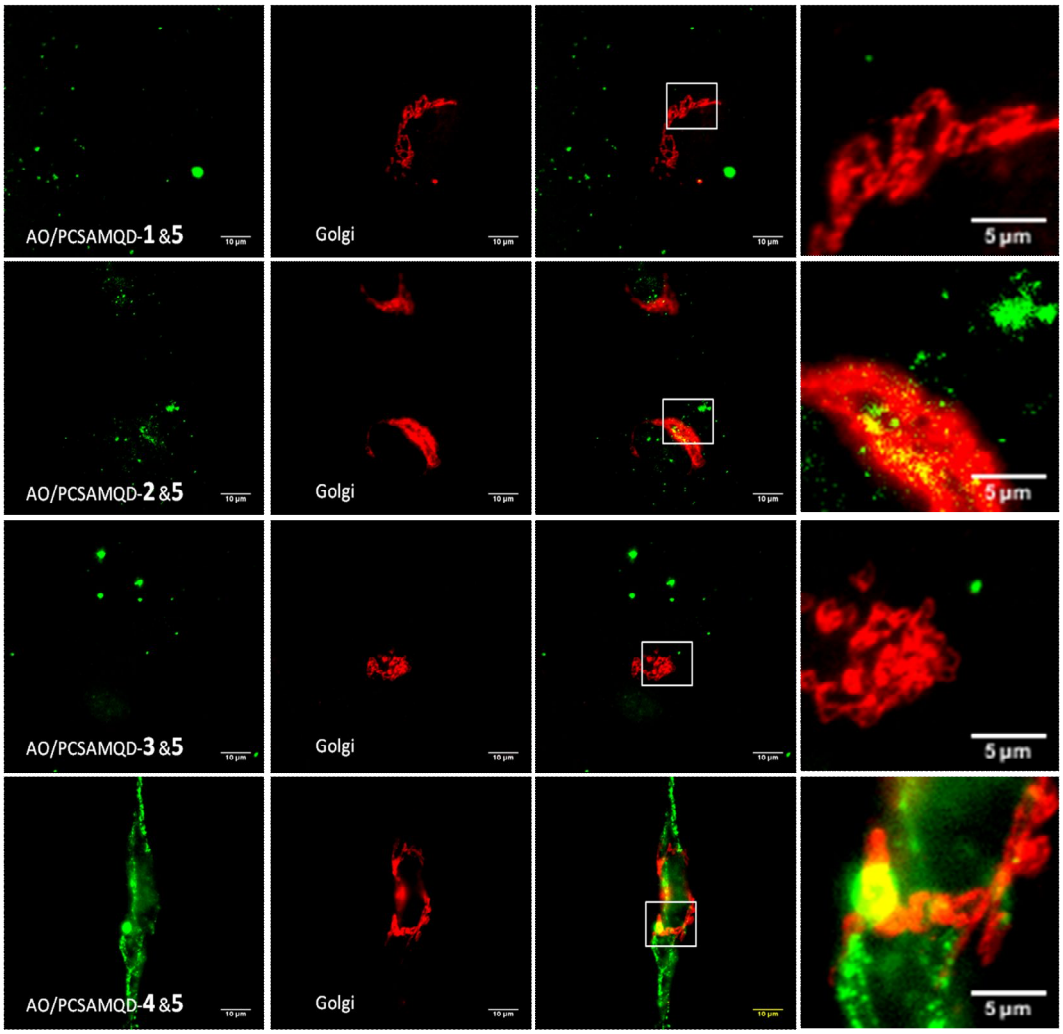

Figure 3.22. Example images of OUS-11 cells showing the colocalization of QD conjugates with the golgi apparatus (yellow color). Golgi was tagged with anti-giantin primary antibody (abcam) and detected with Goat anti-mouse IgG H&L-Alexa Fluor 647 (abcam).Colocalization was measured using imagej software with plugins: Colocalisation Threshold and Colocalisation Test by selecting the entire golgi area inside the region of interest (ROI).

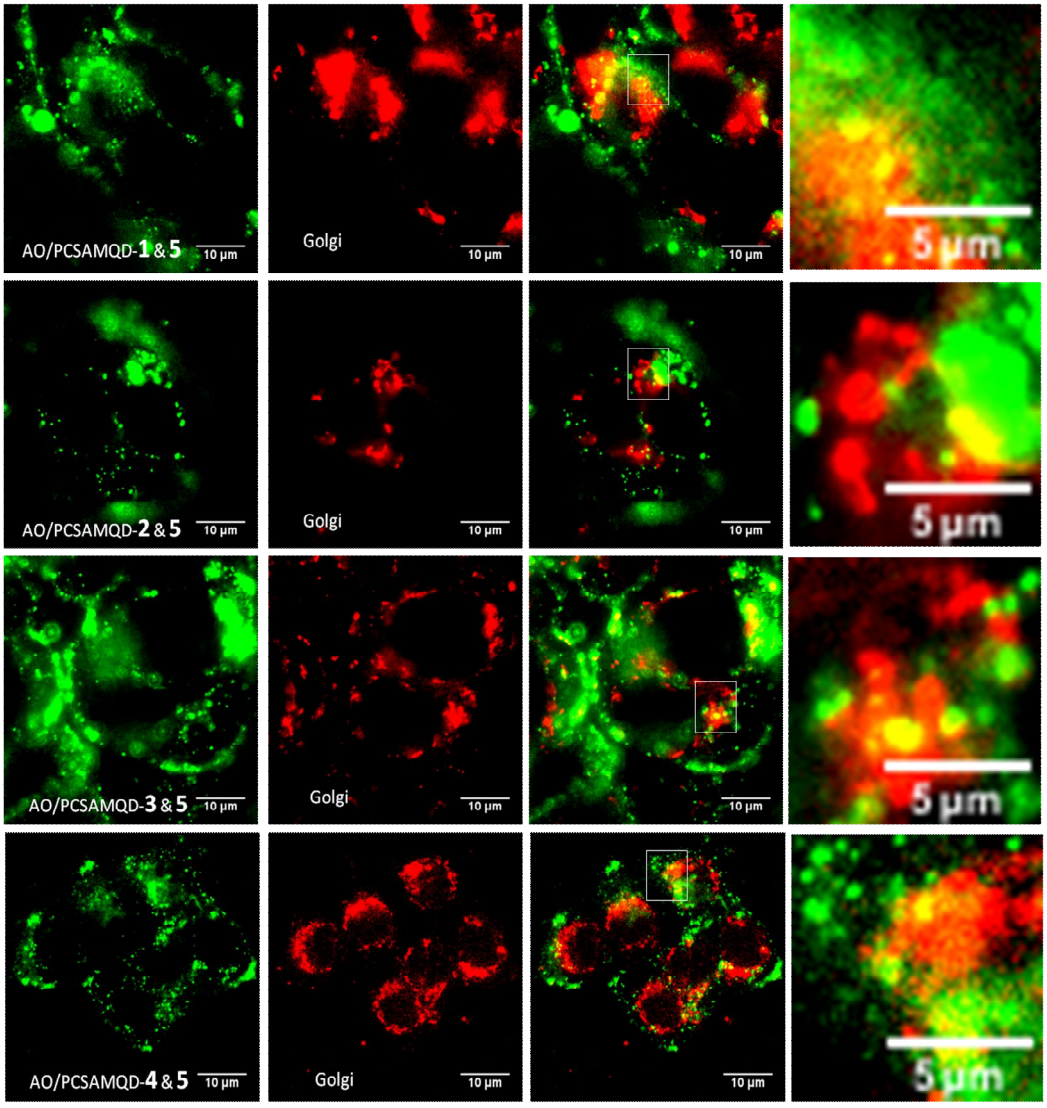

Figure 3.23. Example images of HT-29 cells showing the colocalization of QD conjugates with the golgi apparatus (yellow color). Golgi was tagged with anti-giantin primary antibody (abcam) and detected with Goat anti-mouse IgG H&L-Alexa Fluor 647 (abcam).Colocalization was measured using imagej software with plugins: Colocalisation Threshold and Colocalisation Test by selecting the entire golgi area inside the region of interest (ROI).

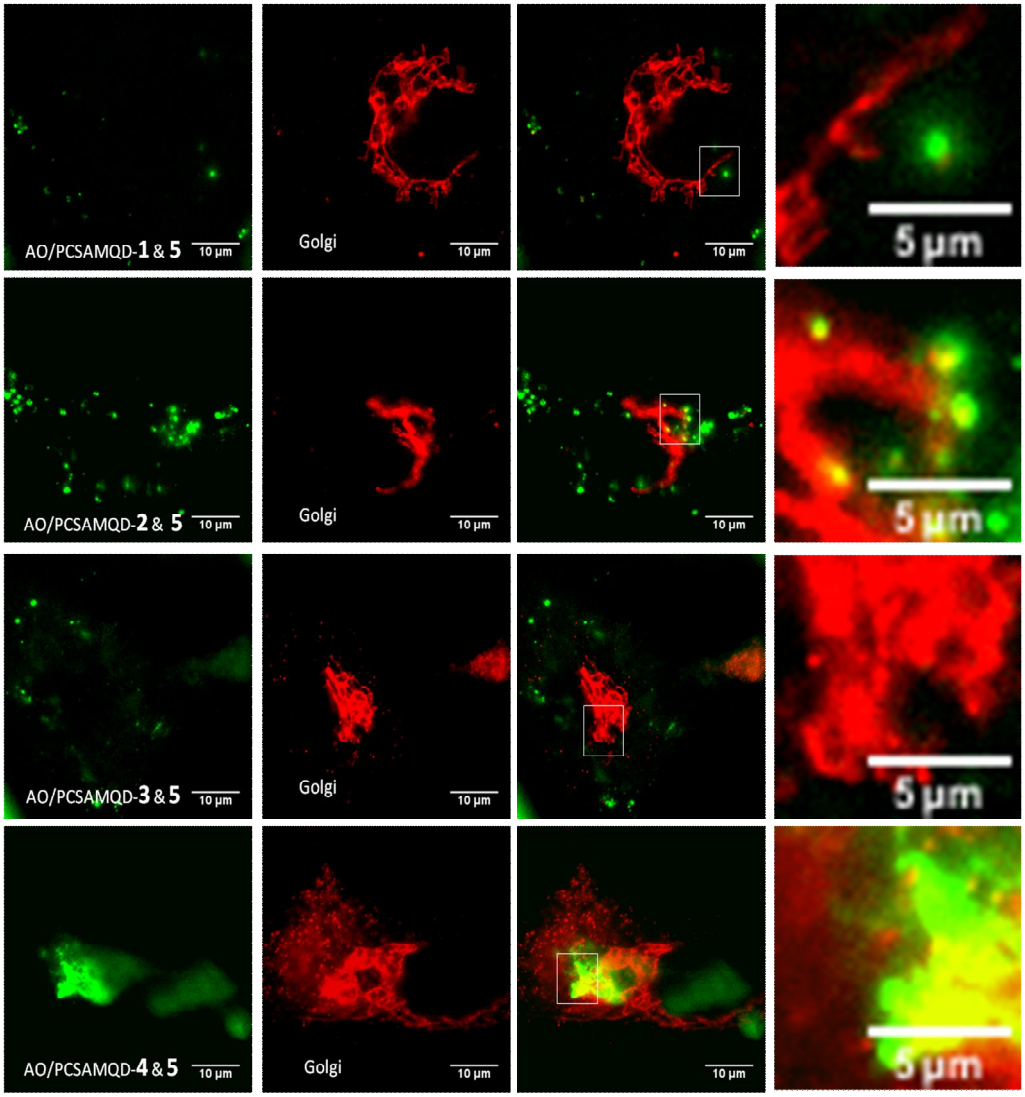

Figure 3.24. Example images of NHAC-Kn cells showing the colocalization of QD conjugates with the golgi apparatus (yellow color). Golgi was tagged with anti-giantin primary antibody (abcam) and detected with Goat anti-mouse IgG H&L-Alexa Fluor 647 (abcam).Colocalization was measured using imagej software with plugins: Colocalisation Threshold and Colocalisation Test by selecting the entire golgi area inside the region of interest (ROI).

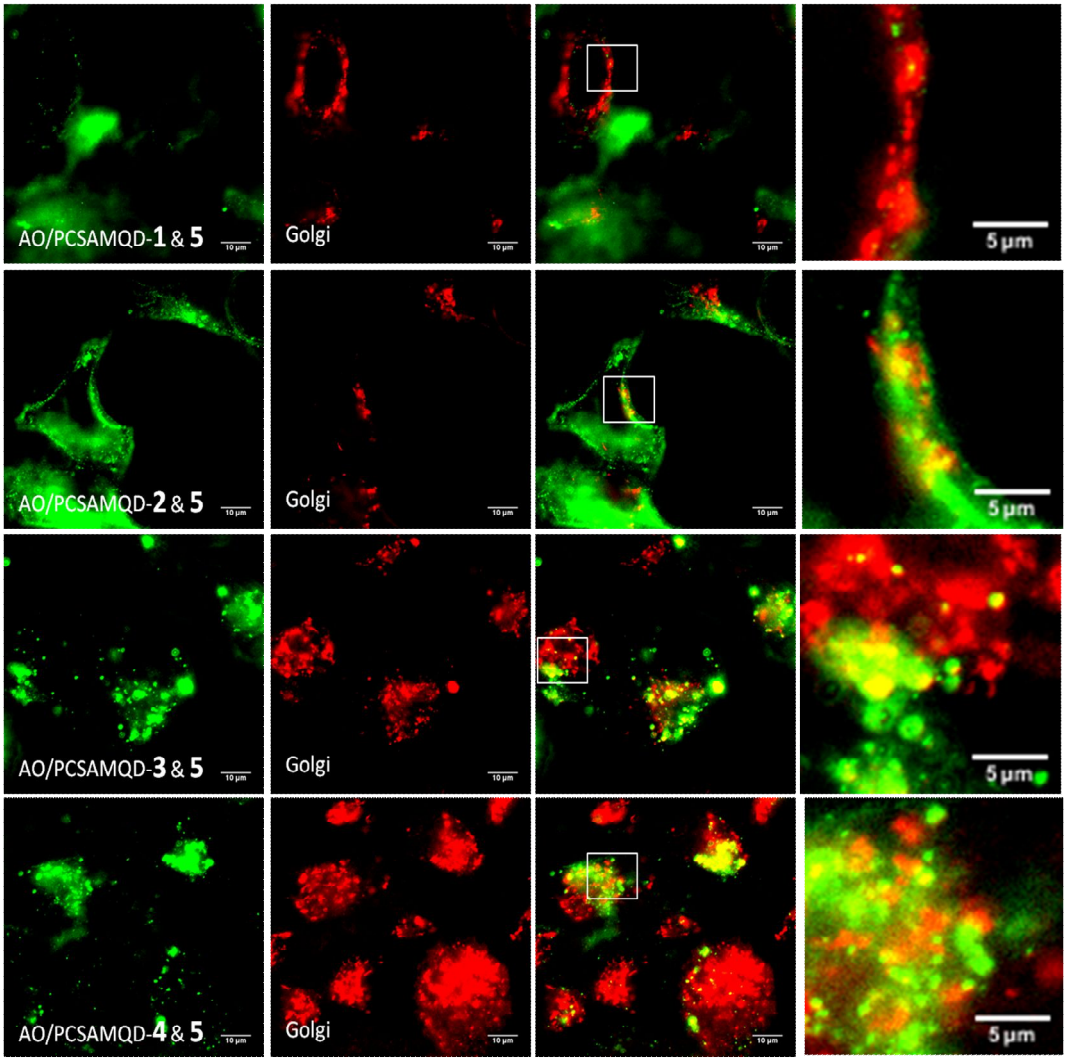

Figure 3.25. Example images of PC-3 cells showing the colocalization of QD conjugates with the golgi apparatus (yellow color). Golgi was tagged with anti-giantin primary antibody (abcam) and detected with Goat anti-mouse IgG H&L-Alexa Fluor 647 (abcam).Colocalization was measured using imagej software with plugins: Colocalisation Threshold and Colocalisation Test by selecting the entire golgi area inside the region of interest (ROI).

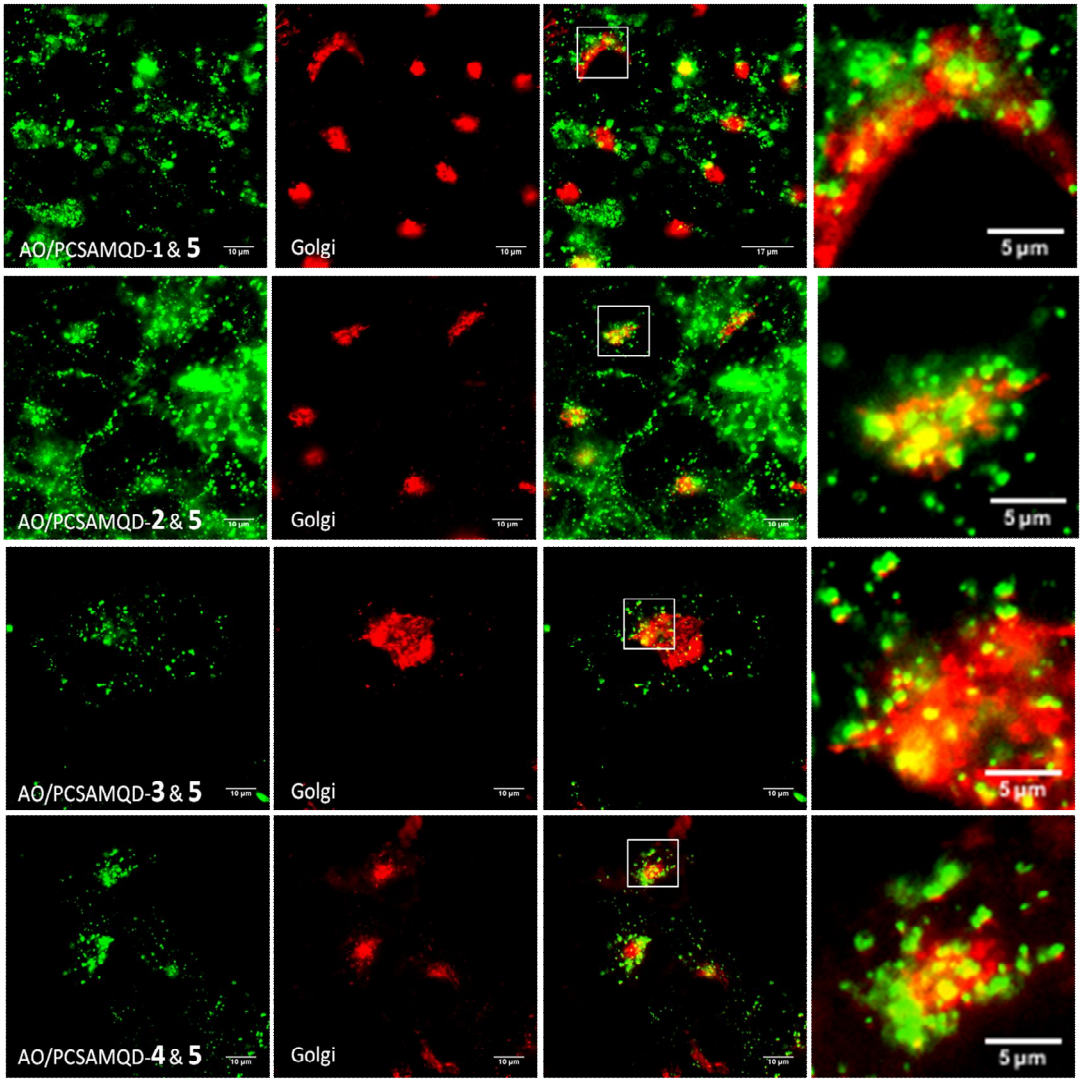

Figure 3.26. Example images of A549 cells showing the colocalization of QD conjugates with the golgi apparatus (yellow color). Golgi was tagged with anti-giantin primary antibody (abcam) and detected with Goat anti-mouse IgG H&L-Alexa Fluor 647 (abcam).Colocalization was measured using imagej software with plugins: Colocalisation Threshold and Colocalisation Test by selecting the entire golgi area inside the region of interest (ROI).

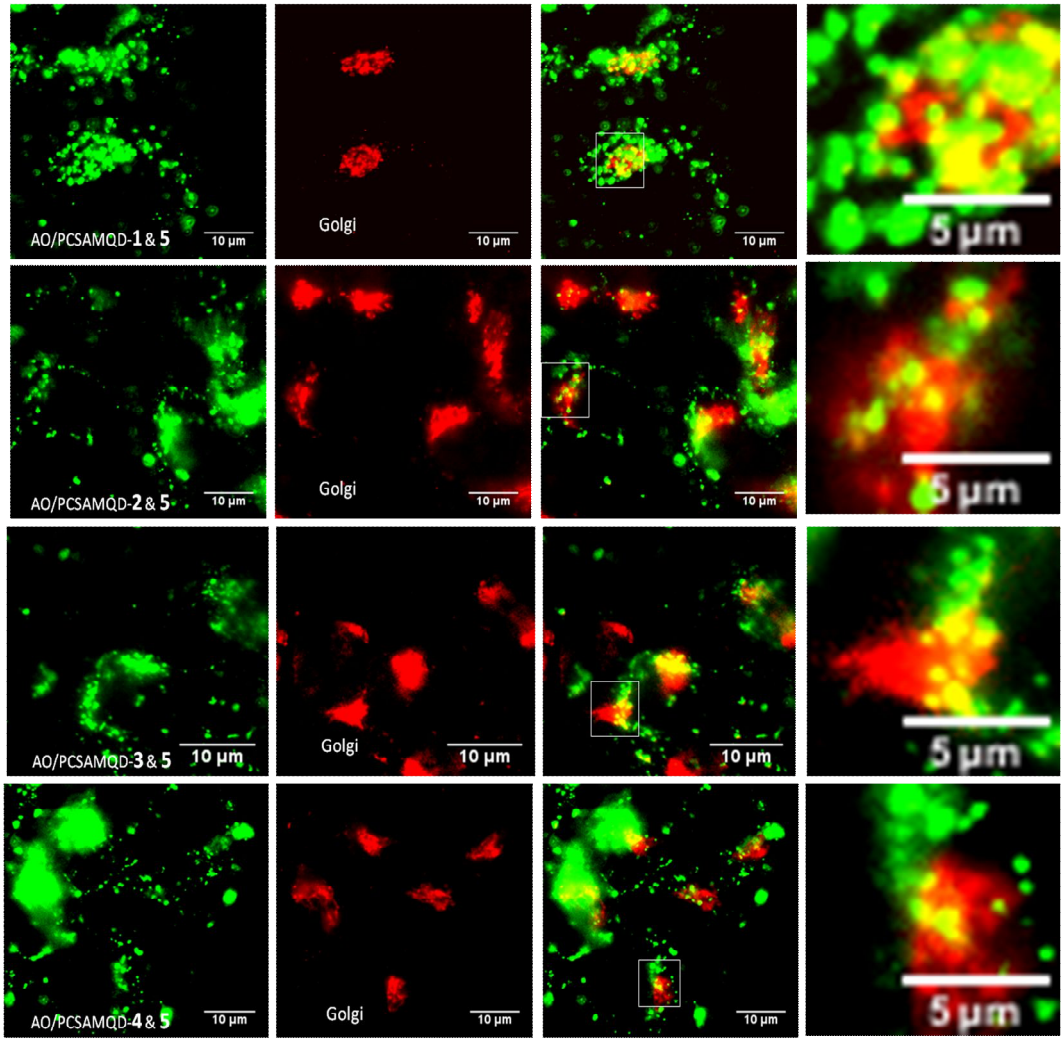

Figure 3.27. Example images of HepG2 cells showing the colocalization of QD conjugates with the golgi apparatus (yellow color). Golgi was tagged with anti-giantin primary antibody (abcam) and detected with Goat anti-mouse IgG H&L-Alexa Fluor 647 (abcam).Colocalization was measured using imagej software with plugins: Colocalisation Threshold and Colocalisation Test by selecting the entire golgi area inside the region of interest (ROI).

The golgi accumulation is predicated by the endolysosomal escape of QDs. Therefore, the degree of golgi localization could be correlated to endolysosomal escape of QD conjugates. As shown in Figure 3.28, only compounds **2** and **4** were able to penetrate the golgi apparatus of OUS-11 selectively, with compound **4** exhibited higher golgi localization, while compounds **1** and **3** were only observed in the cytoplasmic region (see Figure 3.20b-3.22). This phenomenon has been shared by NHAC-Kn (Figure 3.20b and Figure 3.24). However, unlike

OUS-11, NHAC-Kn has higher golgi localization of compound **2** compared to compound **4** (Figure 3.28).

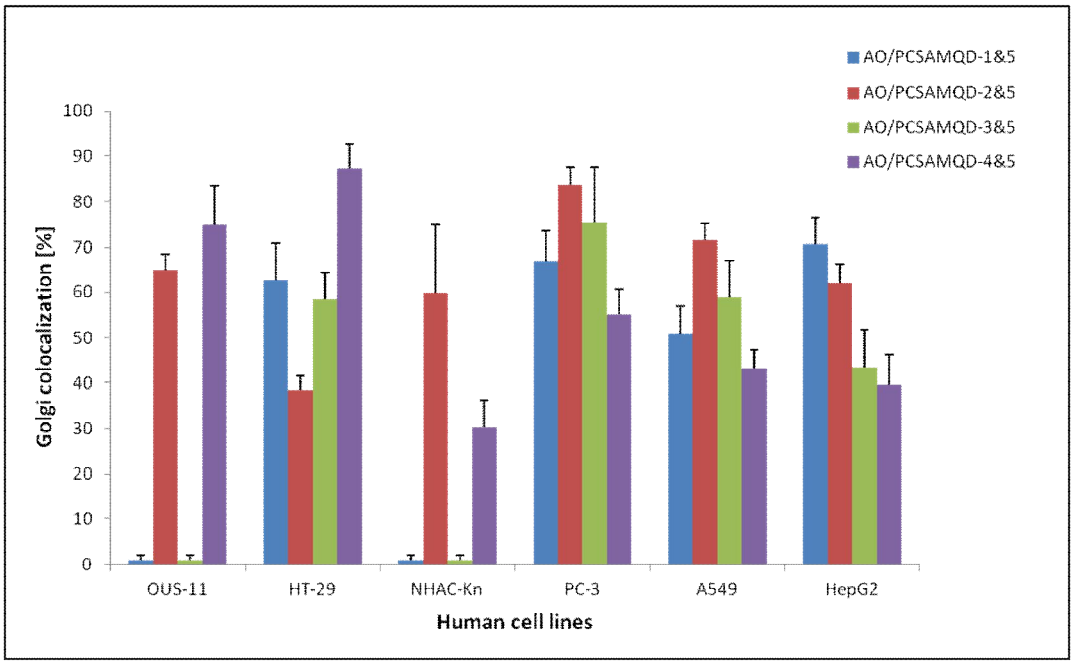

Figure 3.28. Differences in golgi coloclalization of AO/PCSAMQDs displaying compound **5** and with co-displayed compounds **1**, **2**, **3** and **4** on different human cell lines. Error bar represents ±SEM of at least 15 cells.

Having been shown to deliver all QD conjugates into its golgi, like all other cancer cell lines (Figure 3.20a), HT-29 showed higher golgi localization of compound **4** than compound **2** while the two naked peptides (compounds **1** and **3**) have comparable degree of golgi localization (Figures 3.20a and 3.23).

Therefore, considering the ideal condition for intracellular delivery, 30% - 50% was considered ideal ratio that could elicit highest endolysosomal escape and consequent golgi accumulation. The semi-quantitative assessment of QD conjugates inside the cell was summarized in Table 3.2.

Table 3.2. Semi-quantitative assessment of the amount of QDs inside the cell.

	OUS-11		HT-29		NHAC-Kn		PC-3		A549		HepG2	
Compound	Cytoplasm	Golgi	Cytoplasm	Golgi	Cytoplasm	Golgi	Cytoplasm	Golgi	Cytoplasm	Golgi	Cytoplasm	Golgi
1&5	+	-	++	++	+	-	++	++	+++	++	+++	+++
2&5	+	+	++	+	+++	++	++	++	+++	+++	++	+++
3&5	+	-	+++	++	++	-	+	++	++	++	++	++
4&5	+++	++	++	+++	++	+	+	+	+	+	+++	++

*The assessment was based from the amount of QDs colocalized in the golgi and the QD fluorescent signals in the cytoplasm.

Cytotoxicity of peptides, glycopeptides, and QD conjugates

The problem with most of the nanoparticle-based delivering agents is their cytotoxicity. Aside from the core metal, molecules displayed on their surface could likely contribute to their cytotoxicity. To demonstrate that the cells are not adversely affected by QD conjugates, cytotoxicity assays were performed for all synthetic compounds and their QD conjugates. Results showed that all QD conjugates have no significant cytotoxicity towards all cell lines used (Figures 3.22-29), although a decrease in cell viability is observed in a concentration dependent manner in some cell lines.

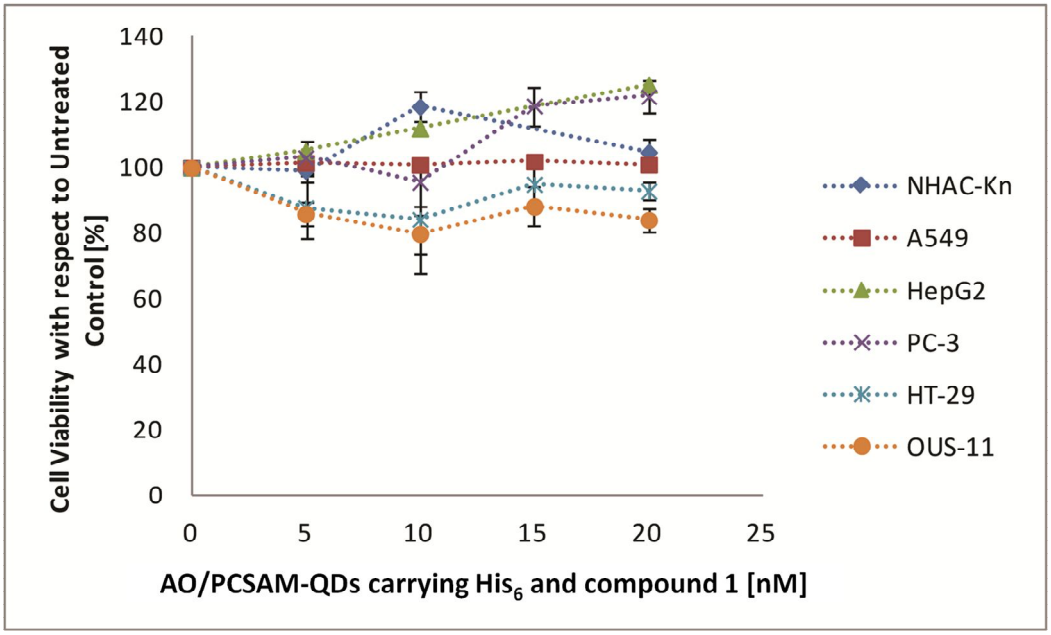

Figure 3.29. Cytotoxicity of AO/PCSAM-QDs carrying His_6 and compound **1** on different human cell lines.

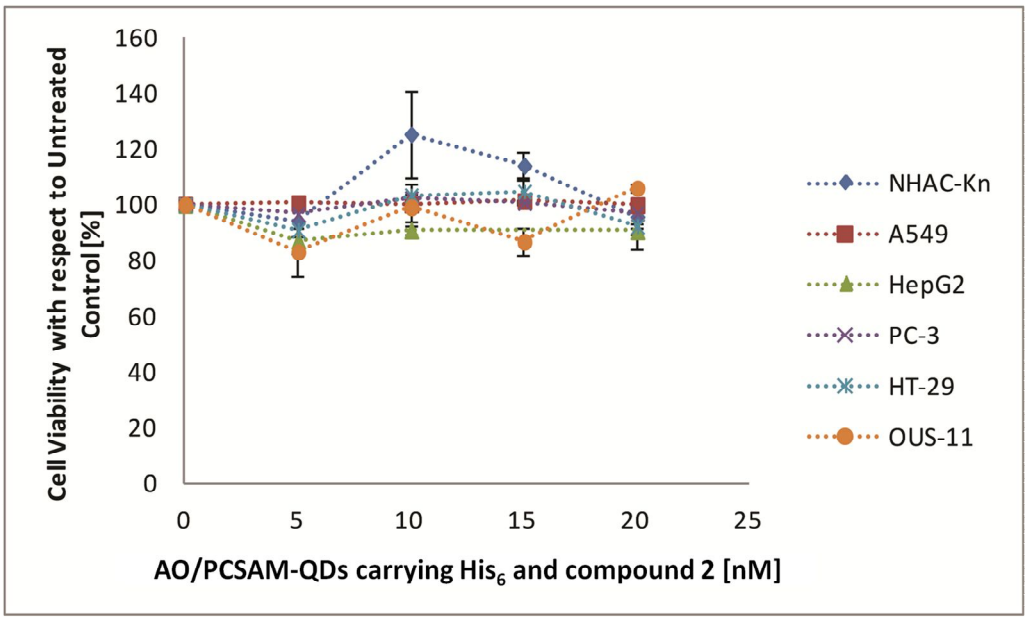

Figure 3.30. Cytotoxicity of AO/PCSAM-QDs carrying His_6 and compound **2** on different human cell lines.

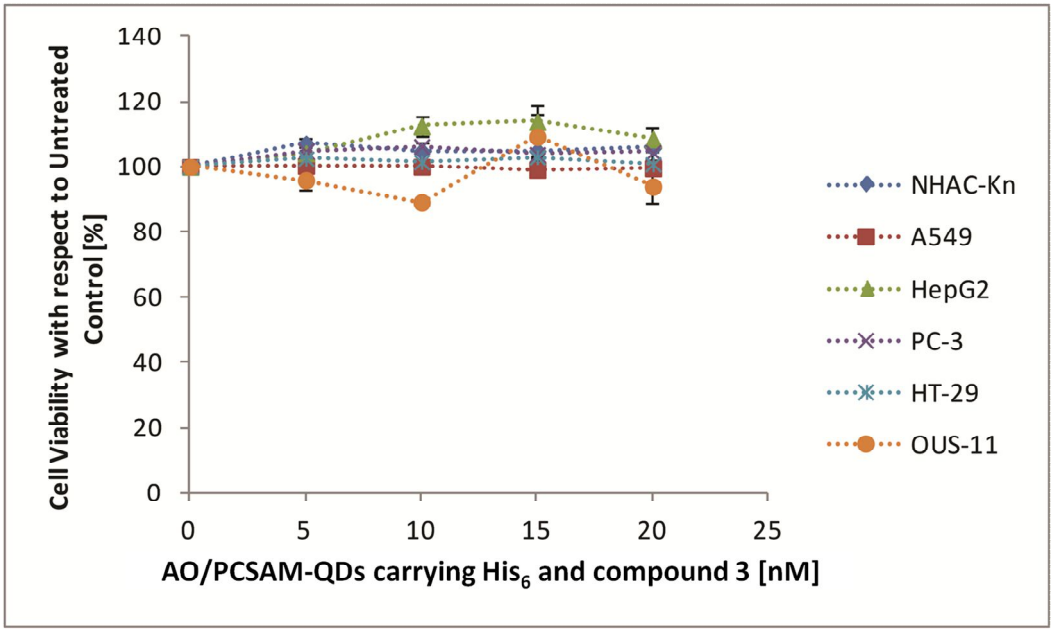

Figure 3.31. Cytotoxicity of AO/PCSAM-QDs carrying His_6 and compound **3** on different human cell lines.

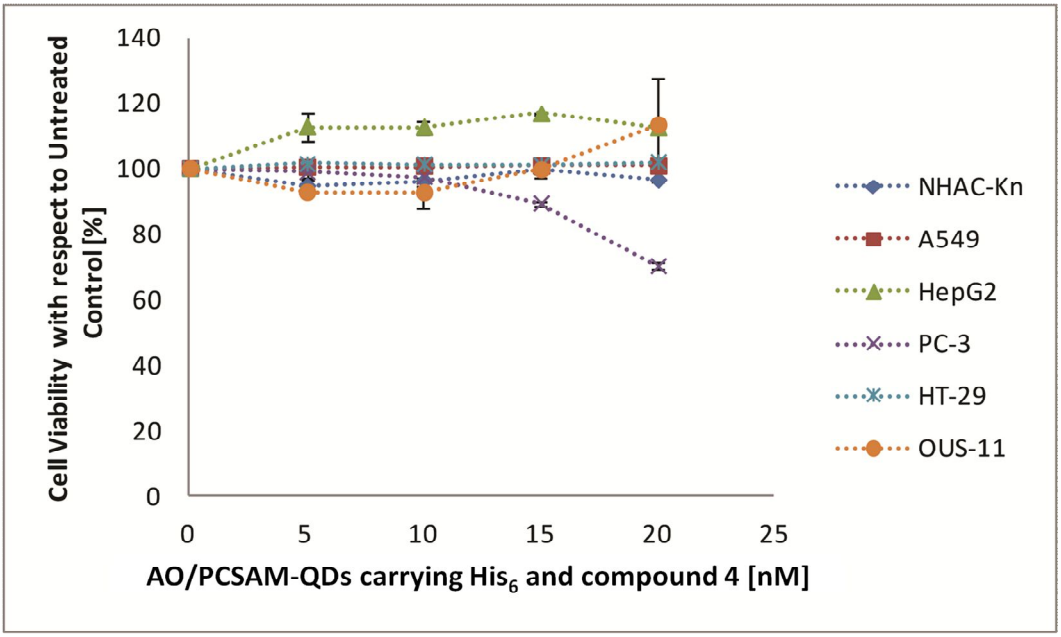

Figure 3.32. Cytotoxicity of AO/PCSAM-QDs carrying His_6 and compound **4** on different human cell lines (see also chapter 2).

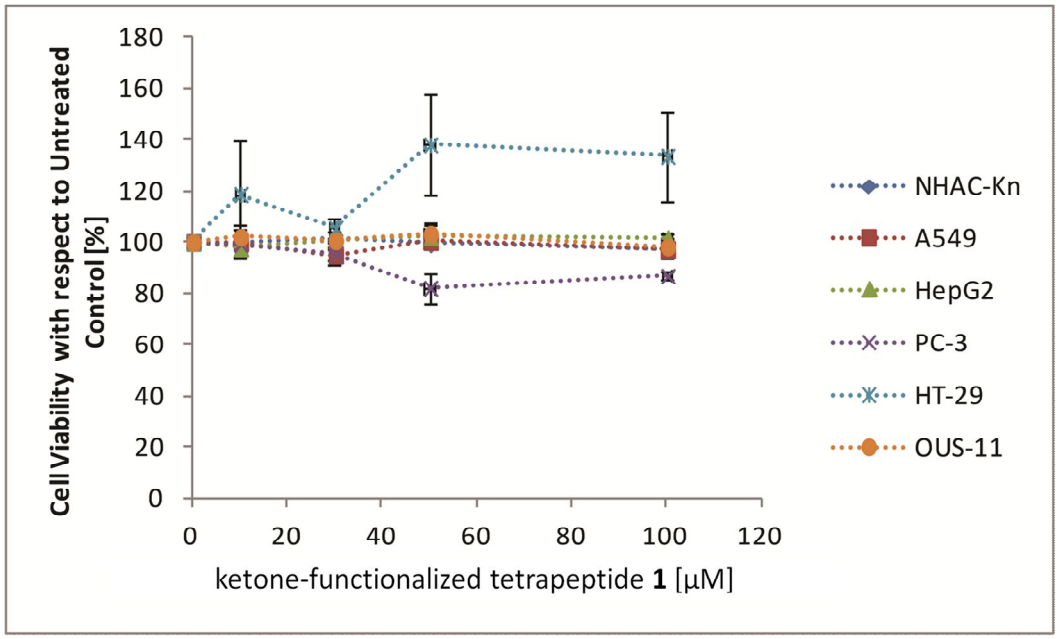

Figure 3.33. Cytotoxicity of tetrapeptide **1** on different human cell lines.

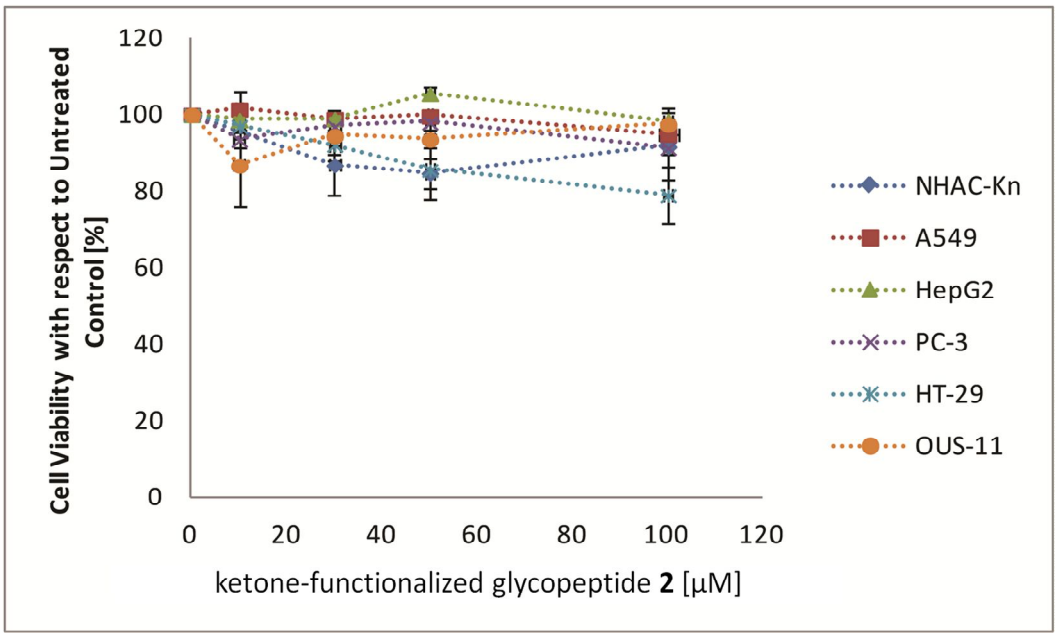

Figure 3.34. Cytotoxicity of glycopeptide **2** on different human cell lines.

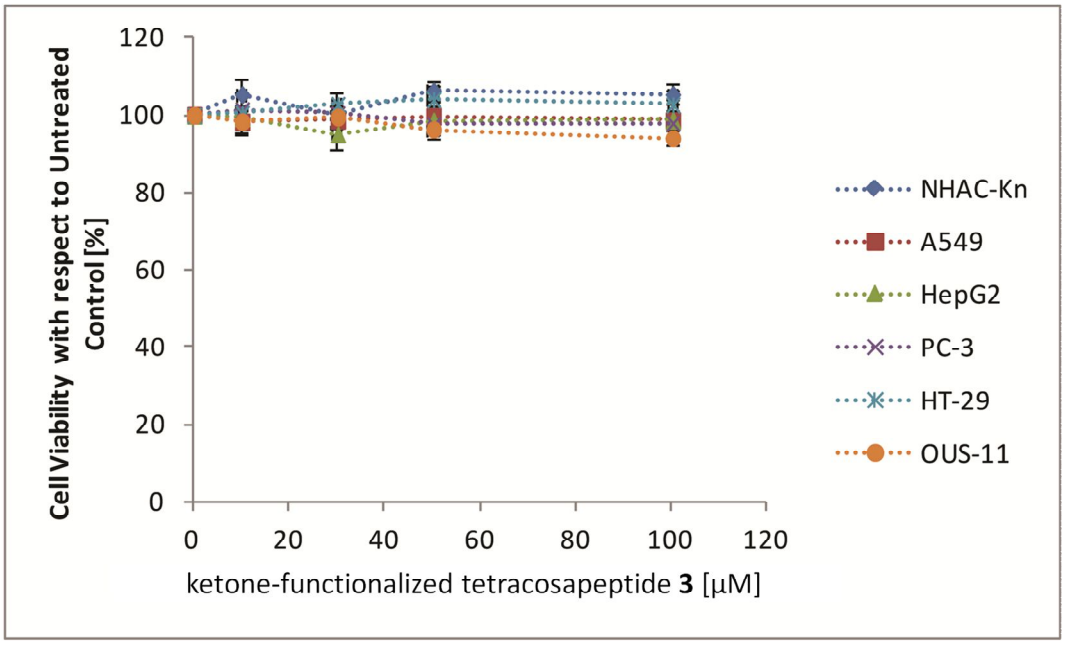

Figure 3.35. Cytotoxicity of tetracosapeptide **3** on different human cell lines.

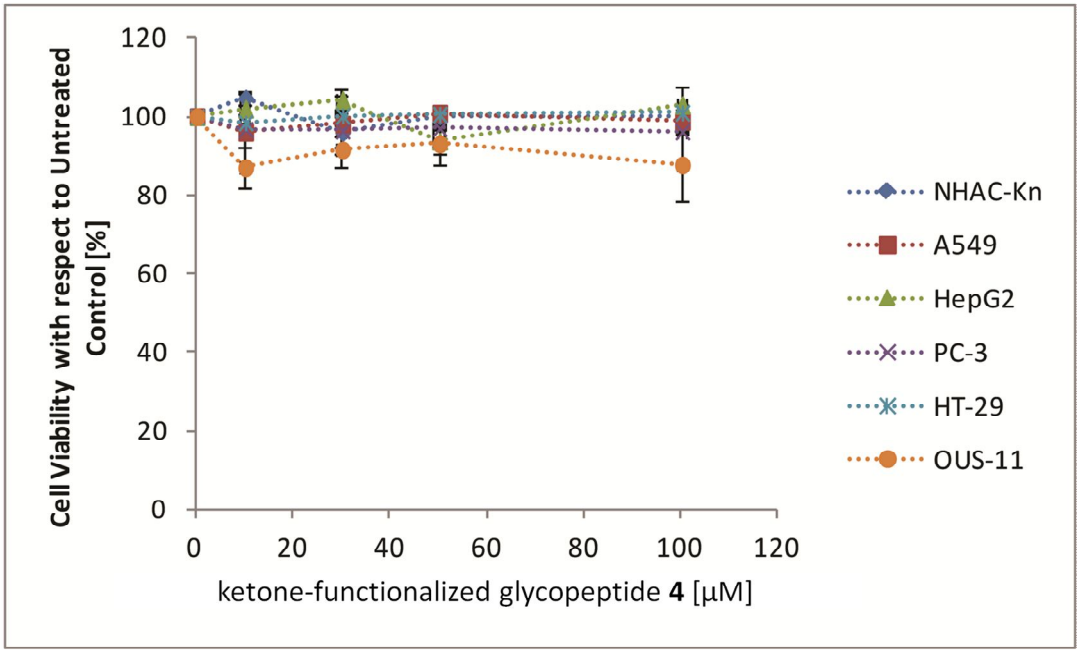

Figure 3.36. Cytotoxicity of glycopeptide **4** on different human cell lines.

The compounds were individually non-cytotoxic, some of them were even mitogenic. The observed concentration-dependent decreased in cell viability, as in the case of PC-3 in Figure 3.2, could not be attributed to the surface-displayed compounds but rather to the entirety of the QD conjugates and its behaviour once inside the cell. At an acidic condition inside the lysosome, the *k*-His_6 can elicit a "proton sponge effect" response resulting to lysosome membrame permeabilization. This permeabilizaion causes the QDs to penetrate its way out of the lysosome. Consequently, this will cause the release of hydrolases and all other lysosomal load to the cytosol that could result in an increase in intracellular pH, which will eventually damage mitochondria and other intracellular compartments. The intense intracellular damage incurred due to lysosomal dysfunction can trigger cellular death.[37,38] Therefore, since this QD conjugates have a remarkable endolysosomal escaping capability; cytotoxicity can likely be induced once inside the cell.

This study revealed an interesting finding that glycosylation could possibly govern subcellular localization of peptides on different cell human lines. It seems that golgi localization, in normal cell lines, is only selective to the glycopeptides. Whereas all compounds, either glycosylated or naked, were observed to localize in the golgi of all human cancer cell lines used. As demonstrated, golgi localization of the QD conjugates, in normal human cell lines, was likely to be primarily due to compounds **2** and **4**. This difference in behaviour between the normal and cancer cells in terms of trafficking of QD conjugates could be linked to their defective quality control and intracellular trafficking machineries.

3.3 Experimental

Materials. All Fmoc-protected amino acids and PyBOP were purchased from Novabiochem, HBTU was from Peptide Institute Inc., HOBT from Kokusan Kagaku Corp., HOAt was from GenScript, Rink-Amide-ChemMatrix resin was from Biotage. *N*-(9-Fluorenylmethoxycarbonyl)-*O*-[2,3-di-*O*-acetyl-4-*O*-(2,3,4,6-tetra-*O*-acetyl-β-D-galactopyranosyl)-β-D-xylopyranosyl]-L-Serine was purchased from Medicinal Chemistry Pharmaceutical Ltd., Japan (http://soyaku.co.jp/). Coating reagents, 11,11'-dothio bis[undec-11-yl 12-(aminooxyacetyl)amino hexa(ethyleneglycol)] (AOSH) and a phosphoryl derivative, 11-mercaptoundecylphosphorylcholine (PCSH) were synthesized by the procedures reported previously and available from MCP Co. Ltd., Qdot 545 ITK™, Lysotracker Red DND-99, and Hoechst 33342 were from Invitrogen. DCM, DMF, DIEA and TFA were purchased from Watanabe Chem. IND., LTD. Ultrafiltration membranes were supplied from Millipore, Carrigtwohill, Co. Cork, Ireland. Unless otherwise noted, solvents and other reagents were purchased from Aldrich Chemical Co. (Milwaukee, WI), Tokyo Chemical Industry (Tokyo, Japan), and Wako Pure Chemical Industries Ltd. (Tokyo, Japan).

Synthesis of ketone-functionalized tetrapeptide 1

A 0.24 mmol/g of Rink-amide-ChemMatrix resin, Fmoc-Ser(tBu)-OH (96 μmol, 4.0 equivalents), Fmoc-Gly-OH (96 μmol, 4.0 equivalents), and 5-oxohexanoic acid (4.0 equivalents) were used. Briefly, 0.24 mmol/g of Rink-amide-ChemMatrix resin was placed in a 5 mL Libra tube, washed sequentially with DMF and DCM followed by DCM swelling for 30 minutes. The swollen resin was washed with DMF. Fmoc-amino acid was pre-activated using 4 equivalents of HBTU, 4 equivalents of HOBt in DMF and 3 equivalents of DIEA for 30 seconds. The pre-activated Fmoc-amino acid was then added to the resin and allowed to couple for 15 minutes at 50°C under microwave irradiation. The resin was then washed subsequently

with DMF, DCM and then DMF. To block the unreacted/uncoupled animo groups in the resin, acetyl capping was performed using DMF:Ac_2O:DIEA (8.5:1.0:0.5) for 5 minutes at room temperature, washed with DMF, DCM and then DMF, then Fmoc deprotection using 20% piperidine in DMF followed by washing with DMF, DCM and then DMF and the cycle repeated for alternating Ser-Gly sequence. After Fmoc deprotection of the last Fmoc-amino acid, 5-oxohexanoic acid was pre-activated using 4 equivalents of HBTU, 4 equivalents of HOBt in DMF and 3 equivalents of DIEA for 30 seconds. The pre-activated 5-oxohexanoic acid was then added to the peptide-resin mixture and allowed to couple for 15 minutes at 50°C under microwave irradiation. The mixture was washed subsequently with DMF, DCM and then DMF. Deprotected and cleavage of the peptide from the resin was done by adding TFA:H2O (95: 5) cocktail to the washed resin in ice for 30 minutes with shaking and then the shaking was continued at room temperature for additional 1 hour. The deprotection and cleavage processes were monitored using MALDI-TOF/MS. The solution containing the synthesized peptide was drained. The resin was flushed subsequently with the same cocktail solution, acetic acid, and methanol. The filtrates were combined and concentrated by air drying, dissolved in 50% acetonitrile and lyophilized. The peptide was then purified using RP-HPLC with acetonitrile (B) and water (A) both with 0.1% TFA using Intersil® ODS-3 (5 µm, 4.6 x 250 mm) column at room temperature, 1 ml/min flow rate, 220 nm wavelength for detection, and solvent gradient (A:B) of 99:1 (0 min), 85:15 (50 mins), and 5:95 (60 mins) to get compound **1** (t = 12.7 mins) and then lyophilized.

HRMS (MALDI): *m/z* calcd for $C_{16}H_{27}N_5NaO_8^+$, $[M+Na]^+$ 440.1757, found 440.1750.

Synthesis of ketone-functionalized glycopeptide 2

A 0.24 mmol/g of Rink-amide-ChemMatrix resin, Fmoc-Ser(tBu)-OH (96 µmol, 4.0 equivalents), Fmoc-Gly-OH (96 µmol, 4.0 equivalents), *N*-(9-Fluorenylmethoxycarbonyl)-*O*-[2,3-di-*O*-acetyl-4-*O*-(2,3,4,6-tetra-*O*-acetyl-β-D-galactopyranosyl)-β-D-xylopyranosyl]-L-Serine (MCP Co., Ltd, Japan) (36 µmol, 1.5 equivalents) and 5-oxohexanoic acid (4.0

equivalents) were used. Briefly, 0.24 mmol/g of Rink-amide-ChemMatrix resin was placed in a 5 mL Libra tube, washed sequentially with DMF and DCM followed by DCM swelling for 30 minutes. The swollen resin was washed with DMF. Fmoc-amino acid was pre-activated using 4 equivalents of HBTU, 4 equivalents of HOBt in DMF and 3 equivalents of DIEA for 30 seconds. The pre-activated Fmoc-amino acid was then added to the resin and allowed to couple for 15 minutes at 50°C under microwave irradiation. The resin was then washed subsequently with DMF, DCM and then DMF. To block the unreacted/uncoupled animo groups in the resin, acetyl capping was performed using DMF:Ac_2O:DIEA (8.5:1.0:0.5) for 5 minutes at room temperature, washed with DMF, DCM and then DMF, then Fmoc deprotection using 20% piperidine in DMF followed by washing with DMF, DCM and then DMF and the cycle repeated for alternating Ser-Gly sequence. For the introduction of *N*-(9-Fluorenylmethoxycarbonyl)-*O*-[2,3-di-*O*-acetyl-4-*O*-(2,3,4,6-tetra-*O*-acetyl-β-D-galactopyranosyl)-β-D-xylopyranosyl]-L-Serine, 1.2 equivalents of PyBOP, 1.2 equivalents of HOAt in DMF and 3 equivalents of DIEA as the coupling cocktail. After coupling for 15 minutes at 50°C under microwave irradiation, the same coupling cocktail, without Fmoc-glycoamino acid, was added for a "double activation-like" approach for 15 minutes at 50°C under microwave irradiation. After Fmoc deprotection of the last Fmoc-amino acid, 5-oxohexanoic acid was pre-activated using 4 equivalents of HBTU, 4 equivalents of HOBt in DMF and 3 equivalents of DIEA for 30 seconds. The pre-activated 5-oxohexanoic acid was then added to the peptide-resin mixture and allowed to couple for 15 minutes at 50°C under microwave irradiation. The mixture was washed subsequently with DMF, DCM and then DMF. Deprotected and cleavage of the peptide from the resin was done by adding TFA:H2O (95: 5) cocktail to the washed resin in ice for 30 minutes with shaking and then the shaking was continued at room temperature for additional 1 hour. The deprotection and cleavage processes were monitored using MALDI-TOF/MS. The solution containing the synthesized glycopeptide was drained. The resin was flushed subsequently with the same cocktail solution, acetic acid, and methanol. The filtrates were combined and concentrated by air drying, dissolved in 50%

acetonitrile and lyophilized. The peptide was then purified using RP-HPLC with acetonitrile (B) and water (A) both with 0.1% TFA using Intersil® ODS-3 (5 μm, 4.6 x 250 mm) column at room temperature, 1 ml/min flow rate, 220 nm wavelength for detection, and then lyophilized. The purified glycopeptide was de-*O*-acetylated by dissolving in trifluoroethanol and added with sodium hydroxide to pH 10.5-11.0 for 30 minutes. The removal of the acetyl groups from the sugar moiety was monitored using MALDI-TOF/MS. After the complete deacetylation process, the solvent was removed either under reduced pressure or air-drying. The de-*O*-acetylated glycopeptide was purified by RP-HPLC with acetonitrile (B) and water (A) both with 0.1% TFA using Intersil® ODS-3 (5 μm, 4.6 x 250 mm) column at room temperature, 1 ml/min flow rate, 220 nm wavelength for detection, and solvent gradient (A:B) of 99:1 (0 min), 85:15 (50 mins), and 5:95 (60 mins) to get compound **2** (t = 13.8 mins) and then lyophilized.

HRMS (MALDI): *m/z* calcd for $C_{27}H_{45}N_5NaO_{17}^+$, $[M+Na]^+$ 734.2708, found 734.2672.

Synthesis of ketone-functionalized tetracosapeptide 3

A 0.24 mmol/g of Rink-amide-ChemMatrix resin, Fmoc-Ser(tBu)-OH (96 μmol, 4.0 equivalents), Fmoc-Gly-OH (96 μmol, 4.0 equivalents), and 5-oxohexanoic acid (4.0 equivalents) were used. Briefly, 0.24 mmol/g of Rink-amide-ChemMatrix resin was placed in a 5 mL Libra tube, washed sequentially with DMF and DCM followed by DCM swelling for 30 minutes. The swollen resin was washed with DMF. Fmoc-amino acid was pre-activated using 4 equivalents of HBTU, 4 equivalents of HOBt in DMF and 3 equivalents of DIEA for 30 seconds. The pre-activated Fmoc-amino acid was then added to the resin and allowed to couple for 15 minutes at 50°C under microwave irradiation. The resin was then washed subsequently with DMF, DCM and then DMF. To block the unreacted/uncoupled animo groups in the resin, acetyl capping was performed using DMF:Ac_2O:DIEA (8.5:1.0:0.5) for 5 minutes at room temperature, washed with DMF, DCM and then DMF, then Fmoc deprotection using 20% piperidine in DMF followed by washing with DMF, DCM and then DMF and the cycle repeated for alternating Ser-Gly sequence. After Fmoc deprotection of the last Fmoc-amino

acid, 5-oxohexanoic acid was pre-activated using 4 equivalents of HBTU, 4 equivalents of HOBt in DMF and 3 equivalents of DIEA for 30 seconds. The pre-activated 5-oxohexanoic acid was then added to the peptide-resin mixture and allowed to couple for 15 minutes at 50°C under microwave irradiation. The mixture was washed subsequently with DMF, DCM and then DMF. Deprotected and cleavage of the peptide from the resin was done by adding TFA:H2O (95: 5) cocktail to the washed resin in ice for 30 minutes with shaking and then the shaking was continued at room temperature for additional 1 hour. The deprotection and cleavage processes were monitored using MALDI-TOF/MS. The solution containing the synthesized peptide was drained. The resin was flushed subsequently with the same cocktail solution, acetic acid, and methanol. The filtrates were combined and concentrated by air drying, dissolved in 50% acetonitrile and lyophilized. The peptide was then purified using RP-HPLC with acetonitrile (B) and water (A) both with 0.1% TFA using Intersil® ODS-3 (5 µm, 4.6 x 250 mm) column at room temperature, 1 ml/min flow rate, 220 nm wavelength for detection, and solvent gradient (A:B) of 99:1 (0 min), 85:15 (50 mins), and 5:95 (60 mins) to get compound **3** (t = 19.7 mins) and then lyophilized.

HRMS (MALDI): *m/z* calcd for $C_{66}H_{107}N_{25}NaO_{38}^{+}$, $[M+Na]^{+}$ 1880.7106, found 1880.7100.

Synthesis of ketone-functionalized glycopeptide 4

A 0.24 mmol/g of Rink-amide-ChemMatrix resin, Fmoc-Ser(tBu)-OH (96 µmol, 4.0 equivalents), Fmoc-Gly-OH (96 µmol, 4.0 equivalents), *N*-(9-Fluorenylmethoxycarbonyl)-*O*-[2,3-di-*O*-acetyl-4-*O*-(2,3,4,6-tetra-*O*-acetyl-β-D-galactopyranosyl)-β-D-xylopyranosyl]-L-Serine (MCP Co., Ltd, Japan) (36 µmol, 1.5 equivalents) and 5-oxohexanoic acid (4.0 equivalents) were used. Briefly, 0.24 mmol/g of Rink-amide-ChemMatrix resin was placed in a 5 mL Libra tube, washed sequentially with DMF and DCM followed by DCM swelling for 30 minutes. The swollen resin was washed with DMF. Fmoc-amino acid was pre-activated using 4 equivalents of HBTU, 4 equivalents of HOBt in DMF and 3 equivalents of DIEA for 30 seconds. The pre-activated Fmoc-amino acid was then added to the resin and allowed to couple

for 15 minutes at 50°C under microwave irradiation. The resin was then washed subsequently with DMF, DCM and then DMF. To block the unreacted/uncoupled animo groups in the resin, acetyl capping was performed using DMF:Ac_2O:DIEA (8.5:1.0:0.5) for 5 minutes at room temperature, washed with DMF, DCM and then DMF, then Fmoc deprotection using 20% piperidine in DMF followed by washing with DMF, DCM and then DMF and the cycle repeated for alternating Ser-Gly sequence. For the introduction of *N*-(9-Fluorenylmethoxycarbonyl)-*O*-[2,3-di-*O*-acetyl-4-*O*-(2,3,4,6-tetra-*O*-acetyl-β-D-galactopyranosyl)-β-D-xylopyranosyl]-L-Serine, 1.2 equivalents of PyBOP, 1.2 equivalents of HOAt in DMF and 3 equivalents of DIEA as the coupling cocktail. After coupling for 15 minutes at 50°C under microwave irradiation, the same coupling cocktail, without Fmoc-glycoamino acid, was added for a "double activation-like" approach for 15 minutes at 50°C under microwave irradiation. After Fmoc deprotection of the last Fmoc-amino acid, 5-oxohexanoic acid was pre-activated using 4 equivalents of HBTU, 4 equivalents of HOBt in DMF and 3 equivalents of DIEA for 30 seconds. The pre-activated 5-oxohexanoic acid was then added to the peptide-resin mixture and allowed to couple for 15 minutes at 50°C under microwave irradiation. The mixture was washed subsequently with DMF, DCM and then DMF. Deprotected and cleavage of the peptide from the resin was done by adding TFA:H2O (95: 5) cocktail to the washed resin in ice for 30 minutes with shaking and then the shaking was continued at room temperature for additional 1 hour. The deprotection and cleavage processes were monitored using MALDI-TOF/MS. The solution containing the synthesized glycopeptide was drained. The resin was flushed subsequently with the same cocktail solution, acetic acid, and methanol. The filtrates were combined and concentrated by air drying, dissolved in 50% acetonitrile and lyophilized. The peptide was then purified using RP-HPLC with acetonitrile (B) and water (A) both with 0.1% TFA using Intersil® ODS-3 (5 μm, 4.6 x 250 mm) column at room temperature, 1 ml/min flow rate, 220 nm wavelength for detection, and then lyophilized. The purified glycopeptide was de-*O*-acetylated by dissolving in trifluoroethanol and added with sodium hydroxide to pH 10.5-11.0 for 30 minutes. The removal of the acetyl groups from

the sugar moiety was monitored using MALDI-TOF/MS. After the complete deacetylation process, the solvent was removed either under reduced pressure or air-drying. The de-*O*-acetylated glycopeptide was purified by RP-HPLC with acetonitrile (B) and water (A) both with 0.1% TFA using Intersil® ODS-3 (5 μm, 4.6 x 250 mm) column at room temperature, 1 ml/min flow rate, 220 nm wavelength for detection, and solvent gradient (A:B) of 99:1 (0 min), 85:15 (50 mins), and 5:95 (60 mins) to get compound **4** (t = 26.7 mins) and then lyophilized.
HRMS (MALDI): *m/z* calcd for $C_{132}H_{215}N_{25}NaO_{92}^{+}$, $[M+Na]^{+}$ 3645.2811, found 3645.2750.

Preparation of AO/PCSAM-QDs. To the 50 μL of 1 μM TOPO-QDs were added Isopropanol:Methanol (100 μL:50 μL), then centrifuged at 15,000 g for 3 minutes. The solvent was removed and the pelleted TOPO-QDs were re-suspended in 50 μL *n*-hexane and homogenized by sonication. TOPO-QDs/*n*-hexane solution was added with 30 μL of Milli Q water, 1 μL of $NaBH_4$ (12 wt % in 14 N NaOH), 5 μL of 5 mM 11,11'-dothio bis[undec-11-yl 12-(aminooxyacetyl)amino hexa(ethyleneglycol)] (HS-ao)[12c] and 10 μL of 50 mM 11-mercaptoundecylphosphorylcholine (HS-PC). The mixture was mixed for 30 minutes at room temperature. The *n*-hexane layer containing TOPO were removed, and washed three times with hexane. The water layer containing AO/PCSAM-QDs was purified using ultra filtration (YM 10) and washed with ultrapure water (400 μL) three times. The AO/PCSAM-QDs solution was directly analyzed by MALDI-TOFMS (Bruker Daltonics, Bremen, Germany) using DHB (1 μL, 10 mg/mL) as a matrix.

Conjugation of QDs with ketone-functionalized derivatives. To the 10 μL of AO/PCSAM-QDs solution was added 1 μL of 10 mM ketone-functionalized peptides/glycopeptides and 1 μL of 10 mM ketone-functionalized glycopeptide mixed thoroughly with 1 μL of 10 mM *k*-His_6. The mixture was added with 10 μL of 200 mM acetate buffer (pH 4.0), mixed for 15-30 minutes at room temperature and concentrated to dryness by centrifugal evaporator, to complete the oxime formation reaction, for 30 minutes at 40°C. The obtained solid was

resuspended in Milli Q, purified using ultra filtration (YM 10) and washed with Milli Q (400 μL) three times. The products AO/PCSAM-QDs co-displaying the glycopeptide and His_6, AO/PCSAM-QDs carrying glycopeptides, AO/PCSAM-QDs carrying His_6 and AO/PCSAM-QDs carrying Arg_6 were dissolved in Milli Q (10 μL) to obtain 1 μM solution. The samples were directly analyzed by MALDI-TOFMS using DHB (1 μL, 10 mg/mL) as a matrix.[12c]

Cell Culture. NHAC-Kn (Kurabo Inc.), A549 (Health Science Research Resource Bank), HT-29 (American Type Culture Collection) and HepG2 (RIKEN cell bank) cell lines were grown in Dulbecco's Modified Eagle Medium (DMEM), PC-3 cells (Health Science Research Resource Bank) were grown in RPMI-1640 and OUS-11 (Health Science Research Resource Bank) were grown in MEM at 37°C with 5% CO_2. All media used were supplemented with 10% (v/v) FBS, Penicillin G (500 units/mL) and Streptomycin (500 unit/mL).

Cellular uptake of QD conjugates. Cellular internalization experiments were performed on an 8-well Nunc Lab-Tek II Chamber Slide System (Thermo Scientific™). Cells ($5x10^3$ cells/well) were seeded in the wells and cultured overnight. For the delivery experiments, QD-conjugates were diluted with the complete culture medium and incubated with cells at 37°C with 5% CO_2 for 2 hours. For assessing lysosomal colocalization, the QD-conjugates were incubated with cells for 5 minutes or 2 hours and cells were stained with lysosomal marker LysoTracker Red DND-99 (Invitrogen). The nuclei were stained with Hoechst 33342 (Invitrogen) and observed under fluorescence microscope. For the golgi colocalization assessment, the incubation was only up to 2 hours. The excess QD-conjugates were removed by washing the cells with DPBS three times. The cells were then fixed with 4% paraformaldehyde for 10 minutes at room temperature and permeabilized with 0.4% Triton X-100 and washed. The cells were incubated with the golgi marker anti-giantin antibody [9B6] mouse IgG1 (abcam), as the primary antibody, for 1 hour at room temperature or overnight at 4 °C, washed with DPBS three times and then incubated with secondary anti-body anti-IgG mouse Cy3 (Funakoshi, Japan) for 30

minutes to 1 hour at room temperature. The nuclei were stained with Hoechst 33342 (Invitrogen), as the final hybridization process, and observed under fluorescence microscope.

Fluorescence Microscopy and Image Analysis. The fluorescence microscope used for image acquisition and image analysis was an all-in-one fluorescence microscope BIOREVO BZ-9000 series generation II (Keyence, Japan) equipped with 4x, 20x, 40x, and 60x (oil immersion) lenses. Images were taken using standard filter set for DAPI (for Hoechst), FITC (for QD545) and TRITC (for anti-mouse IgG-Cy3). Merge images were generated and analyzed using BZ-II software.

Cytotoxicity Study. NHAC-Kn, HepG2, HT-29, A549, OUS-11 and PC-3 cells were seeded in a 96-well plate (Thermo Scientific), at $5.0x10^3$ cells/well, and incubated at 37^oC with 5% CO_2 for 24 hours. The cells were treated with kpH_6, $k(2s4p)_6$, PC-QD-ao-kpH_6, and PC-QD-ao-$k(2s4p)_6$/-kpH_6 for 24 hours. Cell growth was determined by adding 10 μL of cell counting kit 8 (Dojindo, Kumamoto, JAPAN), incubated for 2-4 hours and optical density was measured using a model 550 Microplate reader (BioRad, Hercules, CA, USA). Data were reported in percent viability with respect to the untreated control (± SEM) of the trials (n = 3).

Postimaging Analysis. All images in a given experiment were taken and processed identically for colocalization experiments. Colocalization values were calculated for at least 15 cells per cell line, using the Costes algorithm[39,40] that is available through ImageJ (rsb.info.nih.gov/ij) with the additional plugins: "Colocalization Test" and "Colocalization Threshold" (by T. Collins and W. Rasband). The region of interest (ROI) was set such that the total golgi area is included. 3D analysis and Quantification of images were performed using ImageJ after subtracting the background reading. All photomicrographs in a given experiment were exposed and processed identically.

3.4 References

1. Weerapana, E.; Imperiali, B. Asparagine linked protein glycosylation: From eukaryotic to prokaryotic systems. *Glycobiology* **2006**,16:91R–101R.
2. Mann, M.; Jensen, O.N. Proteomic analysis of post-translational modifications. *Nat Biotechnol.* **2003**, 21:255–261.
3. Walsh, C.T.; Garneau-Tsodikova, S.; Gatto G.J. Protein posttranslational modifications: The chemistry of proteome diversifications. *Angew Chem Int Ed.* 2005, 44:7342–7372.
4. Sears, P.; Wong, C.H.; Enzyme action in glycoprotein synthesis. *Cell Mol Life Sci.* **1998**, 54:223–252.
5. Lehle, L.; Strahl, S.; Tanner, W. Protein glycosylation, conserved from yeast to man: A model organism helps elucidate congenital human diseases. *Angew Chem Int Ed Engl.* **2006**, 45:6802–6818.
6. Sola´, R.J.; Rodriguez-Martinez, J.A.; Griebenow, K. Modulation of protein biophysical properties by chemical glycosylation: Biochemical insights and biomedical implications. *Cell Mol Life Sci.* **2007**, 64:2133–2152.
7. Freeze, H. H. Genetic defects in the human glycome. *Nature Reviews*. **2006**, 7, 537-551.
8. Matsushita, T.; Ohyabu, N,; Fujitani, N.; Naruchi, K.; Shimizu, H.; Hinou, H.; Nishimura, S-I. "Site-specific conformational alteration induced by sialylation of MUC1 tandem repeating glycopept ides at an epitope region for anti-KL-6 monoclonal antibody",*Biochemistry* **2013,** 52, 402-414.
9. Hashimoto, R.; Fujitani, N.; Takegawa, Y.; Kurogochi, M.; Matsushita, T.; Naruchi, K.; Ohyabu, N.; Hinou, H.; Gao, X-D.; Manri, N., Satake, H.; Kaneko, A.; Sakamoto, T.; Nishimura, S-I. An efficient approach for the characterization of mucin type glycopeptides: The effect of O-glycosylation on the conformation of synthetic mucinpeptides, *Chem. Eur. J*. **2011**, **17**, 2393-2404.

10. Shimizu, H. K.; Hosoguchi, K.; Liu, Y.; Fujitani, N.; Ohta, T.; Hinou, H.; Matsushita, T.; Shimizu, H.; Feizi, T.; Nishimura, S.-I. Chemical synthesis, folding and structural insights into O-fucosylated epidermal growth factor-like repeat 12 of mouse Notch-1 receptor, *J. Am. Chem. Soc*. **2010**, 132, 14857-14865.
11. Shental-Bechor, D.; Levy, Y. Effect of glycosylation on protein folding: A close look at thermodynamic stabilization**.** *PNAS,* **2008**, 105, 8256 – 8261.
12. Öberg, F.; Sjöhamn, J.; Fischer, G.; Moberg, A.; Pedersen, A.; Neutze, R.; Hedfalk, K. Glycosylation Increases the Thermostability of Human Aquaporin 10 Protein. *J. Biol. Chem*. **2011**, 286, 31915-31923.
13. Sinclair, A. M.; Elliott, S. Glycoengineering: The effect of glycosylation on the properties of therapeutic proteins. *J Pharm Sci.* **2005**, 94:1626–1635.
14. Liu, D. T. Glycoprotein pharmaceuticals: Scientific and regulatory considerations, and the US Orphan Drug Act. *Trends Biotechnol.* **1992**, 10:114–120.
15. Dennis, J. W.; Lau, K. S.; Demetriou, M.; Nabi, I. R.; Adaptive regulation at the cell surface by N-glycosylation. *Traffic* **2009**,10, 1569–1578.
16. Hoseki, J.; Ushioda, R.; Nagata, K. Mechanism and components of endoplasmic reticulum-associated degradation. *J. Biochem*. **2010**, 147, 19–25 .
17. Kollmann, K. et al. Mannose phosphorylation in health and disease. *Eur. J. Cell Biol*. **2010**, 89, 117–123.
18. Watson, P.; Jones, A. T.; Stephens, D. J.; Intracellular trafficking pathways and drug delivery: fluorescence imaging of living and fixed cells, *Adv. Drug Delivery Rev.* **2005**, 57, 43–61.
19. Lloyd, J.B. Lysosome membrane permeability: implications for drug delivery, *Adv. Drug Deliv. Rev.* **2000**, 41, 189– 200.
20. Wattiaux, R.; Laurent, N.; Wattiaux-De Coninck, S.; Jadot, M. Endosomes, lysosomes: their implication in gene transfer, *Adv. Drug Deliv. Rev.* **2000**, 41, 201–208.

21. Jones, A.T.; Gumbleton, M.; Duncan, R. Understanding endocytic pathways and intracellular trafficking: a prerequisite for effective design of advanced drug delivery systems, *Adv. Drug Deliv. Rev.* **2003**, **55**, 1353– 1357.

22. Conner, S.D.; Schmid, S.L. Regulated portals of entry into the cell, *Nature* **2003**, 422, 37– 44.

23. Bonifacino, J.S.; Glick, B.S. The mechanisms of vesicle budding and fusion, *Cell* **2004**, 116, 153–166.

24. Maxfield, F.R.; McGraw, T.E. Endocytic recycling, *Nat. Rev., Mol.Cell Biol.* **2004**, 5, 121– 132.

25. Hoshi, H.; Shimawaki, K.; Takegawa, Y.; Ohyanagi, T.; Amano, M.; Hinou, H.; Nishimura, S-I. Molecular shuttle between extracellular and cytoplasmic space allows for monitoring of GAG biosynthesis in human articular chondrocytes. *Biochim. Biophys. Acta*, **2012**, 1820, 1391-1398.

26. Cai, W.; Shin, D. W.; Chen, K.; Gheysens, O.; Cao, Q.; Wang, S. X.; Gambhir, S. S.; Chen, X. Peptide-Labeled Near-Infrared Quantum Dots for Imaging Tumor Vasculature in Living Subjects. *Nano lett*. **2006**, 6, 669– 676.

27. De la Fuente, J. M.; Penades, S. Glyco-quantum dots: a new luminescent system with multivalent carbohydrate display. *Tetrahedron Asymm*. **2005**, 16, 387–391.

28. Robinson, A.; Fang, J. M.; Chou, P. T.; Liao, K. W.; Chu., R. M.; Lee., S. Probing Lectin and Sperm with Carbohydrate-Modified Quantum Dots. *J. ChemBioChem.* **2005**, 6, 1899–1905.

29. Ohyanagi, T.; Nagahori, N.; Shimawaki, K.; Hinou, H.; Yamashita, T.; Sasaki, A.; Jin, T.; Iwanaga, T.; Kinjo, M.; Nishimura, S-I. Importance of Sialic Acid Residues Illuminated by Live Animal Imaging Using Phosphorylcholine Self-Assembled Monolayer-Coated Quantum Dots. *J. Am. Chem. Soc*. **2011**, 133, 12507–12517.

30. Shimawaki, K.; Fujisawa, Y.; Sato, F.; Fujitani, N.; Kurogochi, M.; Hoshi, H.; Hinou, H.; Nishimura, S-I. Highly Efficient and Versatile Synthesis of Proteoglycan Core

Structures from 1,6-Anhydro-b-lactose as a Key Starting Material. *Angew. Chem. Int. Ed.* **2007**, 46, 3074-3079.

31. Chen, S.; Zheng, J.; Li, L.; Jiang, S. Strong Resistance of Phosphorylcholine Self-Assembled Monolayers to Protein Adsorption: Insights into Nonfouling Properties of Zwitterionic Materials. *J. Am. Chem. Soc*. **2005**, 127, 14473-14478.
32. Nagahori, N.; Abe, M.; Nishimura, S-I. Structural and Functional Glycosphingolipidomics by Glycoblotting with an Aminooxy-Functionalized Gold Nanoparticle. *Biochemistry* **2009**, 48, 583-594.
33. Kuo, P-L.; Huang, M-S.; Cheng, D-E.; Hung, J-Y.; Yang, C-J.; Chou, S-H. Lung Cancer-derived Galectin-1 Enhances Tumorigenic Potentiation of Tumor-associated Dendritic Cells by Expressing Heparin-binding EGF-like Growth Factor. *J. Biol. Chem.* **2012**, 287:9753-9764.
34. Coombs, P. J.; Taylor, M. E.; Drickamer, K. Two categories of mammalian galactose-binding receptors distinguished by glycan array profiling. *Glycobiology* **2006**, vol. 16 no. 8 pp. 1C–7C.
35. Kolb-Bachofen, V.; Abel, F. Participation of D-galactose-specific receptors of liver macrophages in recognition of fibronectin-opsonized particles. *Carbohydrate Research* **1991**, 213, 201-213.
36. Fuster, M. M.; Esko, J. D. The sweet and sour of cancer: glycans as novel therapeutic targets. *Nat. Rev. Cancer* **2005**, 5, 526-542.
37. Stern, S.T.; Adiseshaiah, P. P.; Crist, R. M. Autophagy and lysosomal dysfunction as emerging mechanisms of nanomaterial toxicity. *Part. Fiber Toxicol.* **2012**, 9:20.
38. Kroemer, G.; Jaattela, M. Lysosomes and Authopagy in Cell Death Control. *Nat. Rev. Cancer* **2005**, 5, 886-897.
39. Costes, S. V.; Daelemans, D.; Cho, E. H.; Dobbin, Z.; Pavlakis, G.; and Lockett, S. Automatic and quantitative measurement of protein-protein colocalization in live cells. *Biophys. J.* ***86***, 3993–4003 (2004).

40. Adler, J., and Parmryd, I. “Colocalization Analysis in Fluorescence Microscopy” In: Taatjes, Douglas J.; Roth, Jürgen (ed.), Cell Imaging Techniques: Methods and Protocols, New York: Humana Press, 97-109 (2012).

Chapter 4

Conclusion

4.1 Conclusion

The study resulted to establishing a standard protocol for the preparation of versatile and multifunctional nanoparticles by means of cell surface mimetic AO/PCSAM-QDs as a key platform for displaying a variety of peptides and glycopeptides. This allows a straightforward attachment of general peptides/glycopeptides on the AO/PCSAM-QD surface, by tagging them with ketone during solid-phase synthesis, without the use of any special coupling reagents. These QD conjugates derived from AO/PCSAM-QDs satisfy some important criteria required for the ideal NDD vehicles such as: (1) versatility and reproducibility in the procedure for the surface manipulation and the attachment of ligands having a ketone group or some functionalities that can be conjugated chemoselectively by an aminooxy functional group, (2) efficient endolysosomal escaping ability, (3) controlled orientation and density of the ligands displayed, and (3) biocompatibility needed for the live cell and animal imaging. This study also revealed the great advantage of ketone-functionalized hexahistidine to facilitate a rapid endolysosomal escape of cell surface mimetic QD conjugates to the cytosol and subsequent delivery to the target intracellular compartment in various human cell lines. Real-time cellular imaging revealed that combined use of hexahistidylated AO/PCSAM-QDs with PGI glycopeptides **1**~**4** showed a rapid and dynamic processes of the entry, controlled intracellular trafficking, specific Golgi localization, and excretion of the nanoparticles from the cytoplasmic area.

Although many histidine-rich peptides such as CPPs and NLS peptides had been proven to be an efficient mediator for gene transfer, this study presented an ideal platform for the design of entirely novel class of NDD systems targeting specific intracellular compartments. Therefore, it is noteworthy that PCSAM coating strategy may also become universal tools for spatially oriented immobilization of engineered proteins including antibody and antibody-drug conjugates on various metal-based nanoparticles.

Through the use of this general platform, difference in intracellular dynamics between naked and glycosylated serglycin-like peptides on different human cell lines as well as the involvement of glycans in governing subcellular localization of serglycin-like peptides were shed into light. The unveiled selective golgi localization on the normal lung tissue (OUS-11) due to the presence of glycosylation on serglycin-like peptide backbone, but not observed in the lung adenocarcinoma (A549), exemplified the possible important use of glycosylation or glycan moieties in targeted drug delivery. This observation if incorporated in a correct targeted drug delivery system design could potentially be used to prevent collateral damages on normal cells/tissues during cancer targeting and treatment.